ESTIMATING THE MICOPHYTOBENTHIC CONTRIBUTION TO ECOSYSTEM NET COMMUNITY PRODUCTION IN A GULF OF MAINE ESTUARY: DAMARISCOTTA RIVER ESTUARY, MAINE, USA

by

Emilee Burris

Submitted in partial fulfillment of the requirements
for the degree of Master of Science

at

Dalhousie University
Halifax, Nova Scotia
April 2021

TABLE OF CONTENTS

LIST OF TABLES

LIST OF FIGURES

ABSTRACT

Productivity in shallow coastal regions of the ocean on a per area basis can outweigh that of the open ocean due to high nutrient inputs from land. Within these shallow regions light can reach the sediment surface resulting in the growth of benthic algae, such as mat forming diatoms. Primary productivity in coastal environments can have a significant benthic component but can vary due to parameters such as light that influence the spatial and temporal distribution of biomass. Light is often the limiting factor for benthic primary producers and an understanding of the of the benthic PE (photosynthesis versus downwelling irradiance) relationship is necessary for quantifying the benthic contribution to ecosystem photosynthesis. In this thesis I used a combination of whole core *ex situ* flux incubations for the total oxygen exchange rate (TOE) and microsensor oxygen profiling for the diffusive oxygen exchange rate (DOE) to determine benthic PE curves. The PE relationship was determined for the benthic community in the Damariscotta River Estuary (DRE), a highly dynamic productive estuary in mid-coast Maine, USA. PE relationships were measured in sediments from different depths by sampling a transect across the estuary. Based on the natural range of light (6 to 63 µmol photons m^{-2} s^{-1} measured during sampling) at the sampling sites, the corresponding sediment total O_2 exchange rate ranged from -40 mmol O_2 m^{-2} d^{-1} in the dark to 53 mmol O_2 m^{-2} d^{-1} at the highest light level. Rates across the transect were similar between sites except at the deepest site in the middle of the channel was lower. The average transect TOE photosynthetic capacity (P_{max}) was 395 mmol O_2 m^{-2} d^{-1}, the average photosynthetic efficiency (α) was 3.9 mmol O_2 m^{-2} d^{-1} (µmol photons m^{-2} s^{-1})$^{-1}$ and the average respiration (R) was 70.8 mmol O_2 m^{-2} d^{-1}. Chlorophyll a sediment concentrations showed no variation between sites while microphytobenthos biomass varied across the transect with the deepest site having significantly less biomass. Combining the TOE PE parameters with measurements of light attenuation, and surface irradiance, the net community production (NCP) was estimated for the month of July 2019. Positive NCP was found in the two shallow sites on either side of the transect reflecting net autotrophy, while negative NCP was found in the deeper sites of the transect, reflecting net heterotrophy. This pattern across the transect is driven by higher light availability at the shallow sites and not differences in the PE relationship except for the middle of the channel site. Quantifying benthic photosynthesis is needed for determining the productivity of the whole estuary. This is an important question as the DRE hosts a lucrative shellfish aquaculture industry and understanding the benthic contribution to primary productivity in the estuary is necessary for understanding how much shellfish aquaculture the estuary can support and its effect on the local ecosystem.

LIST OF ABBREVIATIONS AND SYMBOLS USED

Abbreviations	Descriptions
Chl a	chlorophyll a
BBL	benthic boundary layer
DIC	dissolved inorganic carbon
DOE	diffusive oxygen exchange
DOC	dissolved organic carbon
DRE	Damariscotta river estuary
ED	east deep site
ES	east shallow site
GPP	gross primary production
HD	high definition
LED	light emitting diode
LOBO	Land/Ocean Biogeochemical Observatory
MC	middle of channel site
ME	Maine
MHW	mean high tide water
MPB	microphytobenthos
MPB PP	microphytobenthic primary production
MSO	maximum subsurface oxygen
NCP	net community production
NE	north east
NOAA	national oceanic and atmospheric administration
NOP	net oxygen production
NPP	net primary productivity
PAM	pulse amplitude modulation
PAR	photosynthetic available radiation
PE	photosynthetic irradiance
PME	Precision Measurement Engineering
SEANET	Sustainable Ecological Aquaculture Network
TOE	total oxygen exchange
UV	ultraviolet
WS	west Shallow Site

Symbols	Descriptions	Units
A	area	m^2
α	alpha	mmol O_2 m^{-2} d^{-1} (µmol photons m^{-2} s^{-1})$^{-1}$
C_{chla}	concentration of Chl a in sediment	µg mL^{-1}
C_{slurry}	concentration of sediment slurry cells	cells mL^{-1}
Δ	change	-
D	dilution factor	mL
D_{O_2}	diffusivity of O_2	mmol O_2 m^{-2} s^{-1}
E	downwelling irradiance	µmol photons m^{-2} s^{-1}
E_D	downwelling irradiance at sediment surface	µmol photons m^{-2} s^{-1}
E_k	minimum saturating irradiance	µmol photons m^{-2} s^{-1}
E_o	irradiance at surface	µmol photons m^{-2} s^{-1}
E_z	downwelling irradiance at given depth	µmol photons m^{-2} s^{-1}
H	height	cm
k	attenuation coefficient	-
∂	partial derivative	-
φ	porosity in sediment	g cm^{-3}
P	production of O_2	mmol O_2 m^{-2} d^{-1}
PAR	photosynthetic available radiation	µmol photons m^{-2} s^{-1}
period	length of tidal cycle	hours
P_{max}	maximum photosynthetic capacity	mmol O_2 m^{-2} d^{-1}
O	multiplication factor from slide to sample	-
O_2	O_2 concentration	mg l^{-1}
$O_{2(blank)}$	O_2 concentration in blank core	mg l^{-1}
$O_{2(core)}$	O_2 concentration in sediment core	mg l^{-1}
offset	duration of time high tide is off from midnight	hours
R	respiration or consumption of O_2	mmol O_2 m^{-2} d^{-1}
S	salinity	psu
T	temperature	°C
t	time	hours
TOE Flux	total oxygen exchange rate	mmol O_2 m^{-2} d^{-1}
Δt	change in time	minutes
V	volume of sample on slide for counts	µL
V_{sample}	volume of sample from sediment core	mL
V_1	volume of preserved sediment slurry	mL
V_2	volume of aliquot taken from sediment core sample	mL
z	depth	-

ACKNOWLEDGEMENTS

First and foremost, I would like to thank my supervisor Chris Algar for offering me this opportunity to further my studies into benthic diatoms. I would like to thank him for accommodating my situation of living between Nova Scotia and Maine throughout my research and always putting an optimistic point of view on any circumstance.

I would also like to acknowledge my committee members Jeremy Rich and Katja Fennel for their support and critiques. Further, I would like to thank the Rich Lab at the University of Maine's Darling Marine Center for allowing me to use their space and resources to conduct my research. Without the help of Jeremy Rich and his research associate Sean O'Neill the experiments in this thesis would not have been possible. I would also like to thank the undergraduate interns from the summer of 2019 for their help in the collection of sediment cores by the means of scuba diving and Rachel Presley for her help with the sediment Chlorophyll a samples.

I also would like to thank the Algar/Buchwald lab for always being there for me even when I wasn't always present in the lab. I would like to thank my husband Ryan for supporting me throughout this journey even though it meant moving away from him for the time being. Lastly, I would like to thank my mom and dad who have pushed me to do my absolute best in my academic career and further my education.

CHAPTER 1

INTRODUCTION

Benthic microalgae contribute significantly to ecosystem primary production of temperate and tropical shallow coastal regions (Grøntved 1962; Colijn & de Jonge, 1984; Cahoon & Cooke 1992, Glud et al. 2002b). Productivity within nearshore regions of the ocean can outweigh that of the open ocean by up to 3-5 times because of increased diversity and nutrient availability influenced by daily tidal mixing (Zhao et al. 2019). For example it has been found that the benthic habitat can contribute 31% to the total annual primary production to an overall temperate soft sediment ecosystem (Ask et al. 2016). Benthic microalgae are likely to be widespread around the world's oceans and can be found in estuaries and continental shelf sediments, where sufficient light penetrates through the water column to reach the sediment to support photosynthesis (Gattuso et al. 2006). Benthic microalgae contribute to multiple ecosystem services as they are essential primary producers at the base of the marine food web with rapid transfer of organic matter and mediation of energy and nutrients (Christianen et al. 2017, Hope et al. 2019). Benthic microalgae communities in intertidal and shallow subtidal estuaries with mud or sand as the bottom substrate are largely dominated by diatoms and/or cyanobacteria (Cartaxana et al. 2016).

On the basis of biomass and biogeochemical cycling, benthic diatoms play a significant role in productivity, trophic dynamics and sediment stability (MacIntyre et al. 1996). Intertidal estuaries are dynamic environments, where tidal currents lead to deposition and resuspension of sediments, effecting the distribution of diatoms within the

estuary (Mitbavkar & Anil 2002). Short-term variations in water depth and light attenuation affect spatial and temporal distribution of diatom biomass and corresponding photosynthetic activity (Denis et al. 2012).

1.1 Measuring Benthic Primary Productivity

To determine the benthic net community production (NCP) the total oxygen exchange (TOE) rate has been measured in the sediment core chamber incubations. This measurement reflects the balance between respiration and photosynthesis from the sediment (Rodil et al. 2019) or in other words the sediment is considered a "black box" (Denis et al. 2012) with one net flux of either consumption or production of oxygen. Since the development of fine scale oxygen microelectrode sensors, the spatial resolution of net activity within the sediment can be increased by determining the diffusive oxygen exchange (DOE) from the production or consumption rates within the sediment. Both the TOE and DOE method of determining O_2 flux from the benthic community can be used to define the relationship between production and light levels (PE curve). This has been demonstrated by Glud et al. (2002a) and (2009) who using similar methods determined a PE curve for Arctic sediments using both the TOE and DOE, and reported higher DOE photosynthetic parameters then TOE. The DOE oxygen microprofiling method is done by breaking the sediment into zones of oxygen consumption or production rates with depth based on the curvature of the microsensors O_2 profiles (Berg et al. 1998). The DOE oxygen microprofiles provide insight into the sediment redox reaction cascade determining the oxygen penetration depth (OPD) in the sediment. For example the farther oxygen diffuses into the sediment the more it will increase the amount of nitrification

occurring during light periods resulting in nitrogen retention and the drawdown of nitrogen at night can initiate denitrification during dark periods (Hope et al. 2019).

Most recent studies have measured the dissolved oxygen exchange rates *in situ* to determine benthic primary production, Sospedra et al. (2015) reported seasonal change in O_2 production in temperate fine sands with significantly more production in the spring. Chlorophyll a (Chl a) measurements are taken to fully understand what is driving the benthic rate (e.g., increased biomass or higher Chl a concentrations per cell) as done in McMinn et al. (2012) and many other studies. O_2 exchange can be measured by either whole core incubations or microelectrode profiles either *in situ* or *ex situ*. There are other techniques of measuring benthic production like PAM (Pulse Amplitude Modulation) done *in situ,* used by Salleh & McMinn (2011) in the Antarctic, or the older C^{14} incubation method used by Vilbaste et al. (2000) which is more commonly used for pelagic production (Ask et al. 2016). The exchange rate of dissolved inorganic carbon (DIC) by a whole core incubation can also be used to measure benthic primary production (Ask et al. 2016). In shallow temperate coastal regions, subtidal benthic net primary production has been estimated to range from -0.8 to 2.9 mmol O_2 m^{-2} h^{-1} with Murrell et al. (2009) the lowest values reported from a bay in Florida and Cibic et al. (2008) with the highest from the northern Adriatic Sea based on a literary review from Santema & Huettel (2018). The many different methods of measuring and presenting benthic primary production estimates can lead to difficulties in comparing rates across studies.

1.2 Study Site

The Damariscotta River Estuary (DRE) is a highly dynamic productive estuary in mid-coast Maine, USA. Pelagic phytoplankton abundance has been found to be typically highest at the head of the DRE (Thompson et al. 2006). However, the present study was the first to investigate the benthic microalgae with an objective of determining the primary production contribution of the benthic community at the head of the DRE. The DRE is light limiting for benthic primary production because it experiences daily tidal fluctuations changing the downwelling irradiance reaching the sediment surface. Side-scan sonar surveys from a 1997 study of the middle DRE discovered that the dominant sediment types are silt and mud (Chandler et al. 2016). These sediment types create an optimal environment for benthic diatoms to form mats on the sediment and carry out primary production when sufficient downwelling irradiance reaches the sediment surface. The DRE also hosts a large shellfish aquaculture industry and quantifying the benthic contribution to primary production is necessary for the future of the growing industry in the head of the river.

Progress has been made during the past decades in researching and understanding the benthic O_2 dynamics and how it effects the marine carbon cycle, however there are still many questions that have not been answered (Glud, 2008). Since diatoms act as an environmental indicator for stress based on their sensitivity to the environment (Tang et al. 2017), this can help predict the future of the aquaculture industry in the state of Maine with the bulk of it grown in the Damariscotta River Estuary (Cole et al. 2017). The estuary hosts a large portion of bivalve aquaculture for US coastal bays and estuaries that is increasing at a rate of 75% from 2005 to 2013 (Testa et al. 2015). Ecosystem modeling

and management of the oyster cultivation is key to continuing the future of the DRE aquaculture industry alongside a warming Gulf of Maine system due to climate change (Mills et al. 2013). The production of microphytobenthos is often linked to coastal fish and shellfish production (Kritzer et al. 2016, Morioka et al. 2017, Hope et al. 2019) because they are at the base of the benthic marine food web and transfer organic matter rapidly they mediate energy and nutrients to higher trophic levels (Christianen et al. 2017, Hope et al. 2019). Microphytobenthos are significant food sources for shellfish and can contribute up to 70% of the diet of harvested mussels, oysters and cockles (Hope et al. 2019). Microphytobenthos are often overlooked in decision making for complex ecosystems like the DRE but have been proven to play a key role in interactions and feedbacks that provide crucial ecosystem services.

1.3 Objectives and Thesis Outline

This study will determine whether the benthic community in the upper part of the DRE is either net autotrophic or heterotrophic during July 2019 and the role of light or biomass (determined from cell counts or sediment chlorophyll a) in determining the rate of primary production. The importance of MPB in shallow water ecosystems is well established and the most common limiting factors reported are light and biomass while the fate of these communities are unknown (Middelburg et al. 2000) but what role these factors play in the DRE has not been examined. By determining a relationship between irradiance and primary production (PE relationship) for the DRE sediments the contribution of the benthic community can be estimated for any point in the year using downwelling irradiance recorded by the University of Maine's LOBO buoy. Furthermore, while the water column of the DRE has been highly studied, few benthic investigations

have been done. This research aims to improve the understanding of how sediments in shallow coastal regions can contribute to primary production.

The thesis is organized in the style of a publication. Chapter 2 outlines the details of the methods used. Key background information about the DRE is detailed along with a description of the techniques (TOE and DOE) used for determining the PE relationship of the MPB community. The details of the diatom cell counts and chl a measurements are explained along with the final estimation of net community production across the transect. In Chapter 3, the results of both methods of establishing a PE relationship for the benthic community are presented. The distribution of the MPB community across the transect is also evaluated by both cell and chl a concentrations and related to primary production rates. Then, using the experimentally determined PE region and *in situ* irradiance measurements, the daily oxygen production for the month of July 2019 is determined for each site across the transect. Finally, in Chapter 4, the results from Chapter 3 are discussed and compared to literature values to determine if the DRE has high MPB production and why. Whether each site is net autotrophic or heterotrophic for the benthic community is determined for the month of July 2019 and the impacts of the large aquaculture industry within the study site in the DRE are discussed. The final conclusions of the study are summarized in Chapter 5, and the errors and limitations are discussed with the final part being a discussion of the potential for future work in the DRE.

CHAPTER 2

METHODS

2.1 Study site, sampling and experimental set-up

The Damariscotta River Estuary stretches 30 km inland, southwest from the Gulf of Maine to the town of South Bristol, ME (Mayer et al. 1996). The estuary experiences semi-diurnal tides with an amplitude varying between 2.2 and 3.6 m according to the Walpole ME tide gauge (43°46.02 N, 69°34.8 W). Freshwater input from the Damariscotta Lake at the head of the estuary is limited (1-3 m^3 s^{-1}) and the average salinity is 31.7 (Chandler et al. 2016).

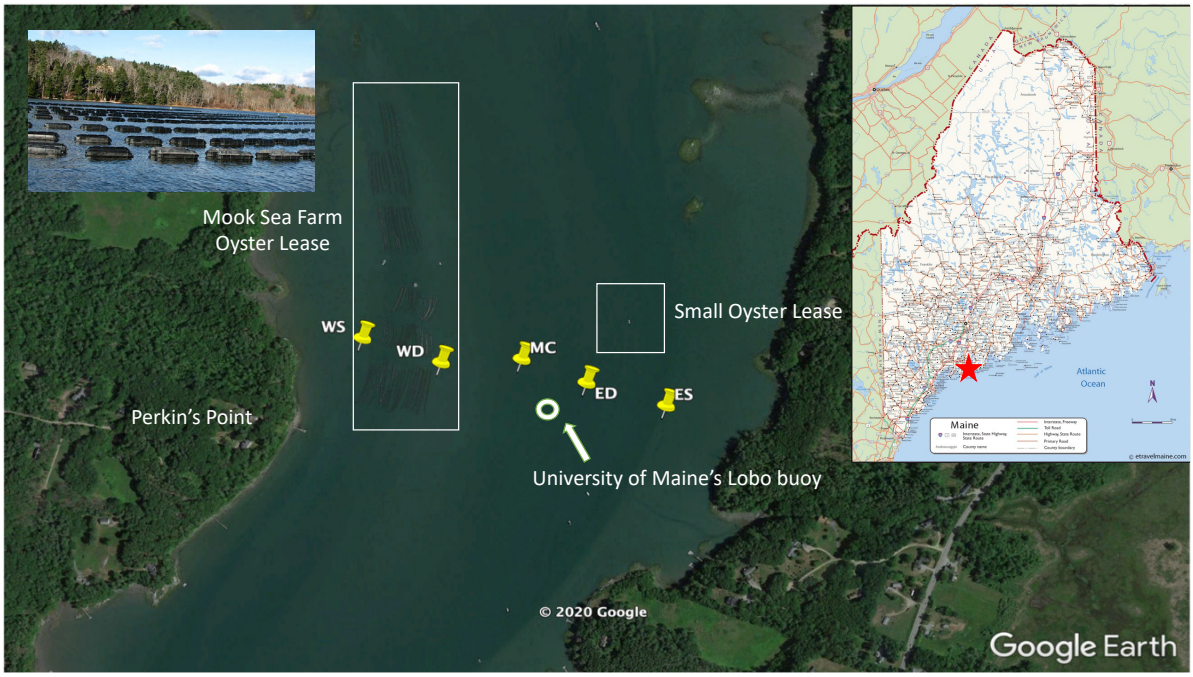

Figure 2.1: The location of the sampling site within the upper Damariscotta River Estuary (DRE). Oyster aquaculture leases marked in white squares and the University of Maine's LOBO buoy in white circle (Google Earth, 2019). The DRE marked with a red star on the state of Maine map (On the World Map, 2020).

Table 2.1: Sample Sites with coordinates, water depth, bottom water temperature, sampling date and the in situ PAR at the sediment surface during sampling of each site.

Site Name	Latitude and Longitude	Sampling Date	Water Depth (m)		Bottom Water Temperature ($°C$)	Light (PAR @ Sediment level during sampling μmol photons $m^{-2}s^{-1}$)
			Mean High Tide	Mean Low Tide		
West Shallow (WS)	$44°00'03.64"\ N$, $69°32'44.06"\ W$	July 30th, 2019	3.3	0.6	22.2	63.41 μmol photons $m^{-2}s^{-1}$
West Deep (WD)	$44°00'01.98"\ N$, $69°32'37.32"\ W$	June 24th, 2019	6.9	4.3	17.7	40.0 μmol photons $m^{-2}s^{-1}$
Middle of Channel (MC)	$44°00'02.22"\ N$, $69°32'30.24"\ W$	August 12th, 2019	7.5	4.9	19.1	15.43 μmol photons $m^{-2}s^{-1}$
East Deep (ED)	$44°00'00.60"\ N$, $69°32'24.86"\ W$	July 22nd, 2019	6.9	4.2	20.3	43.87 μmol photons $m^{-2}s^{-1}$
East Shallow (ES)	$43°59'59.04"\ N$, $69°32'18.06"\ W$	July 11th, 2019	4.7	2.0	19.0	70.22 μmol photons $m^{-2}s^{-1}$

The study took place between 13 June and 12 August 2019 in the upper part of the DRE across from Perkins Point (44°0.05 N, 69°32.881 W) spanning an oyster aquaculture site. Five sampling locations were chosen along a cross sectional transect east of Perkins Point (Fig. 2.1, 2.2 and Table 2.1) to investigate the impact of benthic diatoms on sediment oxygen dynamics. The water depth of the transect ranged from less than 1 m closest to the shoreline to 8 m in the center of the estuary. On the west side of the estuary, site West Shallow (WS) had a water depth of 3.3 m at high tide and was located along the western edge of Mook Sea Farm's oyster aquaculture lease. Site West Deep (WD) was located on the opposite side of the lease at 6.9 m depth. In the middle of the estuary channel, site Middle Channel (MC) was 7.5 m deep at high tide. The sites East Deep (ED, 6.9 m depth) and East Shallow (ES, 4.7 m depth) are located downstream of a small oyster aquaculture lease. The University of Maine's Sustainable Ecological Aquaculture Network's (SEANET) Land/Ocean Biogeochemical Observatory (LOBO; Seabird

Scientific) buoy is located within the study site and provides real time oceanography measurements (e.g., T, S, PAR) at hourly resolution during the period of the study. Benthic microalgal mats, dominated by vertically migrating pennate diatoms, e.g., *Gyrosigma* occur at the study site.

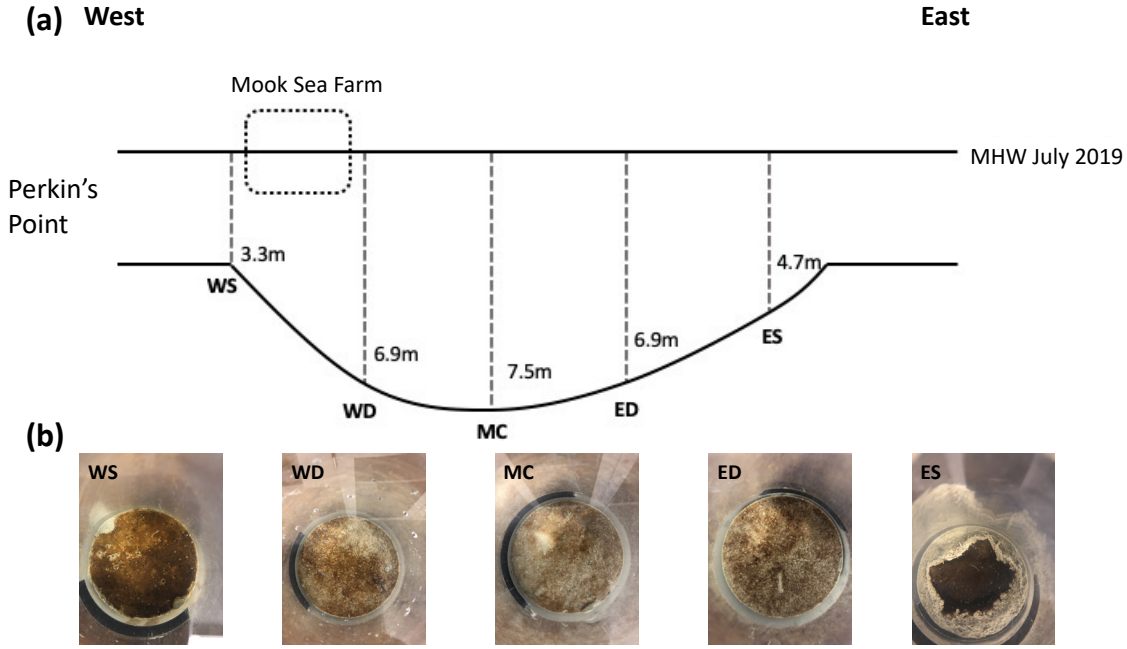

Figure 2.2: (a) Depth profile of transect from west to east in the DRE with mean high tide water levels for the month of July 2019. (b) Top views of a sediment core from each site after the TOE experiment was complete. Therefore, each core was exposed to high light for 1 hour and has full diatom coverage on top of the sediment.

Sediment cores from each site were collected by scuba divers on the dates indicated in Table 1. At each site 6 long (30 cm) and 2 short (15 cm) sediment cores were collected. Light at the sediment surface was recorded using a PME miniPAR sensor at each location during the sampling process (Table 2.1). All cores were transported back to the laboratory in a dark insulated box with ice and placed in an environmental chamber. Once in the environmental chamber, the long cores were placed in a large tank with UV filtered water from the DRE at *in situ* bottom water temperature on the sampling day. The 2 short cores were placed in a smaller tank for microsensor profiling. A light:dark cycle

was set to mimic the *in situ* diel cycle of irradiance at the sediment-water interface on the sampling day. Four Aqua Illumination Hydra 64 HD, LED aquarium lights with a yellow-green filter provided preincubation *in situ* incident irradiance ranging from 5 to 100 µmol photons m^{-2} s^{-1} on the surface of the cores depending on what time of day the core were sampled at. The tanks were aerated continuously to maintain natural air saturation within the tank. The cores were preincubated overnight in the dark to allow for any disturbances from the sampling process to be minimized. The following morning whole core flux incubation experiments were carried out to determine the relationship between irradiance and total oxygen exchange (TOE) across the sediment-water interface, while microsensor profiling on the short cores was used to determine diffusive oxygen exchange (DOE) and vertical oxygen distribution. The following morning after each sediment core sampling event the TOE and DOE experiments began with the lights remaining off from the night before.

During each whole core flux experiment a miniPAR sensor was placed in the TOE flux tank in core position 1(b) (Fig. 2.3b). After all the experiments were completed the light levels in the tank were tested because of variation in the higher light measured during the experiments in core 1(b). The light level in the tanks were tested by setting the tank up the same way as the TOE experiments and repeating the light cycle in the same way (Tables 2.2 and 2.3) only with a miniPAR sensor rather than sediment placed in the core tubes in positions 1-3 (Fig. 2.3b). The light test concluded that there was significant shadowing in the highest light level for all experiments. The was determined based on a comparison of position 1(b) and positions 1-3. The shadowing occurred during the experiments because the miniPAR sensor was in position 1(b) which was next to position

1 but not directly under the light source therefore shadowed in the last light level because in order to achieve the highest light the light source was moved downward closer to position 1. Each position in the tank 1-4 had its own light directly above the sediment core position. The final light level was adjusted based on a correction factor determined, by a linear regression between the positions 1-3 test PAR measurements and 1(b) experimental PAR measurements. The 1(b) PAR measurements for the highest light level from each experiment was multiplied by the correction factor of 1.70 to get the new calculated highest light level.

Table 2.2: Light levels for the TOE flux incubation experiments with light intensity and distances to the corresponding light. The distances of the sediment level to the light for each different light level in cm as well as the light to the water with a 5.08 cm filter housing on the light and 22 cm of water to the sediment level in the tank.

Light Level	Light for each TOE experiment by site ($\mu mol\ photons\ m^{-2}s^{-1}$)					Light distance from Sediment (*cm*) 1	Light distance from water (*cm*) 2	Light color Intensity		
	West Shallow (07/31/19)	West Deep (06/25/19)	Middle of Channel (08/13/19)	East Deep (07/23/19)	East Shallow (07/12/19)			Green%	Blue%	White%
1	0 ± 0.07	0 ± 0.08	0 ± 0.03	0 ± 0.08	0 ± 0.06	91.44	69.85	0	0	0
2	13.31 ± 0.22	11.88 ± 3.37	23.56 ± 0.53	13.32 ± 0.34	13.92 ± 2.05	91.44	69.85	90	80	0
3	13.24 ± 0.99	21.77 ± 2.51	47.49 ± 1.62	28.27 ± 0.62	28.84 ± 1.18	91.44	69.85	209	116	30
4	52.62 ± 1.07	40.98 ± 1.50	88.40 ± 1.10	56.39 ± 1.01	55.84 ± 0.81	91.44	69.85	209	116	137
5	111.91 ± 5.71	72.75 ± 4.93	112.54 ± 2.85	105.67 ± 4.61	69.01 ± 4.55	66.04	44.45	209	116	137
6	150.22 ± 4.27	92.49 ± 2.08	155.49 ± 4.68	116.18 ± 2.59	92.61 ± 0.69	55.88	34.29	209	116	137
7	150.63 ± 2.49	105.84 ± 3.61	224.65 ± 10.39	131.31 ± 0.87	111.70 ± 3.98	48.26	26.67	209	116	137
8	317.85 ± 3.55	213.54 ± 6.33	428.82 ± 4.23	254.49 ± 1.35	179.24 ± 2.60	35.56	13.97	209	116	137

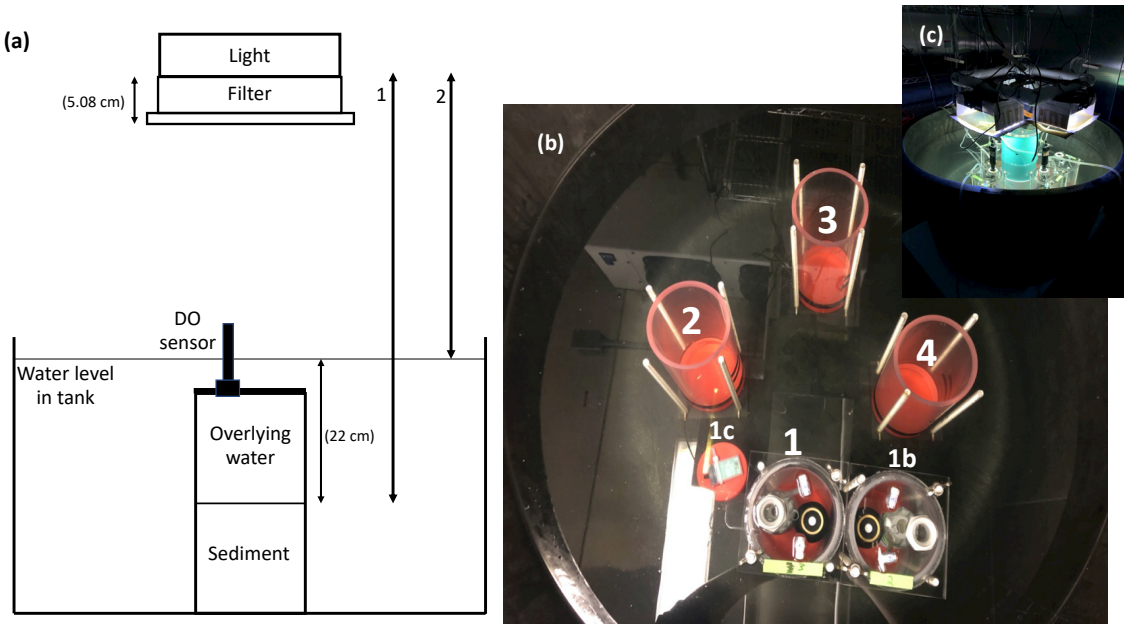

Figure 2.3: (a) TOE flux tank set up diagram for distances that were set during each experiment as a supplement to table 1.1 with the filter housing and sediment to water level. Distance 1 is the light to the sediment surface and distance 2 is water surface in the tank to the light. (b) Overview of TOE flux tank for light test based on the experimental set up with cores 1-3 being the sediment core positions, core 4 the blank and 1(b) being the position of the miniPAR sensor during the experiments. (c) Image of TOE tank set up for WD site on June 25th, 2019.

Light color Intensity			Light distance from sediment (*cm*)	Light distance from water (*cm*)	Average Light for DOE Core for all experiments ($\mu mol\ photons\ m^{-2}s^{-1}$)
Green%	Blue%	White%			
0	0	0	68.58	63.50	0 ± 0.09
50	40	0	68.58	63.50	14.24 ± 3.94
90	80	0	68.58	63.50	22.70 ± 6.25
209	116	30	68.58	63.50	39.80 ± 10.23
209	116	100	68.58	63.50	60.66 ± 14.55
209	116	137	63.50	58.42	81.29 ± 14.26
209	116	137	48.26	43.18	154.97 ± 15.37
209	116	137	38.10	34.29	221.19 ± 20.08

Table 2.3: *Light levels for the DOE microprofiling experiments with light intensity and distances to the corresponding light. The distances of the sediment level to the light for each different light level in cm. The light to the water with a 5.08 cm filter housing on the light and 22 cm of water to the sediment level in the tank.*

2.2 Total Core Incubation for Total Oxygen Exchange

To determine the photosynthetic vs irradiance relationship for the benthic diatom community the total amount of oxygen being produced or consumed as a function of light must be determined. To do this, TOE was measured using whole-core flux incubations at 8 different irradiance levels for the long cores collected at each study site. The irradiance was changed by first adjusting the intensity of the light and then regulating the distance of the light source relative to the surface of the lid on top of the sediment core (Fig. 2.3), similar to the procedure of Glud et al., 2002. Each irradiance interval lasted for 1 hour and the entire overlying water contents of each core was flushed to reset the O_2 concentration before each well-defined irradiance level.

The incubation was initiated by the capping of the core and the start of the stirring. A fourth core was added to the tank with filtered UV water from the DRE as a blank. Each core was capped with a clear plastic lib avoiding any bubbles and screwed on to ensure the contents of the core stays within. A Hach LDO oxygen sensor was placed in the top of the lid alongside the magnetic stir bar to ensure a well-mixed overlying water phase above the sediment surface. In the lid there were in and out water ports connected to a UV filtered DRE water reservoir so the overlying water contents could be exchanged between each irradiance level of the experiment. The first hour of the incubation the cores remained in the dark while dissolved oxygen was measured every 5 minutes throughout the hour in the overlying water. After the first hour the light was turned on and adjusted to 11 μmol photons m^{-2} s^{-1} and the overlying water contents of each core was flushed. This sequence continued for 6 more levels ranging from 22 to 428 μmol photons m^{-2} s^{-1}, the

exact light intensities are listed in Table 2.2. Total oxygen exchange rates (TOE) for each core in mmol O_2 m^{-2} d^{-1} were calculated from the change in overlaying water oxygen concentrations Eq. (2.1) measured every 5 minutes during each flux incubation.

$$TOE\ Flux = \frac{\Delta(O_{2(core)} - O_{2(blank)})}{\Delta t} * H \quad (2.1)$$

Where $O_{2(blank)}$ is the oxygen measured in the blank core with just UV filtered sea water, $O_{2(core)}$ the oxygen measured in the overlying water for the sediment core, Δt is the change in time, and H is the height of the overlying water column. To ensure activity in the water column wasn't contributing to the change in oxygen, the oxygen concentration of the blank core filled with just UV filtered sea water was subtracted out. A PE (Photosynthetic rate vs irradiance) relationship Eq. (2.2) (Platt & Gallegos 1980) was fit to the total oxygen exchange rate with light curves for each site according to,

$$P = P_{max}\left(1 - e^{\frac{-\alpha E}{Pmax}}\right) - R \quad (2.2)$$

where P_{max} represents the maximum photosynthetic capacity in mmol O_2 m^{-2} d^{-1} and α is the initial slope of the PE curve representing the photosynthetic efficiency in mmol O_2 m^{-2} d^{-1} (µmol photons m^{-2} s^{-1})$^{-1}$. R is the O_2 consumption rate in the sediment in mmol O_2 m^{-2} d^{-1} and E is the downwelling irradiance in µmol photons m^{-2} s^{-1}. Each photosynthetic parameter P_{max}, α, R was determined from individual fits of the three-replication sediment core TOE rates with light from each site.

2.3 Oxygen Microprofiles for Diffusive Oxygen Exchange

Oxygen profiles were determined in the short (15 cm) cores using a Clark Type microelectrode (Unisense OX-100) attached to a motor driven micromanipulator. The oxygen electrode has a tip diameter of 100 µm which allows for non-destructive

measurements of oxygen that can take place in less than 0 to 3 seconds. Oxygen was measured at 100 µm depth increments until the oxygen penetration depth was reached, approximately 0.5 to 1 cm. To ensure oxygen profiles were at steady state each core remained under each light level for 45 minutes prior to the initiation of profiling and aeration within the tank remained on throughout the 8 1-hour intervals. For each light level 3 sediment profiles were made where diatom coverage was observed, avoiding any repeat locations. From these profiles the upward oxygen flux was calculated based on the integrated rate of oxygen production or consumption with depth determined based on a series of least square fits to the oxygen concentration profile and then compared based on a statistical F-test for the least number of zones the profile could be broken into based on equivalent oxygen activity (Eq 2.3). The downward flux is towards the heterotrophic or chemolithotroph communities which lie in the deeper sediment layers (Glud et al. 1992, 2002b, Kühl et al. 1996). To quantify a rate of diffusive oxygen exchange (DOE) from the microprofiles the approach of Berg et al. (1998) was used. This approach determines the least number of zones of production and consumption rates needed to balance the reaction and diffusive exchange Eq. (2.3).

$$-\varphi D o_2 \frac{\partial^2 o_2}{\partial z^2} = P - R \tag{2.3}$$

Where D_{O_2} is the diffusivity of O_2, φ is the porosity of the sediment, O_2 is the concentration of oxygen and z is the corresponding depth of the O_2 concentration. This is then balanced by the integrated production (P) and consumption (R) rate.

2.4 Microphytobenthos Biomass

Following the TOE incubation experiments cores were sectioned for diatom cell counts. The top of each core was photographed before sectioning to compare diatom

coverage after full light exposure (Fig. 2.2b). Then the distinct benthic diatom mat that had formed on top of the sediment was carefully removed for diatom counts. The next 1cm of sediment underneath the diatom mat was sectioned and divided into quarters and 1 quarter was removed for diatom counts. The diatom mat and underneath layer were mixed with NaCl water (10 mL for Mat and 20 mL for 1cm below) to make uniformly mixed slurry and weighted both before and after NaCl was added. Two 0.5 mL aliquots were collected from each slurry and one was frozen at -80℃ to measure chlorophyll a while the other was further diluted with NaCl (8.5 mL) and preserved in formalin (6 mL). 15 μL of formalin preserved cells were pipetted onto a microscope slide with cover slip. Diatoms were counted at 400X magnification along three transects across the cover slip and expressed using Eq. (2.4):

$$C_{slurry} = O * \left(\frac{Cells}{V}\right) * D * 1000 \tag{2.4}$$

Where C_{slurry} is the number of diatoms mL^{-1} of original slurry, (O) is a multiplication factor of one transect to the area of the cover slip (88, taking into account a 10mm x 10mm counting grid on the underside of a 10X ocular, with 40X objective, and 22mm x 22mm cover slip) (*Cells*) is the average number of diatoms in a transect, (*V*) is 15 μL under the cover slip, and (*D*) is a dilution factor of 30 accounting for the formalin mixture. The number of diatoms per area of the core was calculated using Eq. (2.5):

$$\frac{Cells}{m^2} = \frac{\left(\frac{V_1 * C_{slurry}}{V_2}\right) * V_{sample}}{A} \tag{2.5}$$

Where (V_1) is the volume of original slurry and (V_2) is the volume of original mat or 1cm underneath layer that went into the slurry, V_{sample} is the total volume of the mat or 1cm underneath layer in the sediment core, and (*A*) is the area of the sediment core.

The chlorophyll a content in the sediment was measured from both the mat and 1 cm below samples. This was done by using the second 0.5 mL aliquots taken from the first samples that were frozen at -80℃. The analysis was done on a Turner Designs model Trilogy fluorometer based on the Parsons, Maita, & Lalli, 1984 method and used 2.5 mL extracts to determine μg mL^{-1} of Chl a for each sample which was calculated as described in the JGOFS protocols (Knap, A., A. Michaels, A. Close & (eds.) 1996). From μg ml^{-1} of Chl a the per core area concentration was calculated using Eq. (2.6) with the original volume of the sample (V_{sample}) from the core with the concentration of Chl a (C_{chla}) and (A) is the area of the sediment core and converted to mg.

$$\frac{mg\ of\ Chl\ a}{m^2} = \left(\frac{C_{chla} * V_{Sample}}{A}\right) * 0.001 \tag{2.6}$$

2.5 *In situ* Light Measurements

To determine the incidence downwelling irradiance (PAR) at each site across the transect light profiles were taken at several times during the tidal cycle on July 18th, August 9th and 12th 2019. Profiles were recorded using a PME miniPAR logger mounted to a tripod which was lowered into the water column and measurements were recorded every meter. The light attenuation coefficient k, was determined from these light profiles using an exponential fit to Eq. (2.7).

$$E_z = E_o e^{-kz} \tag{2.7}$$

where k is the light attenuation coefficient for the water column and z is the water column depth. E_o is the irradiance at the surface of the water and E_z is the downwelling irradiance at a given depth. Light profiles were taken as close as possible to noon depending on the tide with minimal cloud coverage. Both average low and high tide attenuation coefficient

were determined from the light profiles due to changes in turbidity corresponding to the tides, and the coefficient for every hour in between was calculated using Eq. (2.8).

$$k_{(t)} = \frac{k_{high} - k_{low}}{2} \cos\left(\frac{2\pi(t - offset)}{period}\right) + \frac{k_{low} + k_{high}}{2} \quad (2.8)$$

Where t is time, *offset* is the amount of time high tide is away from midnight and *period* is the length of the tidal cycle. k is the attenuation coefficient determined for high and low tide. The *period* and *offset* where determined using the NOAA tide and current buoy (Walpole, Damariscotta River, ME, 43°56.0 N, 69°34.8 W) located near the study site.

2.6 Benthic Net Primary Production Estimates

A timeseries of benthic net community production (NCP) based on the TOE experiments was estimated for each site along the transect for the summer of 2019 between 16 June to 31 August 2019. This was calculated using Eq. (2.2) with P_{max}, α, and R determined from the TOE incubation experiments. The bottom irradiance E_D was estimated hourly by Eq. (2.7) where E_o was the surface PAR recorded at the University of Maine's Lobo buoy, z was the water column depth and the light attenuation coefficient k, calculated from Eq. (2.8) and measured water column light profiles.

CHAPTER 3

RESULTS

3.1 Total Oxygen Exchange

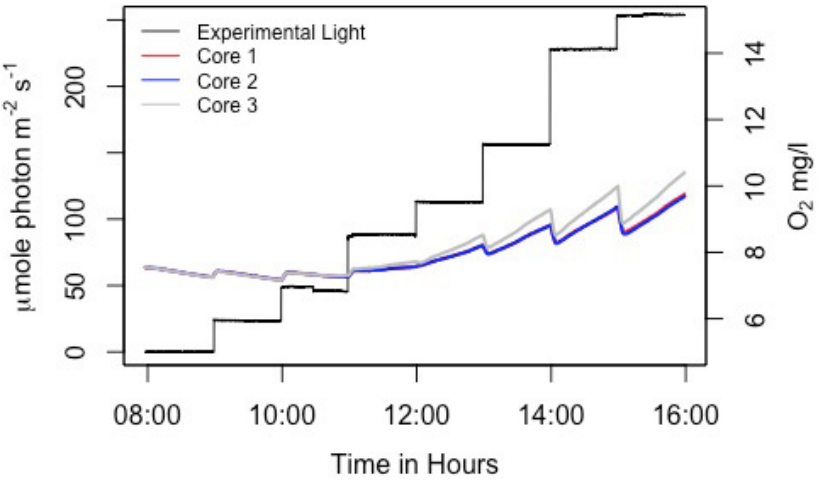

Figure 3.1: Middle of Channel Site (August 13th, 2019) TOE raw oxygen concentrations in mg L^{-1} for all 8 different intervals of light with three replication sediment cores (grey, red and blue lines). In black the corresponding light levels from the experiment in a core next to replication sediment core 1.

The total O_2 exchange (TOE) across the sediment-water interface measured in the whole core incubations represents the combined activity of O_2 production by the benthic diatom community and consumption due to respiration of both diatoms and the heterotrophic organisms present in the sediment. During each experiment O_2 decreased in the overlying water during the dark incubation (08:00 to 09:00 in Fig. 3.1), reflecting the O_2 demand of the heterotrophic community. O_2 also decreased at the next two lowest light levels (refer to Table 2.1, level 2) and didn't begin to increase until the third light levels (refer to Table 2.1, level 3). Plots of the O_2 concentration, along with the light

reaching the sediment-water interface during each flux incubation experiment are shown in Appendix A for each site and Fig. 3.1 for site MC. Relationships between irradiance and TOE for each site are shown in Fig. 3.2 and the red line in these figures represents the least squared fit of Eq. (2.2) used to determine values of P_{max}, α, and R for each site (Table 3.1). At low light levels TOE increased linearly with increasing irradiance, α ranged from a low of 1.4 ± 0.2 mmol O_2 m^{-2} d^{-1} (μmol photons m^{-2} s^{-1})$^{-1}$ in the middle of the channel (MC) to a high of 4.8 ± 0.5 mmol O_2 m^{-2} d^{-1} (μmol photons m^{-2} s^{-1})$^{-1}$ at site ES. At around 100-200 μmol photons m^{-2} s^{-1} TOE began to plateau indicating that P_{max} was reached. P_{max} ranged from 286.5 ± 37.8 mmol O_2 m^{-2} d^{-1} at MC to 570.5 ± 41.0 mmol O_2 m^{-2} d^{-1} at WS. The sediment respiration, R, was lowest in the middle of the channel (MD) (33.5 ± 1.6 mmol O_2 m^{-2} d^{-1}) and highest along the edges of the channel; 81.9 ± 6.2 mmol O_2 m^{-2} d^{-1} at WS and 82.8 ± 14.7 mmol O_2 m^{-2} d^{-1} at ES. The compensation irradiance, defined as the light level when the depth-integrated O_2 production by photosynthesis is balanced by the depth-integrated heterotrophic respiration, i.e., TOE flux became zero, was between 11 and 20 μmol photons m^{-2} s^{-1} for all the sites except MC which was 24 μmol photons m^{-2} s^{-1}.

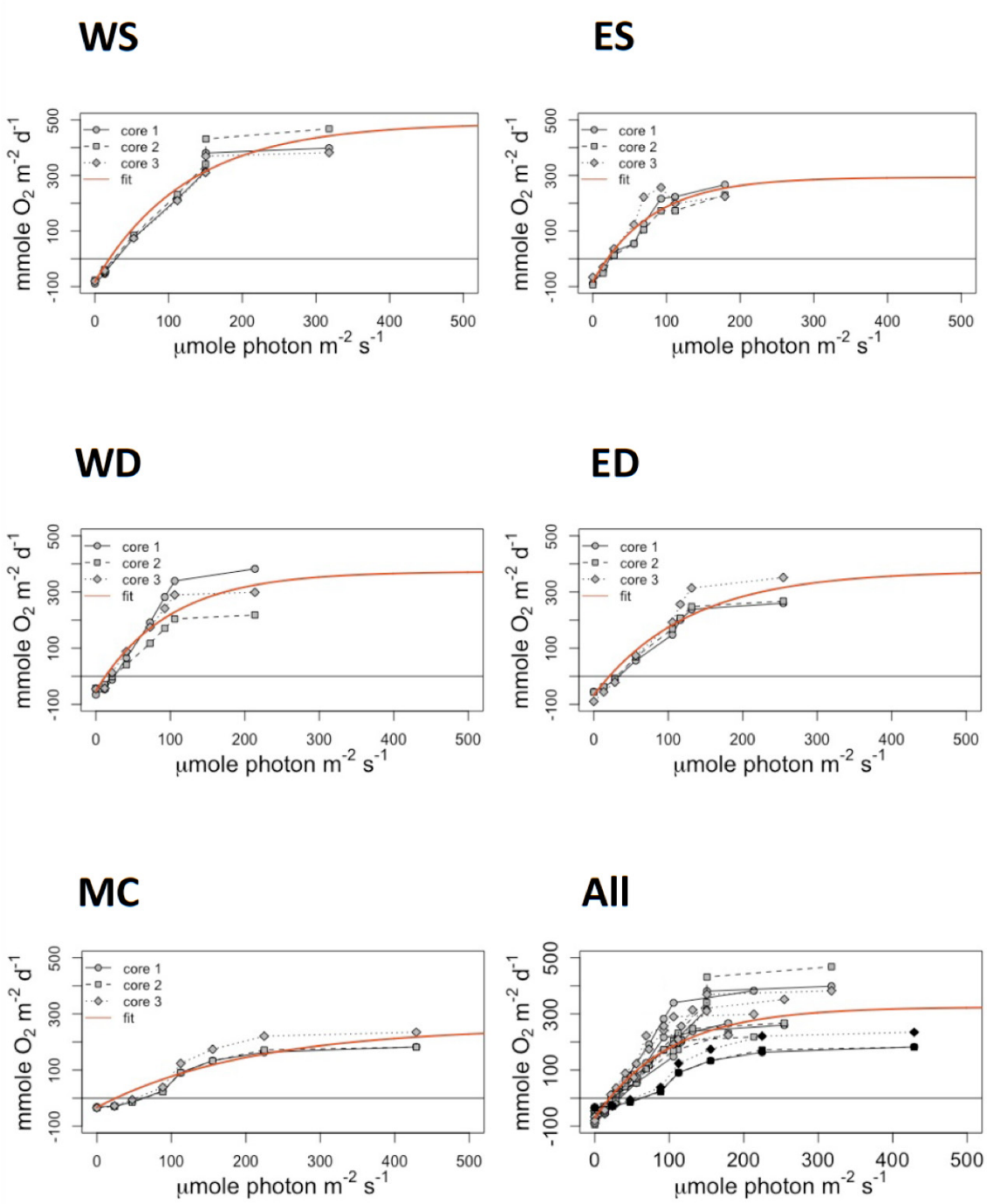

Figure 3.2: PE response curves for each site based on TOE. Three replicate sediment cores incubated under well-defined light for each site along the transect. The red lines represent the least squares fit of Eq (2.2). Site West Shallow (WS), Site East Shallow (ES), site West Deep (WD), site East Deep (ED) and Middle of Channel (MC) all located in the upper part of the DRE across from Perkin's Point. All sites grouped together with the MC site in black and the rest in grey, the red line in all represents the best fit for WS, WD, ES, and ED combined.

An ANOVA was used to compare the fitted values of P_{max}, α and R between sites. The results were statistically significant for each parameter (P_{max} p=0.0159, α p=0.0029, R p=0.0031), indicating difference between sites. However, removing the deepest site, MC and repeating the ANOVA for the four remaining sites resulted in no significant differences (P_{max} p=0.143, α p=0.374, R p=0.0753). Therefore, these four sites were considered not statistically different for the photosynthetic parameters. The average parameter values across the four sites (WS, WD, ES, ED) are shown at the bottom of Table 3.1.

Table 3.1: All parameters determined to make NCP estimates for the TOE and DOE methods. P_{max} ($mmol\ O_2\ m^{-2}d^{-1}$) is the maximum photosynthetic capacity, α ($mmol\ O_2\ m^{-2}\ d^{-1}\ (\mu mol\ photons\ m^{-2}\ s^{-1})^{-1}$) is the photosynthetic efficiency and R ($mmol\ O_2\ m^{-2}d^{-1}$) is the dark respiration. Values in bold are statistically different parameters determined from an ANOVA test run on both methods individually.

Site Name	Total Oxygen Exchange (TOE)				Diffusive Oxygen Exchange (DOE)			
	P_{max}	α (Growth Curve)	α (Linear Fit)	R	P_{max}	α (Growth Curve)	α (Linear Fit)	R
West Shallow (WS)	570.5 ± 41.0	4.5 ± 0.4	2.7 ± 0.1	81.9 ± 6.2	n/a	**1.8 ± 0.1**	**1.8 ± 0.1**	40.6 ± 2.0
West Deep (WD)	424.7 ± 57.9	4.3 ± 0.6	3.2 ± 0.2	51.3 ± 12.4	n/a	1.2 ± 0.1	1.3 ± 0.1	49.6 ± 4.9
Middle of Channel (MC)	**286.5 ± 37.8**	**1.4 ± 0.2**	1.2 ± 0.1	**33.5 ± 1.6**	302.6 ± 93.5	1.4 ± 0.2	0.9 ± 0.1	30.1 ± 14.0
East Deep (ED)	442.5 ± 48.4	3.5 ± 0.4	2.5 ± 0.1	67.1 ± 19.5	n/a	1.2 ± 0.2	1.1 ± 0.1	44.6 ± 11.2
East Shallow (ES)	376.4± 37.7	4.8 ± 0.5	3.2 ± 0.2	82.8 ± 14.7	n/a	**2.7 ± 0.3**	**2.2 ± 0.1**	**72.3 ± 0.9**
Average (Not Including MC)	395.4 ± 24.1	3.9 ± 0.3	2.7 ± 0.1	70.8 ± 14.9				

3.2 Diffusive Oxygen Exchange

O_2 microsensor profiling was conducted in the short (15 cm) cores alongside the TOE incubation experiment and at similar light levels. Three replication profiles were made at each light level resulting in 24 profiles per experiment and 124 profiles total. An

example series of profiles collected during the microsensor experiment for site WD is shown in Fig. 3.3 and the remaining profiles from all sites are shown in Appendix B. The O_2 concentrations within the sediment increased extending deeper as the light increased with each interval for each site in the transect.

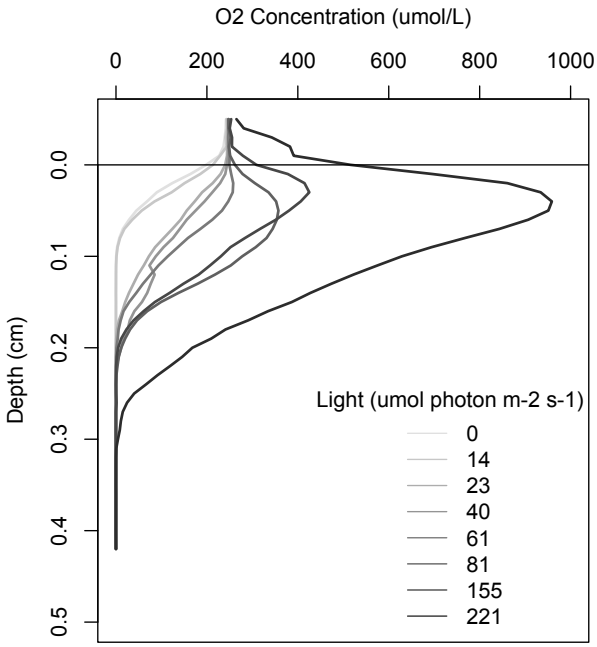

Figure 3.3: Example O_2 sediment profiles from West Deep (WD) site. Three replication profiles averaged from each light level exposed to the sediment core for 1 hour.

The O_2 concentration within the diatom-covered sediment at each site along the transect increased to more than twice that of O_2 in the overlaying water (250 O_2 µmol L^{-1}) at the highest irradiance level of 221 µmol photons m^{-2} s^{-1}. This resulted in maximum subsurface oxygen (MSO) concentrations between 600 to 1000 O_2 µmol L^{-1} within the first 0.1 cm of the sediment. Site MC had the lowest MSO concentration (613.3 ± 87.4 O_2 µmol L^{-1}) and the shallow sites had the highest (1085 ± 52.8 O_2 µmol L^{-1}). In the dark incubation the oxygen penetration depth (OPD) was between 0.05 to 0.1 cm depth and increased with increasing irradiance to between 0.2 to 0.35 cm depth at the highest irradiance levels. The shallow sites had the deepest OPD at the highest irradiance (0.32 ±

0.02 cm), while the deepest site in the middle of the channel (MC) had the lowest (0.25 ± 0.01 cm). All of the sites had higher compensation irradiance for DOE than TOE somewhere between 22 and 41 µmol photons m^{-2} s^{-1} except for site MC which was lower at 21 µmol photons m^{-2} s^{-1} compared to 24 µmol photons m^{-2} s^{-1} for TOE.

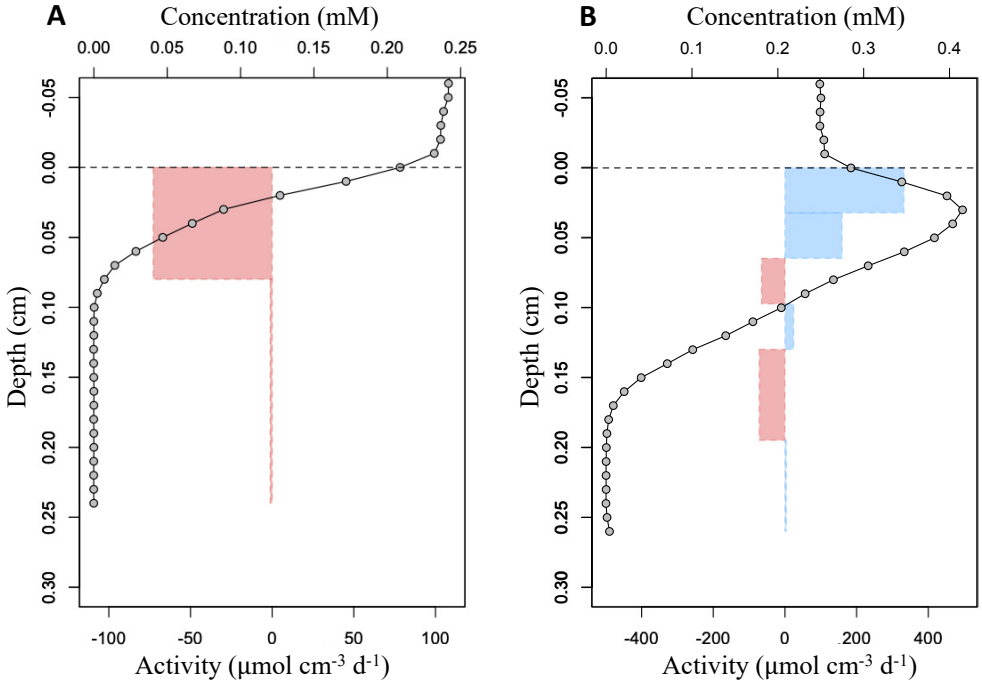

Figure 3.4: Example O_2 sediment profiles from West Deep (WD) site with the Berg et al., 1998 method of determining the flux of O_2 from the sediment at light levels of (A) dark (0 µmol photons m^{-2} s^{-1}) *and (B) 155* µmol photons m^{-2} s^{-1}. *Consumption rates are in red and production rates are in blue with the sediment (diatom mat) surface at zero marked by a dashed line.*

The oxygen activity rates, both production and consumption, were estimated from the microprofiles using the approach of Berg et al., 1998 (Fig. 3.4). The three replication profiles of O_2 concentration with depth fitted with the rates for each light level from the experiments are shown in Appendix B. Fig. 3.4 shows the results of this for both dark (Fig. 3.4A) and light (Fig. 3.4B) incubation from site WD, with production shown in blue and consumption in red. During the dark incubation oxygen consumption at the rate of 72 µmol O_2 cm^{-3} d^{-1} begins immediately below the sediment water interface and oxygen is

depleted by 0.1 cm depth. In the light incubation (155 μmol photons m^{-2} s^{-1}) an actively photosynthesising population of diatoms is indicated by an oxygen production zone occupying the top 0.08 cm of sediment. The production rate is 332 μmol O_2 cm^{-3} d^{-1} immediately below the sediment water interface, then drops to 159 μmol O_2 cm^{-3} d^{-1} by 0.04 cm depth until below this zone oxygen is consumed at a rate similar to the dark incubation.

The diffusive oxygen exchange (DOE) was determined for each profile from each site by the integrated production and consumption rates determined above and used to construct a DOE-based PE relationship for each site. Relationships between irradiance and DOE for each site are shown in Fig. 3.5 and the red line in these figures represents a linear regression of the data points to determine α, except for site MC, which was fit using Eq. (2.2) since only at this site was P_{max} reached. The red line in Fig. 3.5C therefore represents the least squared fit of Eq. (2.2) used to determine values of P_{max}, α, and R for site MC (Table 3.1) rather than a linear fit, as is the case for the other sites. For all cores at lowest light levels, DOE increased linearly, with α ranging from a low of 0.9 ± 0.1 mmol O_2 m^{-2} d^{-1} (μmol photons m^{-2} s^{-1})$^{-1}$ in the middle of the channel (MC) to a high of 2.2 ± 0.2 mmol O_2 m^{-2} d^{-1} (μmol photons m^{-2} s^{-1})$^{-1}$ at site ES. For site MC at 200 μmol photons m^{-2} s^{-1} DOE began to plateau giving a P_{max} of 302.6 ± 93.5 mmol O_2 m^{-2} d^{-1}. P_{max} was not reached at the other sites. The sediment respiration, R, was lowest in the middle of the channel (MC) at 30.1 ± 14.1 mmol O_2 m^{-2} d^{-1} and highest along the eastern edge of the channel; 72.3 ± 0.9 mmol O_2 m^{-2} d^{-1} at ES. The shallow sites had a greater flux of O_2 to the overlying water because there is a larger MSO concentration in the sediment at the higher light levels.

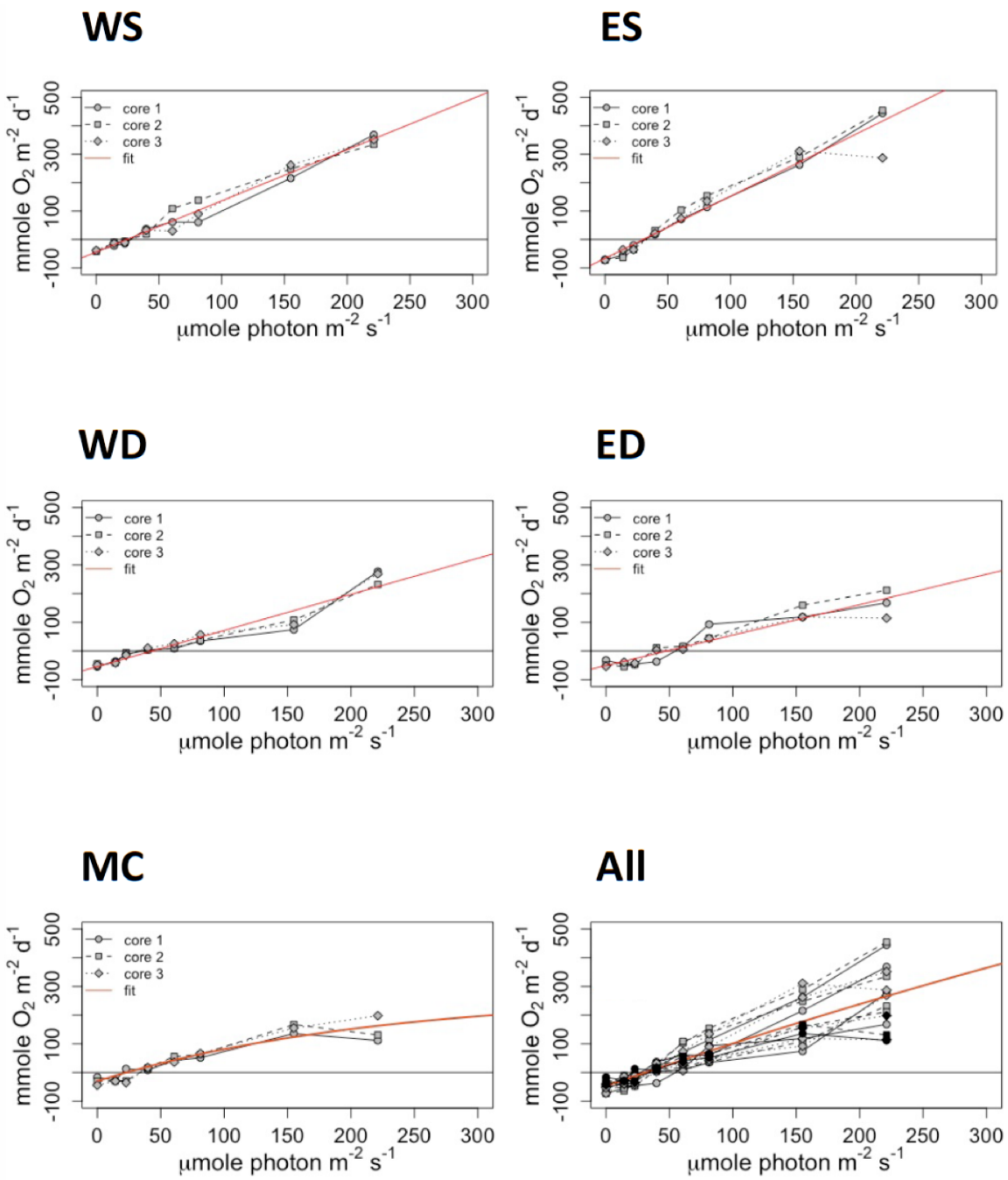

Figure 3.5: PE response curves based upon the DOE measured from microsensors. Three replication O_2 microprofiles were taken under well-defined irradiance (0, 14, 23, 40, 60, 81, 155, 221 µmol photons m^{-2} s^{-1}) levels for each site on the transect. Site West Shallow (WS), site East Shallow (ES), site West Deep (WD), site East Deep (ED) and Middle of Channel (MC) all located in the upper part of the DRE across from Perkin's Point. All is each individual core from each site together with the MC site in black and the rest in grey.

An ANOVA test was used to compare the α and R parameters across sites. For α this indicated there were statistical differences across sites (p=0.0010). Grouping the sites by depth indicated that the deep sites and the middle of the channel were not statistically different (p=0.292) and likewise both shallow sites were not statistically different to each other (p=0.099). For the parameter R there were also differences across sites (p=0.0013), but these differences disappeared if site ES was removed from the ANOVA (p=0.149). An ANOVA was also used to compare the value of alpha determined from the DOE and TOE experiments. When comparing methods, the transect was statistically different (p=0.0159) except for when WD was removed (p=0.0755).

3.3 Microphytobenthos Cell Distribution

Microphytobenthic cell concentration at each site both in the diatom mat, and at 1 cm depth were determined. The site with the greatest number of cells present in the diatom mat was the WS site with 75.53 ± 32.08 10^{10} cells m^{-2} which also had the highest, though not statistically significant, P_{max} (570.5 ± 41.0). The MC site had the least number of cells, 3.65 ± 0.898 10^{10} cells m^{-2}, present in the diatom mat consistent with the PE parameters being statistically lower than the other sites (Table 3.1, Table 3.2). The cell counts from 1 cm below the mat had a greater number of cells in the deeper sites compared to the shallow sites for both the east and west side. The west side of the channel had a larger total number of cells (104.87 ± 17.73 10^{10} cells m^{-2}) in the top 1 cm compared to the east side (61.05 ± 16.16 10^{10} cells m^{-2}) (p=0.0186). The MC site had statistically lower cell counts than the other sites both for the mat (p=0.0274) and 1 cm below (p=0.0238) cell counts.

Table 3.2: Number of cells per core area for each site in the transect with chlorophyll a concentrations per core area for both the diatom mat and 1cm below the mat. Values in bold are statistically different within each measurement comparing sites based on an ANOVA.

Site Name	Number of Cells per area in core (10^{10} cell m^{-2})		Chl a concentration per area in core (mg m^{-2})	
	Mat	1 cm below	Mat	1 cm below
West Shallow (WS)	75.53 ± 32.08	46.22 ± 21.80	6.90 ± 0.96	**4.12 ± 1.06**
West Deep (WD)	52.96 ± 23.67	58.65 ± 33.95	6.74 ± 3.60	14.53 ± 4.57
Middle of Channel (MC)	**3.65 ± 0.898**	**0.138 ± 0.240**	9.10 ± 6.78	**5.00 ± 4.36**
East Deep (ED)	52.34 ± 34.47	40.56 ± 8.35	6.54 ± 3.13	14.29 ± 1.92
East Shallow (ES)	18.90 ± 10.91	20.50 ± 7.86	9.33 ± 3.87	11.30 ± 3.49
Average	40.68 ± 33.63	33.21 ± 26.59	7.73 ± 3.70	9.85 ± 5.44

Based on the chlorophyll a (Chl a) concentration for the area of the cores the sum of the mat and 1 cm below are not statistically different ($p=0.31$). Looking at the individual measurements of Chl a, 1 cm below was statistically different ($p=0.0073$) across the transect. The 1cm below was not statistically different without sites WS and MC ($p=0.751$) The mat concentrations are not statistically different ($p=0.85$). Sites MC 9.10 ± 6.78 mg m^{-2} and ES 9.33 ± 3.87 mg m^{-2} have the highest concentrations and were not statistically different.

3.4 Benthic NCP Estimates for upper DRE

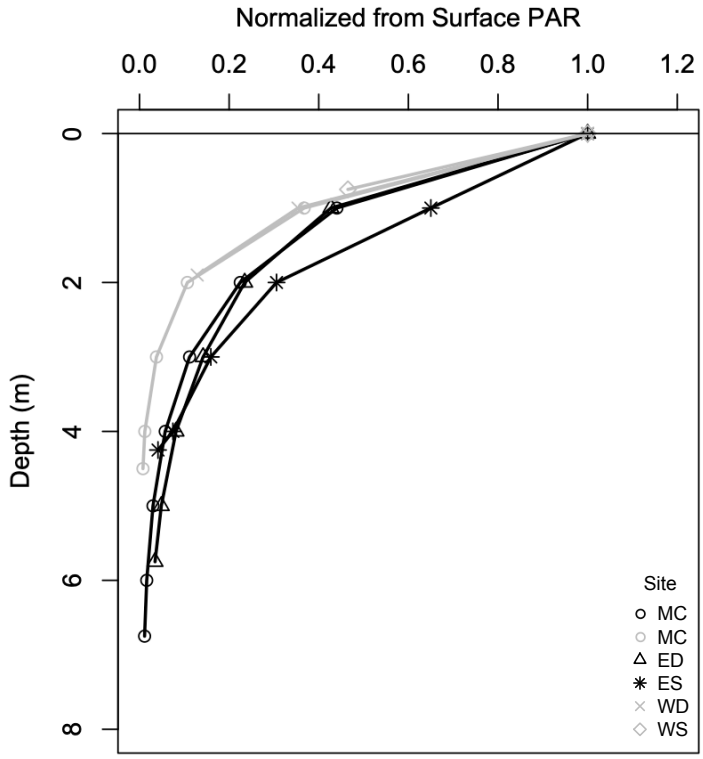

Figure 3.6: Water column light profiles with depth to determine the attenuation coefficient from each site along the transect. Profiles in grey were made at low tide and ones in black done at high tide. Three replication profiles for each site with MC being done at both low and high tide.

The light attenuation coefficient (k) was determined for each site across the transect at both high and low tide using *in situ* water column PAR profiles (Fig. 3.6). There was no horizontal variability in the coefficient across the transect, however there was differences depending on tidal period (Fig. 3.6). The low tide k value (k_{low} = 1.101 ± 0.03) was higher than the high tide k (k_{high} = 0.59 ± 0.05) Using these values and Eq. (2.8) k was estimated throughout the tidal cycle (Fig. 3.7C).

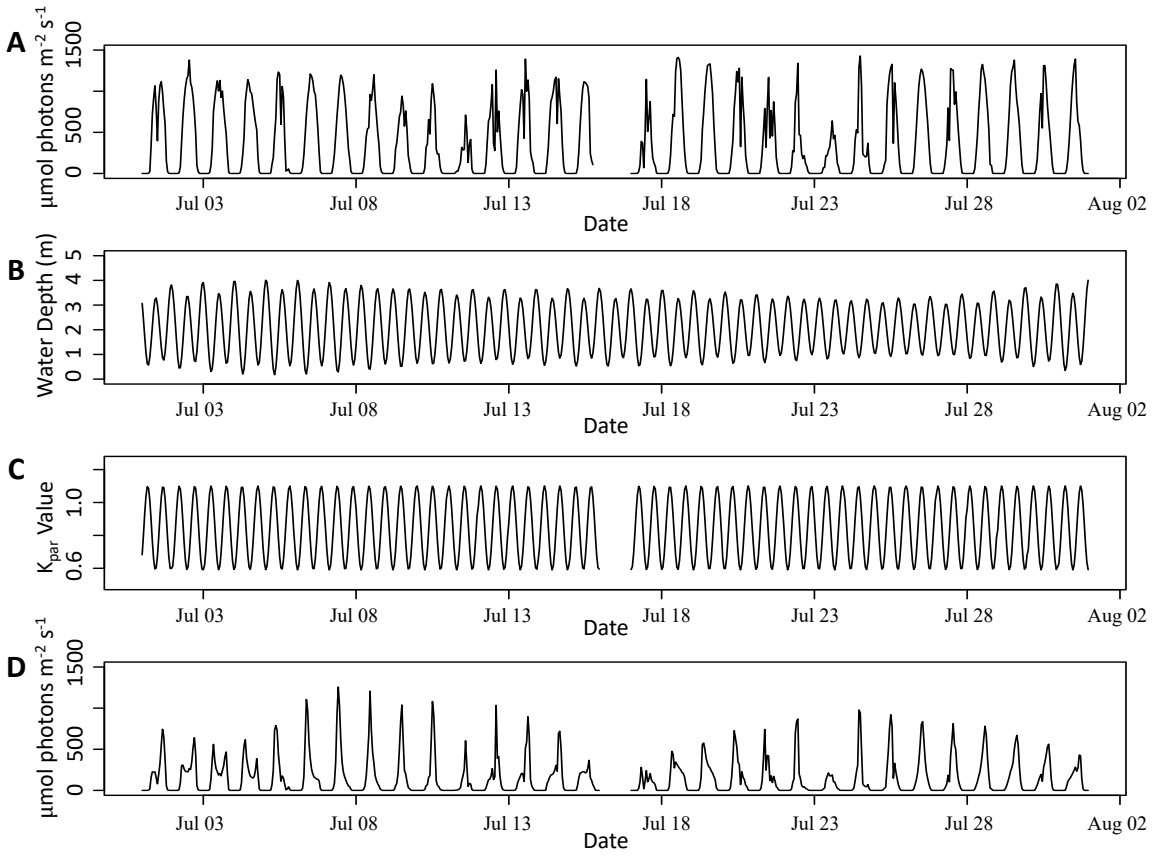

Figure 3.7: In situ daily values from the month of July used to calculate the NCP for site west shallow. (A) is the irradiance at the surface of the water in µmol photons m^{-2} s^{-1}, (B) is the water depth in meters at the specific site and (C) is the attenuation value calculated (k). (D) is the calculated sediment surface downwelling irradiance in µmol photons m^{-2} s^{-1} using plots A-C values with Eq. (2.7). All for site west shallow for the month of July with zero marked in black. July 16th missing for plot (A), (C) and (D) due to Lobo buoy cleaning.

To calculate the net community production (NCP), which is the diatom photosynthetic production minus the respiration of the diatoms and heterotrophic community present in the sediment, a number of *in situ* parameters and coefficients had to be determined. Using the hourly calculated *k* values (Fig. 3.7C) combined with hourly surface irradiance (Fig. 3.7A) from the University of Maine's LOBO buoy and water depth (Fig. 3.7B) the downwelling irradiance (E_D) (Eq. 2.7) at the sediment surface for every hour of the day from July 1st to July 31st in 2019 was calculated (Fig. 3.7D). The downwelling irradiance is dependent on the surface irradiance and the water depth. For

the greatest amount of light to reach the sediment surface at each site high tide water depths have to occur during peak sunlight hours of the day (12:00 PM). Oscillation in tidal amplitude correspond to spring and neap tides, influencing depth and E_D. The spring tide occurred at the beginning of the month when the highest, high tide water depths occur indicated in Fig. 3.7B from July 3rd to 8th affecting Fig. 3.7D.

Based on the ANOVA analysis of the TOE parameters it was decided to use averages across the transect for every site except site MC. Table 3.1 was used to calculate the NCP estimates for the benthic community as a whole for each site (Fig. 3.8). The hourly NCP rates were calculated using Eq. 2.2 with the calculated hourly bottom irradiance for each site and parameters fitted from the TOE method (Table 3.1). The shallow sites at the edge of the transect have a higher production rate and can be net autotrophic during peak sunlight times of day during the month of July (Fig. 3.8A and E). The two deep locations are rarely net autotrophic (Fig. 3.8B and D), and the MC site never was (Fig. 3.8C). Site WS (Fig. 3.8E) is the most constant net autotrophic site as it experiences net production every day for the month of July constantly reaching a maximum NCP rate of 300 mmol O_2 m^{-2} h^{-1}. Site ES (Fig. 3.8A) is net autotrophic each day but has a varying degree of NCP ranging from 100 to 300 mmol O_2 m^{-2} h^{-1}. The Deep sites (Fig. 3.8B and D) for both sides of the transect have almost identical NCP rates and follow a trend of only being net autotrophic during spring tide, high tides at peak sunlight times of the day reaching a maximum NCP rate of 45 mmol O_2 m^{-2} h^{-1}. The MC site (Fig. 3.8C) is always net heterotrophic but production does increase during peak sunlight times of the day but does not exceed consumption rates. The maximum NCP rate for site MC was -1.5 mmol O_2 m^{-2} h^{-1} on July 18th.

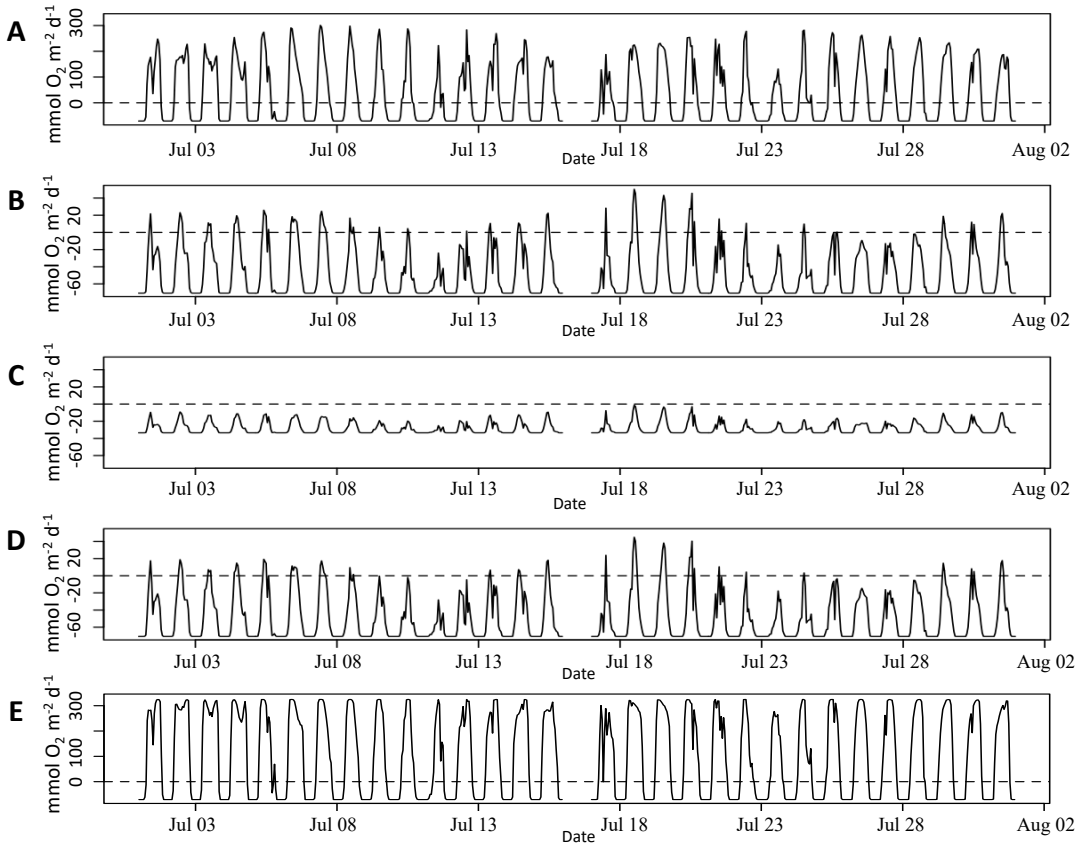

Figure 3.8: Calculated NCP in mmol O_2 m^{-2} d^{-1} for each site for the month of July with zero marked with a dashed line to indicate net autotrophic or heterotrophic. (A) is the estimate for site ES, (B) is site ED, (C) is site MC, (D) is site WD and (E) is site WS for the entire month of July 2019, July 16th missing due to LOBO buoy cleaning.

CHAPTER 4

Discussion

Microphytobenthic primary productivity (MPB PP) can be a significant portion of the primary production in shallow water, coastal environments. For example, Glud et al. (2002a) found that in a Greenland fjord benthic primary production was 7 times higher than pelagic primary production in waters less than 30 m deep and this accounted for 40% of the primary production over the entire fjord. However, despite such evidence of its importance, there are comparatively fewer measurements of MBP PP compared to those of the water column (Krause-Jensen et al. 2012), and to my knowledge most of these are from intertidal environments. This thesis is a step toward addressing this knowledge gap by providing benthic primary productivity measurements from the Damariscotta River Estuary (DRE), a mid-latitude, productive, tidal estuary.

One reason for the lack of measurements is likely due to the challenge of measuring benthic productivity, which is complicated by the presence of a solid phase and the small spatial scale over which it occurs. While the euphotic zone in the pelagic environment can vary from a few meters in a turbid estuary to 100's of meters deep in the open ocean, primary production by microphytobenthos occurs in a thin biofilm, at most a few millimeters thick. So, while pelagic primary production can be determined using the ^{14}C-incubation technique, this is complicated for benthic samples due to the necessity of transporting the label across the sediment-water interface and the resulting challenge in determining what fraction of label has been taken up (Glud et al. 2009). As a result, there is no standard technique for measuring benthic primary production (Ask et al. 2016).

Although, ^{14}C incubations have been used, particularly in the early days (Nielsen & Hansen 1958), most estimates of MPB PP are made using incubation chambers or whole sediment cores and measuring changes in oxygen or dissolved inorganic carbon (DIC) in the overlying water (Cahoon & Cooke 1992, Jahnke et al. 2000, Glud 2008, Glud et al. 2009). *In situ* techniques, such as pulse amplitude modulation (PAM) fluorometry (Barranguet & Kromkamp 2000, Kühl et al. 2001, Glud et al. 2002a, 2009) can measure electron transport rates and can be used to assess activity in heterogeneous environments over larger spatial scales. However, this technique must still be calibrated against whole core or chamber measurements to relate the electron transport rate to primary production measured in terms of substrate either consumed or produced. In addition, oxygen microsensors, either optodes or Clark type electrodes, can be used to infer the fine scale spatial variability of MBP PP.

Another challenge in measuring MPB PP is defining what is meant by "primary productivity". O_2 production and consumption is tightly coupled in benthic communities (Kühl et al. 1996). Phototrophs provide O_2 and organic C to the heterotrophs which in return provide DIC for photosynthesis (Epping et al. 1996, Kühl et al. 1996, Glud et al. 1999, 2002a, Fenchel & Glud 2000). The release of dissolved organic carbon (DOC) by the MBP community during periods of photosynthesis can elevate the background respiration above the dark respiration rate (Cartaxana et al. 2016). As a result, though whole core and chamber incubations measure the net result of production, due to photosynthesis and consumption (respiration), it is not possible to simply use a dark incubation to separate gross and net productivity as is done in pelagic environments. For this study the illuminated respiration was not determined but could have been with more

cores and microsensors using the light-dark shift technique resulting in GPP (Glud et al., 2009; Revsbech & Jorgensen, 1983). The light-dark shift method to determines the gross photosynthesis at a given point based on the decline of O_2 concentration once the light is turned off (Glud et al., 2009). However, determining depth resolved rates using this approach is labour intensive and time consuming and could not have been done concurrently with the flux incubations. For these reasons, in this thesis, results are reported as net community productivity (NCP) and NCP is defined as the production of O_2 by the MPB community minus the consumption due to respiration by MPB and the background heterotrophic community. This is similar to the approach in other MPB PP studies (e.g., (Glud et al. 2002a)).

4.1 Estimating Benthic PE Relationship

In this thesis total oxygen exchange (TOE) across the sediment-water interface was determined using whole core incubations and compared to the dissolved oxygen exchange (DOE) determined from O_2 microsensor profiles. By performing these measurements with different irradiance at the sediment surface, a PE relationship for the sediment of the upper DRE was determined and net community production (NCP) was estimated.

4.1.1 Estimating Benthic PE Relationship Using TOE Parameters

Using the whole core incubation technique to determine the PE relationship has the advantage of being relatively easy and averages out small scale spatial variability. However, the downside is that the sediment is represented as a “black box”. Only the upward flux of O_2 across the sediment surface can be determined and is the net result of

production and consumption integrated over the entire sediment core. The spatial distribution of production and consumption within the sediment core cannot be determined.

The maximum photosynthetic capacity (P_{max}) for the TOE PE relationship showed depth and biomass variation. The deeper the site with less biomass the smaller the P_{max}. Site MC had the smallest P_{max} and was statistically different from the rest of the transect. When comparing to Ní Longphuirt et al. (2007) who used the *in situ* benthic chamber oxygen exchange method during late summer, in a subtidal temperate site with muddy sediments reported a P_{max} of 54 mmol O_2 m^{-2} d^{-1} and α of 0.73 (mmol O_2 m^{-2} d^{-1} (µmol photons m^{-2} $s^{-1})^{-1}$) and compared to the DRE average P_{max} of 395 mmol O_2 m^{-2} d^{-1} for the transect is significantly smaller. However, this study did see at least a two-fold increase in P_{max} from late summer to spring and had comparable dark O_2 consumption rates with R being 64.8 mmol O_2 m^{-2} d^{-1} in late summer and 69.6 mmol O_2 m^{-2} d^{-1} in spring almost the same as the DRE average (minus MC) transect R of 70.8 $\pm$ 14.9 mmol O_2 m^{-2} d^{-1}. Glud et al. (2009) reported a P_{max} value of 39 mmol O_2 m^{-2} d^{-1} for a transect in the artic with muddy sediments using the whole core incubation method for oxygen exchange. This study also reported a much lower α value of 0.45 (mmol O_2 m^{-2} d^{-1} (μmol photons m^{-2} $s^{-1})^{-1}$) (Glud et al., 2009) compared to the DRE average (minus MC) transect α of 3.9 $\pm$ 0.3 (mmol O_2 m^{-2} d^{-1} (µmol photons m^{-2} $s^{-1})^{-1}$). This is not surprising given that the Artic site is much colder, and ice covered for longer periods of time each year with less available sunlight.

The TOE minimum saturating irradiance (E_k) is the downwelling irradiance when the community production reaches the point of saturation and can no longer produce at a faster rate even with increased downwelling irradiance and is determined using Eq. (4.1).

$$E_k = \frac{P_{max}}{\alpha} \tag{4.1}$$

Where P_{max} and α are determined from each site PE curve and used to determine the site specific E_k value. The TOE E_k from each site follow a correlation to light availability at the sediment surface as other similar studies have observed and is independent to biomass (Ní Longphuirt et al. 2007). Overall, the E_k values in Table 4.1 are in the middle of the range of estimates for subtidal temperate microphytobenthos communities (30-265 µmol photons m^{-2} s^{-1}) (Sundbäck & Jönsson 1988, Blanchard & Montagna 1992, Light & Beardall 2001, Ní Longphuirt et al. 2007). Comparing to DOE E_k values all of the sites are significantly higher than Glud et al. (2002a) reporting the minimum saturating irradiance of a high artic fjord transect to be 32 µmol photons m^{-2} s^{-1}.

Table 4.1: TOE and DOE minimum saturating irradiance (E_k) values in µmol photons m^{-2} s^{-1} and TOE compensation irradiance values in µmol photons m^{-2} s^{-1} for each site in the transect. Both including the average (minus MC) for the not statistically different sites in the transect for TOE.

Site Name	E_k (µmol photons $m^{-2}s^{-1}$)	Compensation Irradiance (µmol photons $m^{-2}s^{-1}$)	
		TOE	DOE
West Shallow (WS)	132.7	19.0	22.6
West Deep (WD)	98.8	11.9	41.3
Middle of Channel (MC)	206.1	24.1	21.5
East Deep (ED)	127.0	19.3	37.2
East Shallow (ES)	79.1	17.4	26.8
Average	100.4	18.0	n/a

4.1.2 Estimating Benthic PE Relationship Using DOE Parameters

Oxygen microprofiles of the MPB communities generally have a large subsurface oxygen maximum zone with a relatively large penetration depth that in this study extended to 3.5mm into the sediment. This is in the range of oxygen penetrations depths in coastal temperate regions for cohesive sediments ranging just a few millimetres into the sediment (Ahmerkamp et al. 2017). From the O_2 concentration profiles the flux of O_2 across the diffusive boundary layer can be calculated based on the curvature of the steady state profile just below the sediment water interface (Berg et al. 1998). In the present study the average diffusive net oxygen production (NOP) based on the O_2 profiles across the transect reached 258.3 $\pm$ 108.2 mmol O_2 m^{-2} d^{-1} at the highest light level and was higher than intertidal studies that were performed *in situ*. For instance, on the French coast of the eastern English Channel in an intertidal zone a maximum diffusive NOP obtained was 103.2 mmol O_2 m^{-2} d^{-1} (Denis et al. 2012), while Epping & Jørgensen (1996) obtained a maximum value of 117.6 mmol O_2 m^{-2} d^{-1}. Some studies have reported much higher values from the same location and season with a maximum NOP of 225.6 mmol O_2 m^{-2} d^{-1} indicating large variation from year to year (Denis & Desreumaux 2009). The site with the highest NOP in the sediment was site ES reaching a maximum of 395.3 $\pm$ 7.5 mmol O_2 m^{-2} d^{-1} at an irradiance level of 221.2 $\pm$ 20.1 µmol photons m^{-2} s^{-1} while the lowest was 164.7 $\pm$ 47.5 mmol O_2 m^{-2} d^{-1} at site MC.

Based on parameters fitted using the DOE PE relationship the only P_{max} reached was for site MC (302.6 $\pm$ 93.5 mmol O_2 m^{-2} d^{-1}) and is higher than other reported values. Glud et al. (2002a) reported a P_{max} of 67 mmol O_2 m^{-2} d^{-1} in the Artic and Denis et al.

(2012) in a temperate intertidal site found P_{max} values of 105 and 136 mmol O_2 m^{-2} d^{-1} on two different spring days. Overall compared to the high Arctic fjord transect my transect has higher production and consumption as my respiration parameters are greater than 10.7 mmol O_2 m^{-2} d^{-1} and my α parameters are higher than 2.5 (mmol O_2 m^{-2} d^{-1} (µmol photons m^{-2} s^{-1})$^{-1}$) (Glud et al. 2002a) which is expected because temperate regions have greater nutrient, light availability and temperature. As for a comparison to a temperate location in the English Channel the corresponding R values for the previously reported P_{max} values are 50.4 and 43.2 mmol O_2 m^{-2} d^{-1} which are comparable to my R values for the DOE I measured in Table 3.1.

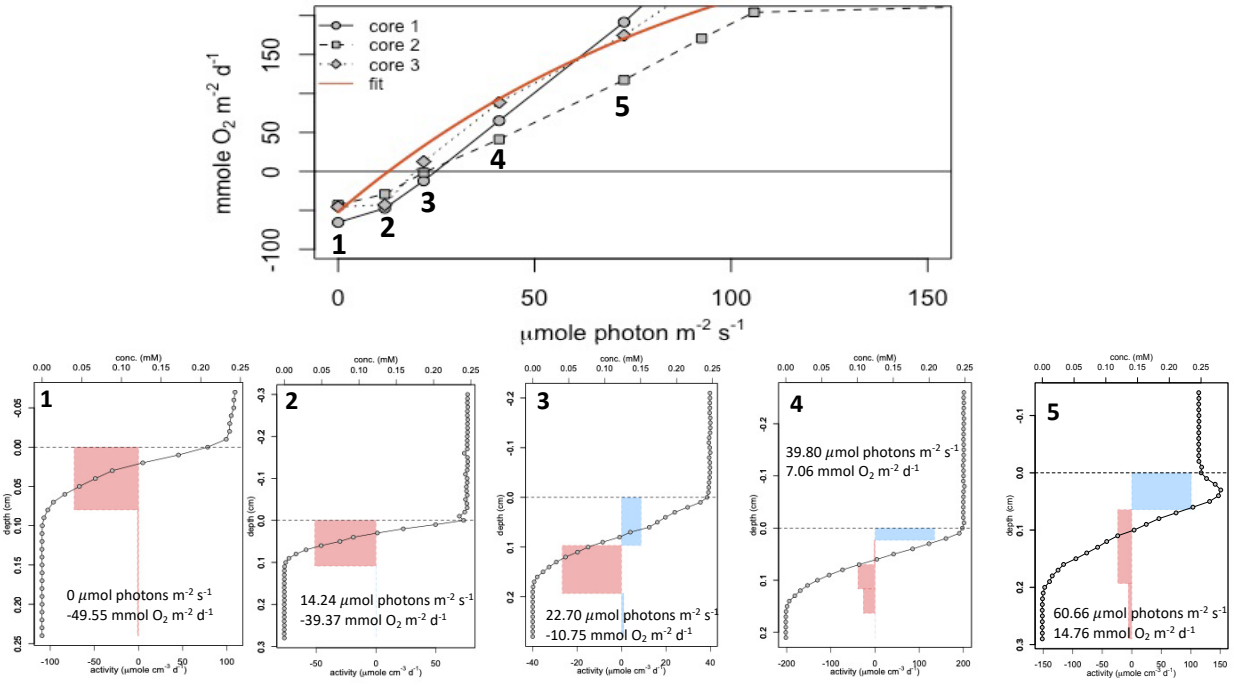

Figure 4.1. DOE PE curve for site WD with corresponding microsensor O_2 profiles to show production in the sediment before the net flux from the sediment is autotrophic at lower light levels.

Microprofiles of O_2 concentration with depth provide insight into the spatial distribution of O_2 below the sediment-water interface and the O_2 production and consumption as a function of depth (Revsbech et al. 1981, Epping et al. 1999, Glud et al.

2009). The O_2 profiles can explain why the compensation point determined from the TOE flux experiments at the deepest site MC (24.1 µmol photons m^{-2} s^{-1}, Table 4.1) was higher than the downwelling irradiance measured during core collection (15.43 µmol photons m^{-2} s^{-1}, Table. 2.1). This is how it is possible that in Fig. 3.7C the sediment at MC appears to be always net heterotrophic, but still has a resident population of actively photosynthesising diatoms. How is it possible this MPB community could exist? This becomes clear by looking at the microsensor profiles, from these you can see that a thin layer of oxygen production appears just below the sediment water interface, even though the DOE flux across the interface is still net consumption (Fig. 4.1). The sign of the oxygen flux for TOE does not switch until the oxygen production in this zone exceeds the depth integrated oxygen respiration of the entire core and the core becomes net autotrophic. Related to this, it is also important to keep in mind that TOE flux experiments do not capture the full rate of oxygen production in the sediment photic zone, but only the fraction that diffuses up out of the sediment. Typically TOE incubations only measure 70-90% of the oxygen production in this photic layer of sediment (Epping et al. 1996, Kühl et al. 1996, Wenzhöfer et al. 2000, Christensen et al. 2003, Glud et al. 2009). The remaining 10-30% of the oxygen produced diffuses downward into the deep sediment layers. An example of the upward and downward diffusion of oxygen for site WS is in Table 4.2 used to calculate the net diffusive oxygen rate from the sediment based on the microprofiles. This demonstrates the importance of using both whole core and microsensor profiling for assessing the influence of MPB on oxygen cycling in the sediment photic zone. To determine when production starts in the sediment the microsensor profiling is needed.

Table 4.2: DOE depth integrated rates of O_2 production and consumption used to calculate the overall net diffusive O_2 from the sediment-water interface into the overlying water column from the oxygen microprofiles. Production is the upward flux of oxygen and consumption is the downward flux from site WS.

Light Interval (μmol photons m^{-2} s^{-1})	Production (upward flux ↑ in mmol O_2 m^{-2} h^{-1})	Consumption (downward flux ↓ in mmol O_2 m^{-2} h^{-1})	Sediment-water Interface Flux (mmol O_2 m^{-2} h^{-1})
0 ± 0.09	0	-4.52 ± 0.23	-4.51 ± 0.22
14.24 ± 3.94	2.64 ± 1.40	-4.34 ± 1.29	-1.81 ± 0.93
22.70 ± 6.25	2.36 ± 1.98	-3.55 ± 1.36	1.19 ± 0.62
39.80 ± 10.23	6.95 ± 2.21	-3.69 ± 1.21	3.26 ± 1.09
60.66 ± 14.55	13.56 ± 4.66	-6.14 ± 0.58	7.41 ± 4.40
81.29 ± 14.26	16.76 ± 6.42	-5.97 ± 2.32	10.79 ± 4.20
154.97 ± 15.37	35.78 ± 3.25	-8.91 ± 1.70	26.87 ± 2.64
221.19 ± 20.08	51.58 ± 3.28	-12.51 ± 0.62	39.06 ± 2.66

4.1.3 Comparing TOE and DOE

Glud et al. (2002a) also compared both methods of benthic O_2 exchange and reported that TOE had a higher compensation point than DOE which is not the case for this study except for site MC. For sites WD, ED and WS (Fig. 4.2A, D and C) the TOE PE curves are larger for the amount of oxygen being produced at the higher light levels, while sites ES (Fig. 4.2B) and MC (Fig. 4.2E) are relatively the same. The linear portion of the PE curve represents the lower *in situ* natural light and is defined by the parameter α and follows the same trend for both methods (TOE and DOE) used to determine α for all the PE curves except for site WD (Fig. 4.2B). Site MC for both the TOE and DOE had the most similar parameters for both methods because it was the only site P_{max} was reached in the DOE method. This is why site MC is statistically different from the rest of

the TOE parameters (Fig. 4.2E). The difference between the two methods of determining the PE relationship is depended upon which part of the sediment photic zone is being measured. The DOE method determines oxygen flux at a single point, however it can be difficult to scale up to a larger area which may not be the same as the small-scale point and accurately take into account the sediment spatial heterogeneity (Glud et al. 1996, 1999, Wenzhöfer & Glud 2004, Denis et al. 2012).The larger area could be impacted by bare spots and patchiness of diatom coverage although it has been found that bare sediments can often contain active autotrophs (Glud et al. 2002a). This was observed during the TOE incubations because diatom coverage increased from start (dark) to the finish of the incubation for all sites. Bioturbation is often underestimated or disrupted in sediment core fluxes (Rabouille et al. 2003, Hammond et al. 2004, Murrell et al. 2009) but in this case burrowing macrofauna or evidence of burrowing microfauna were not observed in any of the cores collected at each site. All of these factors can significantly alter the overall MPB PP contribution when comparing TOE parameters to DOE. DOE is expected to be lower than TOE because TOE quantifies the net community photosynthesis of the integrated benthic community which is accounting for the entire respiration activity any fauna and non-photosynthetic microbes that consume the O_2 production in the sediment photic zone (Glud et al. 2002a). The DOE microsensor technique can have limitations such as modifying the diffusive boundary layer in the sediment when the sensor enters to increase the flux of oxygen from the sediment-water interface (Glud et al. 1994, Denis et al. 2012).

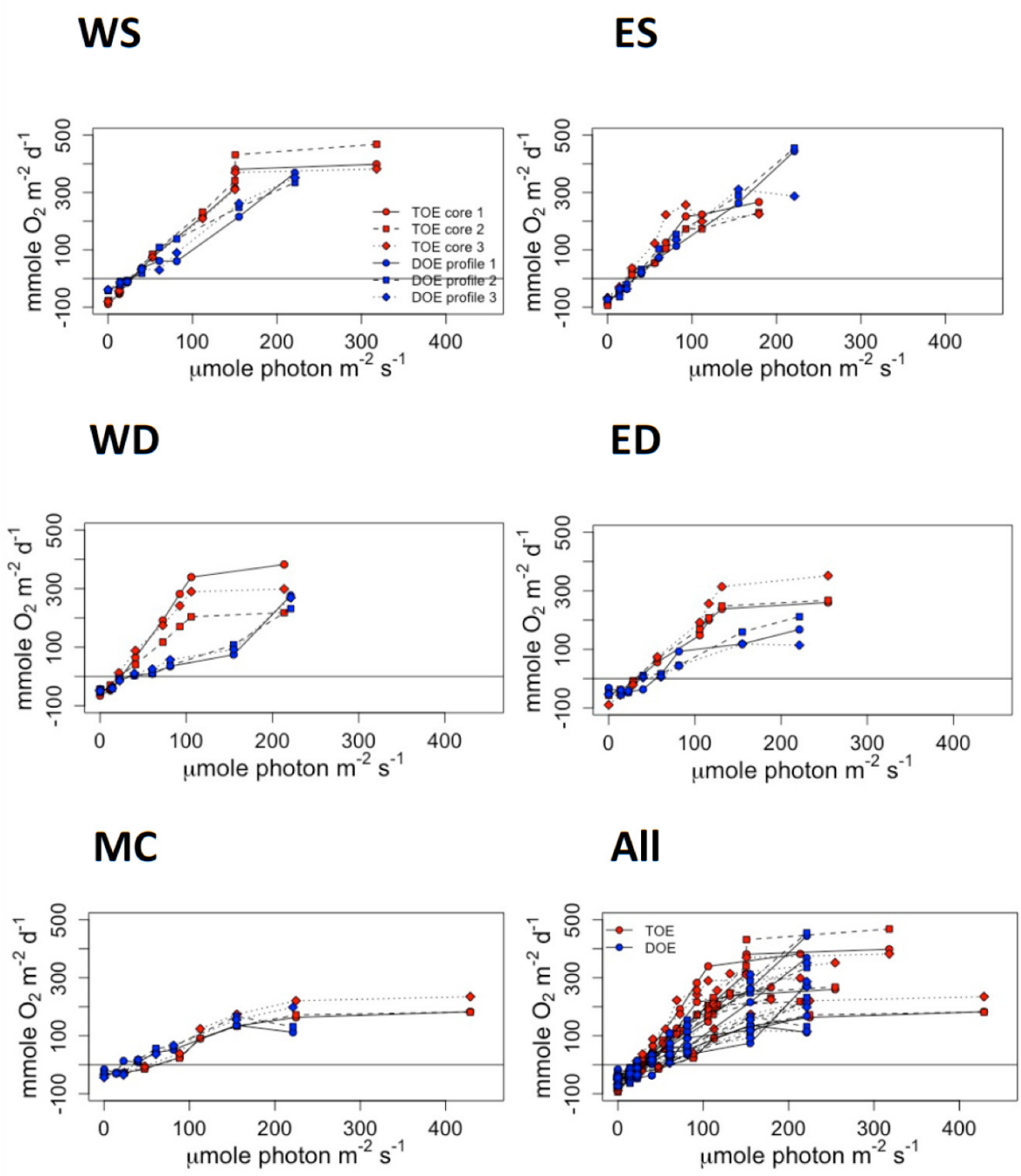

Figure 4.2: All sites across the transect comparing the PE curves for both the TOE in red and DOE in blue method used to determine the flux of O_2 across the sediment water-interface under well-defined light levels. Site West Shallow (WS), site East Shallow (ES), West Deep (WD), site East Deep (ED), and site Middle of Channel (MC) all located in the upper part of the DRE across from Perkin's Point. All is each individual core from each site together for both methods

4.2 Relationship between population size and PE parameters

My observations are consistent with previous studies that report spatial heterogeneity in the distribution of MPB on scales ranging from micrometers to meters (MacIntyre et al. 1996, Moreno & Niell 2004, Jesus et al. 2005, Ní Longphuirt et al. 2007). This can make scaling up estimates of benthic community production over large areas like estuaries challenging (Glud et al., 2009). However, after the cores where exposed to the full light cycle, diatom mats on the surface covered almost all of the sediment core area for the shallow sites (Fig. 2.2b). This indicates that even sediments that appear bare, may contain populations of active phototrophs. Others have found that especially in intertidal areas benthic diatoms demonstrate vertical migration as a function of irradiance or tides (Heckman 1985, Pinckney & Zingmark 1991, Glud et al. 2002a). The MPB PP would be affected by vertical migration of diatoms *in situ* throughout a daily cycle but would not be expected to play a role in altering our *ex situ* estimates. It has been shown MPB respond rapidly to changing environmental conditions (Glud et al. 2002a, Falkowski & Raven 2013, Hopes & Mock 2015, Hope et al. 2019) and maximize their photosynthetic activity to the dynamic environmental conditions within estuaries (Hope et al. 2019). Glud et al. (2002a) reported that benthic diatoms can acclimate within minutes to changes in irradiance. Both vertical migration of diatoms and photoadaptation could bias our flux experiments, if significant changes to the population or physiology of the MPB community was occurring during the experiments. However, the constant linear drawdown of oxygen during flux incubations at each irradiance level (Appendix A, Fig

A.1-5) indicate that oxygen fluxes were constant, and the benthic community was approximately in steady state

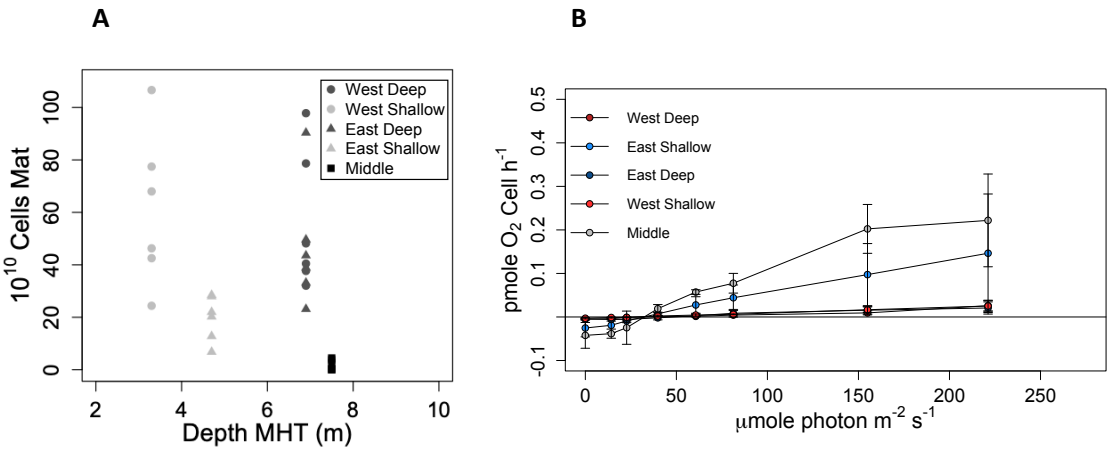

Figure 4.3: (A) Cell counts for the diatom mats with mean high tide water depth for each site with 3 replications (B) All sites across the transect averaged for three replications for the DOE depth integrated cell rate with the experimental light levels from the summer 2019. Oxygen microsensor O_2 flux from the sediment with depth by hour normalized to cell numbers in the diatom mat from each specific site. Cell are assumed to be producing at the same rate for the entire diatom mat.

Cell counts from each diatom mat and 1 cm below the mat revealed that the sites with deeper water depths on average generally had less diatom cells present (Fig 4.3A). The site ES was the only one across the transect that did not follow this trend having the least number of cells other than site MC. At the highest light levels, the diatom mat on all 3 cores from site ES began to curl in on top of itself exposing bare sediment on the edge of the core. The depth integrated cell normalized O_2 rate per hour was calculated from the oxygen microsensor profiles and diatom mat cell counts (Fig 4.3). Assuming that all the cells in the mat are actively photosynthesising this could provide an estimate of cell specific production and suggests that per cell oxygen production ranged from 0.01-0.2

pmol of O_2 $cell^{-1}$ h^{-1}. The sites with the highest cell specific rates were MC and ES which had the least number of cells present, however ES was not statistically different from the rest of the sites (Table 3.2). The higher per cell oxygen activity at MC could suggest these diatoms were adapted to low light environments potentially containing higher amounts of light harvesting pigments (Chlorophyll a). However, there per cell rate estimates assumes all of the cells in the mat are producing at the same rate and does not account for the possibility of shadowing at the bottom of the thicker mats which would cause these cells to produce at a limited rate based on light availability. Therefore, site MC which had statistically less cells in the diatom mat had the highest cell specific rates due to less cells shadowing because of a smaller less dense diatom mat. MC site also had statistically different P_{max}, α, and R parameters fitted to the PE curve determined from the whole core incubations, while ES did not, suggesting that there may be a difference in photoadaptation and biomass composition present at site MC compared to the other sites along the transect.

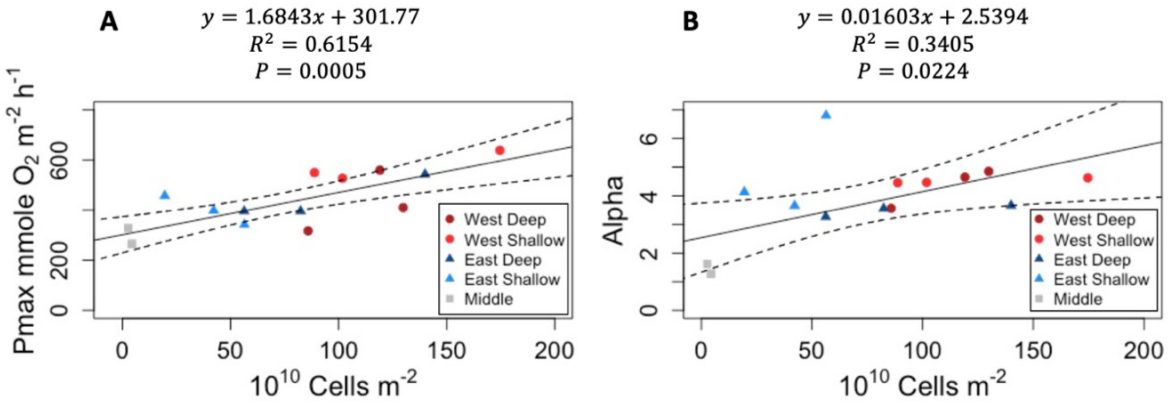

Figure 4.4: (A) TOE P_{max} parameters for each individual site-specific core with the microphytobenthic cell concentration. (B) TOE α parameters for each individual site-specific core with the microphytobenthic cell concentration. Dashed lines are the 95% confidence intervals.

To assess how biomass may influence the PE parameters, and the oxygen flux from the sediment. The relationship between P_{max} and α determined from the whole core flux incubations and biomass is shown in Fig 4.4. The P_{max} linear trend (Fig. 4.4A) infers that cell counts can explain 62% of the variability in the P_{max} across the sites, suggesting that biomass is the main factor determining P_{max} values. MC has a statistically lower P_{max} than the other sites and the smallest population of diatoms. There is a depth trend with biomass across the transect, except for site ES which has less biomass than the comparative shallow water site on the west side shown in Fig 4.3A. Site ES although not statistically different had an increased cell specific O_2 rate in Fig. 4.3. This combined with Fig. 4.4A indicates a smaller population of diatoms present producing at a faster cell specific rate than ED, WD and WS but still with a not statistically different production due to a difference in cell composition or photoadaptation of the cells. The α flat trend (Fig 3.5b) shows that the amount of cells present is independent of the rates of production at the lower light levels.

Unlike the cell counts, the chlorophyll a content both in the mat and 1cm of sediment below the mat were not statistically different. The mat chl a content showed no differences across sites, and in the cm below only WS and MC had sediment chl a concentrations that were different than the other sites. In both cases chl a content at these sites was lower than at the other sites. However, these sediment chl a measurements are below the photic zone of the sediment based on the OPD of at most 0.35 cm determined from the oxygen microprofiles. These chl a concentrations are therefore likely not representative of the chl a content of the active phototrophs. The mean chl a

concentration, 7.73 ± 3.70 mg chl a m^{-2} in the diatom mats and 9.85 ± 5.44 mg chl m^{-2} in the 1 cm below, and where similar to those reported for other subtidal temperate muddy sites, for example Ní Longphurit et al. (2007) reported chl a values of 5.4 ± 1.0 mg chl m^{-2}. It has been observed in Santema & Huettel (2018) that increased mixing causes sediment resuspension resulting in the highest chl a concentrations at depths of 5 cm in the sediment. This could explain why chl a content measured below the mat was somewhat higher than in the mat itself. In addition, other studies have also found that chl a concentrations in the uppermost 1 cm of the sediment are a poor representation of the active phototrophic biomass as the photic zone in the sediment only extends a few millimetres in the sediment (Kühl et al. 1997, Kühl 2005, Glud et al. 2009). It is likely the chl a measured in the sediment below the mat, is largely derived from phytodetrital material settling from the pelagic zone above and senescent or saprophytic living microphytes or spores (Sun et al. 1994, Glud et al. 2009).

4.3 Environmental Limiting Factors

Abiotic (water depth, sediment type and nutrient availability) and biotic (faunal and floral communities) variables present in the ecosystem can influence the spatial and structural distribution of microphytobenthos (Asmus 1982, Davis & Mclntire 1983, Ní Longphuirt et al. 2007). Limiting factors for the production of MPB include small scale factors of nutrient availability or faunal and floral limiting biomass growth spatially, creating patches of mats and larger scale factors include water depth and sediment type limiting production (Brotas et al. 1995, Cahoon 1999, Moreno & Niell 2004, Ní Longphuirt et al. 2007). Other studies have found that concentrations of chl a are higher in muddy sediments then sandy based on the correlation between chl a and the silt

fraction (Underwood & Kromkamp 1999, Ní Longphuirt et al. 2007). For this study all of the sites across the transect are muddy sediments leaving the large limiting factor to be water depth which changes on a scale of about 4m from low to high tide and would therefore influence light availability.

Within the photic zone of muddy or sandy sediments Cartaxana et al. (2016) found that at an incident downwelling irradiance of 1000 µmol photons m^{-2} s^{-1} about 6 to 200 µmol photons m^{-2} s^{-1} was reaching the bottom boundary of the photic zone within the sediment. Indicating that particles within the water column could be playing a large roll in scattering light before it reaches the sediment or shadowing within the diatom mats limiting light attenuation to the bottom of the photic zone. For the DRE system the incidence downwelling irradiance changes based on sunlight and water depth. Therefore, light is dependent on the time of day and tidal cycle lining up for optimal benthic NCP. Based on a study done in the Baltic sea for soft sediments like in the DRE the benthic community has a higher contribution than the pelagic zone to the overall production at depths less than 4 meters (Ask et al. 2016). This could be the result of light attenuation within the system and could vary depending on the turbidity and water depth present at a site. The DRE attenuation of light varies within the tidal period where there is less downwelling irradiance at low tide and a greater attenuation at high tide. The attenuation of light affects the deep sites in the transect more than the shallow sites. Based on Fig. 3.7 of the daily NCP estimates for the month of July the shallow sites are limited by the amount of sunlight each day reaching a consistent peak production every day that light is available. While the deep sites have inconsistent production rates as they only reach optimal production on days where peak sunlight aligns with spring tide, high tide. These

are the days of the month where there is the most amount of clean sea water to dilute the estuary water, which is higher in particles that scatter light, inhibiting downwelling irradiance.

4.4 Benthic Net Community Production for DRE

In addition to the daily light-dark cycle, MPB PP can be influenced by the tidal cycle, as variations in the water depth and attenuation coefficient effect the amount of light reaching the sediment surface. To account for this, the laboratory determined PE relationship from the TOE flux incubations were used with surface irradiance (from the University of Maine's LOBO buoy) and tidal height (from the Walpole NOAA tide gauge) to estimate benthic NCP at 1-hour intervals for the month of July 2019. Integrating over 24 hours produced daily estimates of MPB net community production for each day of the month and these are summarized in Fig 4.5. The maximum NCP across the transect was 100.8 $\pm$ 25.3 mmol O_2 m^{-2} d^{-1} at site WS and the lowest values being -45.8 $\pm$ 5.6 mmol O_2 m^{-2} d^{-1} at site WD. Only the shallow sites in the transect were net autotrophic (Fig 4.5), while the other 3 sites were net heterotrophic. Generally, water depth seemed to be the primary factor determining NCP across the transect. However, MC had slightly higher NCP then either WD or ED, which were slightly shallower. MC, due to its deeper water depth, had less irradiance on the sediment surface, and lower day time O_2 production then either WD or ED, however its dark respiration rate, *R*, was lower (33.5 mmol O_2 m^{-2} d^{-1}). This could be because there is less fauna present at MC to mediate O_2 uptake, possibly because there was less organic matter deposition at MC than the other 2 sites. There could be less fauna present because of lack of nutrients in the deepest water in the middle of the channel where there is boat traffic and no aquaculture

while sites WD and ED are located directly below or above oyster aquaculture farms and enhanced organic deposition from the farms could drive higher rates of heterotrophic respiration at these sites.

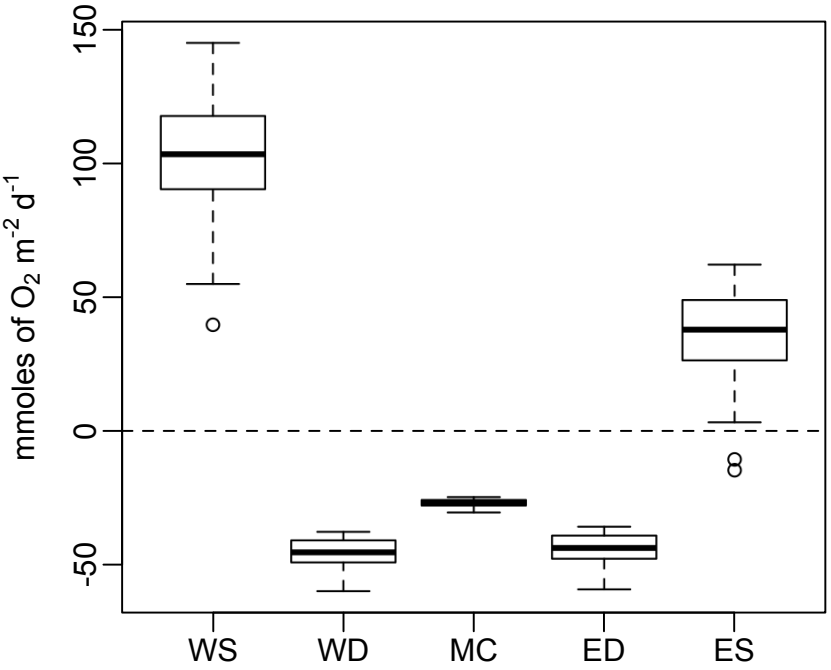

Figure 4.5: NCP box plot of the month of July for periods of potential photosynthesising for each site on the transect. Below zero on the plot is net heterotrophic and above is net autotrophic.

Most of the coastal benthic primary production studies in temperate regions make estimates for intertidal sediments while few have studied subtidal sediments. Comparing to other studies from coastal subtidal temperate regions my estimates are similar. Sospedra et al. (2015) estimated *in situ* spring net primary production of 689.6 mmol O_2 m^{-2} d^{-1} at a depth of 9m in sandy sediments comparable to our WS site for a spring estimation. In the Arctic using the same total core incubation method for NCP Glud et al. (2002a) estimated benthic net primary production at a site of 5m in depth to be 10.2 moles O_2 m^{-2} d^{-1} and 10m in depth to be 9.4 moles O_2 m^{-2} d^{-1} during the month of July. They saw seasonal change throughout the 3 months they sampled decreasing from July to

September. Comparing to the Artic the DRE is more productive which is to be expected due to increased sunlight, higher temperatures and greater nutrient availability. Lastly comparing to another temperate site with similar depths (5-10 m) but sandy sediments, NCP *in situ* values ranged from -1.4 to 5.7 mmol O_2 m^{-2} d^{-1} (Santema & Huettel 2018). The DRE shallow sites had higher productivity than Santema & Huettel (2018) because MPB growing on soft sediment like mud have higher productivity rates than those growing on hard substrates like sand because they have access to nutrients stored in the sediment (Vadeboncoeur et al. 2006, Ask et al. 2016) instead of competing with the phytoplankton in the overlying water for nutrients.

4.5 Influence of MPB on Oyster Aquaculture

Benthic contributions to primary production in continental shelf regions are already an area of biogeochemistry that lacks in research compared to the water column (Pinckney et al., 2018). This thesis demonstrates the potential importance of the microphytobenthos community to the primary production in shallow subtidal temperate estuary. Oyster aquaculture is an important industry in the DRE, and it continues to expand, understanding the interactions between MPB and aquaculture is important to understand its sustainability and environmental impacts of this industry. MPB are a particularly label source of organic carbon and a significant dietary source for benthic meio- and macro- fauna species (Hope et al. 2019). If MPB are suspended into the water column they may also become a food source for pelagic ecosystems. It has been found that microphytobenthos primary production is closely linked to the production of fish and shellfish in coastal regions (Kritzer et al. 2016, Morioka et al. 2017, Hope et al. 2019) and in particular up to 70% of the diet of harvested and farmed oysters may be composed of

MPB (Hope et al. 2019). The presence of microphytobenthos in the DRE could therefore be of benefit to the bivalve aquaculture industry. In addition, microphytobenthos derived carbon to CO_2 respiration which 0.6 mol of CO_2 can account for nearly 1 mol of carbon found in the shells of bivalves (Fodrie et al. 2017, Hope et al. 2019). The microphytobenthic derived carbon to CO_2 is found in shells by the process of calcification to form the bivalve's calcium carbonate shell. Microphytobenthos, like shellfish aquaculture, play a role in water purification by aiding in the removal, transformation or retention of pollutants (Tolhursf et al. 2002, Kowalski et al. 2009, Snelgrove et al. 2018, Hope et al. 2019). They can also act as a barrier for the sediment from the overlying water trapping particles (Kornman & De Deckere 1998, Hope et al. 2019). Evidence from the Chesapeake Bay can support that the presents of oysters can help with water clarity (Kemp et al. 2005, Hope et al. 2019) increasing the amount of light reaching the sediment for MPB PP.

MPB PP can not only increase the amount of oxygen in the overlying water affecting the pelagic zone but also within the sediment affecting the biogeochemical gradient within the sediment (MacIntyre et al. 1996, Hope et al. 2019). With increased production from the microphytobenthos the concentration of oxygen within the sediment extents deeper during optimal day light hours. The extension of O_2 deeper into the sediment can stimulate nitrification and in return can provide a labile carbon source for nitrogen cycling bacteria in the sediment. In turn, at night when O_2 decreases because of increased respiration and no primary production, dentification increases resulting in a larger removal of nitrogen from the system (An & Joye 2001, Hope et al. 2019). This is important for the aquaculture because it may mediate the eutrophication associated with

shellfish aquaculture waste. Large amounts of shellfish aquaculture in the ecosystem creates increased organic matter settling on the sediment from the shellfish secretions (Burkholder & Shumway 2011). Overloading of organic matter can lead to oxygen deficient zones or so called “dead zone”. MPB can counteract this nutrient loading, either through stimulation of coupled nitrification-denitrification or the assimilation of nutrients into their biomass. Increased nitrogen retention and removal can significantly create a more inhabitable benthic environment for organisms therefore interactions between MPB, nitrogen cycling bacteria and invertebrates are important (Douglas et al. 2018, Hope et al. 2019). The impact of MPB on the cycling of nitrogen within the sediment can change not only daily from nutrient uptake and transfer but also seasonally based on biomass (Hope et al. 2019). Therefore, the presence of microphytobenthos in the DRE driving the MPB PP could not only be the base of the marine food web but also play a key role in the sediment biogeochemistry.

Comparing to another site with bivalve aquaculture like the New Meadows River just southwest of the DRE could provide insight to why the DRE has higher MPB production than other sites that are similar like the temperate study done by Santema & Huettel (2018) or Artic study done by Glud et al. (2002a). Therefore, the potential positive impact of aquaculture to an estuaries overall production could be evaluated. Understanding what drives the benthic photosynthetic rate will help for the future of the aquaculture industry as shellfish are secondary consumers. The positive feedback between these two different trophic level species could be influencing the quality of the aquaculture in the DRE. Overall, based on this study the DRE has high rates of benthic

primary production that is light limited, dependant on the tidal period with the shallow edges of the estuary being net autotrophic in the summer.

CHAPTER 5

Conclusion

5.1 Summary

This thesis describes the influence of diatom-dominated MPB communities on sediment-water column O_2 dynamics along a depth transect in a mesotidal temperate estuary, the Damariscotta River Estuary in Maine, USA. Using a combination of whole core flux incubations and microsensor profiling the PE relationship between irradiance and oxygen flux was determined and used to calculate the *in situ* trophic state (heter- or autotrophic) of the sediment. It was concluded that light limitation determined by water depth based on the tidal cycle was the main environmental factor controlling benthic primary production and the balance between oxygen production and consumption across the transect. The deepest site in the middle of the channel, site MC, had the least variation in the oxygen dynamics over both daily and tidal cycles and was always net heterotrophic, while the shallow sites had much wider variability and were net autotrophic. Phototrophic biomass was assessed using diatom cell counts and bulk Chl a measurements. No trends were observed with respect to Chl a, however diatom cell counts were a primary factor explaining the P_{max} parameter in the PE relationship (Eq. 2.2), but did not explain differences in the α parameter which describes the response to changes in irradiance. Differences in the cell specific O_2 rates between ES and the other sites (not including MC) could imply a variation in diatom species composition but this requires further work. More studies are suggesting that in subtidal coastal ecosystems the benthic microalgae community contributes significantly to the primary production (Glud

et al., 2009). In the DRE, the benthic microphyte community is contributing to the overall production of the system at the shallow sites but the heterotrophic consumption is greater than the production at the deeper sites.

5.2 Errors and Limitations

It became apparent during the experiments that accurately determining the amount of light illuminating the sediment during PE incubations was a challenge and a potential source of error in the experiments. Accurately determining sediment irradiance in the experimental setup of the whole core incubations was more challenging than I was expecting. Often in the literature there are few details provided as to how irradiance on the sediment surface was determined. For example, Glud et al. (2002a) describes achieving the irradiance for their TOE incubations by regulating the source of light to the sediment surface and Santema & Huettel (2018) achieved controlled light conditions by shading natural sunlight. These explanations are very brief and did not provide enough detail for me to follow for the experimental setup of the whole core incubations and microprofiling. For experiments I used an approach similar to Glud et al. (2002a). To determine the irradiance on the sediment through the experiment a second empty core tube with a reactor cap was placed beside one of the flux reactors and instead of sediment, a miniPAR sensor was placed inside the reactor (Fig 5.1) to record irradiance throughout the experiment. From this it was determined that the irradiance measured during the experiment was higher (grey line in Fig 5.2) than the target irradiance (red line Fig 5.2) which was discovered after the experiments were complete. To further check the irradiance levels the flux experiment was repeated without sediment but instead a

miniPAR sensor in both the sediment core that would normally contain sediment and the light monitoring core.

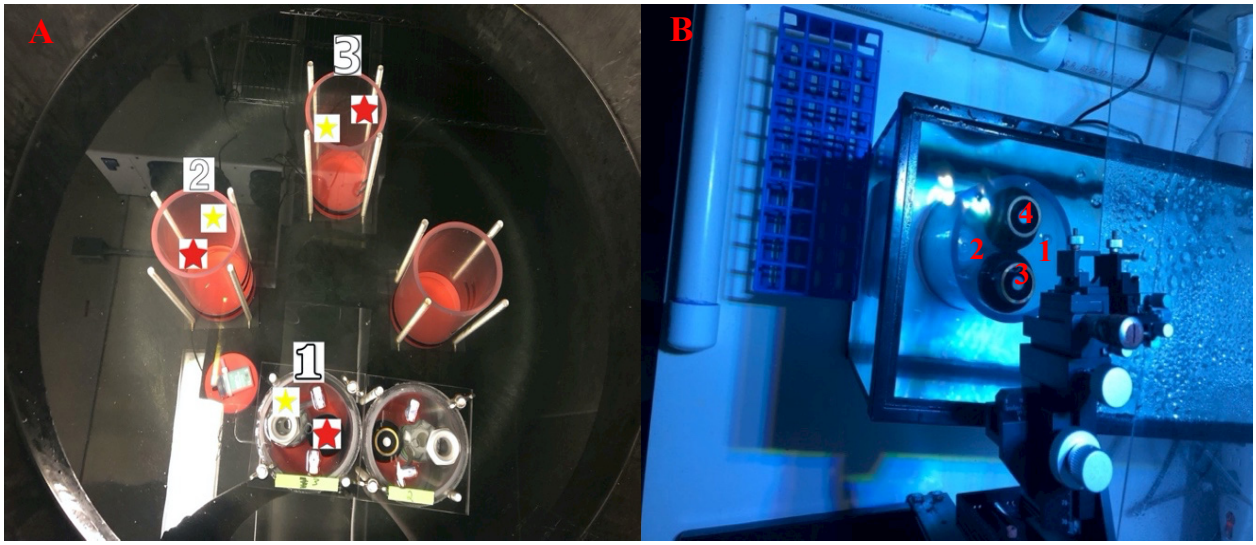

Figure 5.1: (A) overview of the whole core incubation light experiment setup to rule out tank variation and variability within the sediment core. (B) overview of the microprofiling tank light experiment set up to rule out sediment core variability.

The light test was done by setting both tanks up the exact same way as the original experiments, only this time with two PAR sensors one in the sediment core position (cores 1-3 Fig 5.1A) and one in a core beside the sediment core position (core beside core 1 Fig 5.1A) to rerecord the light levels. Then the same light level sequence was run for three replications in all three positions in the whole core tank and the single position in the profiling tank (Fig 5.1). The sensor in the sediment core position was moved around in the core to rule out light variability within the core as well as in the tank. From these results it was concluded that the experimental light during the summer of 2019 was accurate except for the higher light level because as the light source got closer to the sediment core the PAR sensor off to the side of the sediment core was shaded, due to

focusing of the light beam and therefore did not record the highest light level accurately during the whole core incubation experiment (Fig 5.2 grey vs blue lines). To account for this a correction factor was applied to the highest light levels measured during the experiments. For the microprofiling tank the light levels where similar from the test to the experimental values so that the measured value during the microprofiling could be used.

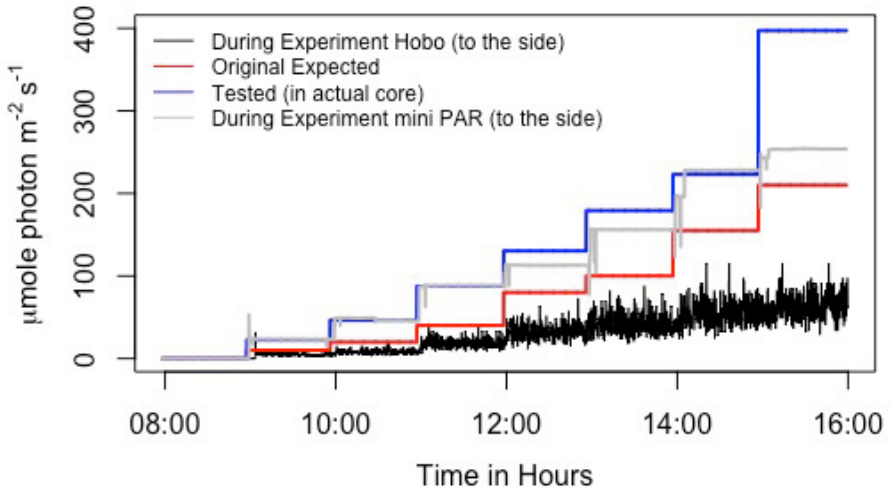

Figure 5.2: All light measured in the whole core incubation tank compared to the experimental light from the MC site experiment from the summer. The red line is the original light levels set during planning of the experiments, the grey line is the experimental light recorded during the experiments, and the blue line is light recorded during the test after the experiments all recorded using a miniPAR sensor. The black line is light recorded during the experiments using a HOBO logger. For the rest of the site light plot refer to Appendix A.

To create the same light environment that the benthic community experiences *in situ* involved a series of light box filters and colour spectrum adjustments within the aquarium lights used. Each light used was fitted with a light filter box with a yellow-green filter attached. As each light interval progressed after the dark period the colour spectrum was adjusted using the blue, green and then the cool white colours to get

different light levels within the incubation and microprofiling experiments. Adjusting the colour spectrum was done to get lower light levels in the tanks because the lights could only be moved so far away from the cores in the environmental chamber used to allow for in situ temperature to be set. Therefore, the light colour spectrum may not have been exactly the same throughout the intervals of light and may have differed from the *in situ* light colour spectrum.

To determine the *in situ* sediment level irradiance a series of calculations was done based on the hourly recorded surface irradiance and attenuation coefficient. By calculating the bottom irradiance instead of recording it, there is room for error based on the attenuation coefficient. If actually measuring the bottom irradiance of each site for the month of July was a possibility it would have been done. Using the method of *ex situ* light to determine the photosynthetic response curve for the benthic community to make *in situ* production estimates has been reported as underestimating the *in situ* values (Santema & Huettel 2018). The use of ex situ light response curves may underestimate production rates because there is no nutrients or CO_2 supply from deeper sediments or the overlying water (Cook & Røy 2006, Santema & Huettel 2018) but in this case the incubation period was not long enough for the nutrients and CO_2 supply to decline. Therefore, these rates reflect the community of the 15 cm of sediment at the time of sampling because UV filtered water is used.

In addition, the *in situ* water column light attenuation throughout the tidal period could have been more accurately obtained. This would improve the estimates of sediment surface irradiance calculated from the LOBO buoy and the tidal varying attenuation coefficient. During the process of profiling the water column for light uncontrollable

environmental factors played a role. Cloud coverage during the light profiles was avoided because of possible shadowing but impacted the duration of time each site could be profiled. This created difficulties in measuring each site at the same point in the tidal cycle on the same day, therefore mid tide light profiles were not measured. I hypothesized prior to light profiling that the attenuation coefficient would not differ greatly between tides but between sites across the transect. However, this was not the case and there was a significant tidal signal in this calculated light attenuation coefficient. To account for this a sinusoidal curve was used to estimate the light attenuation coefficient throughout the tidal cycle. However, I only had a few points at high and low tide to fit this curve and they were not always taken on the same day. A more detailed survey of light attenuation throughout the tidal cycle would provide greater confidence in our modelled attenuation coefficient. An additional measurement that could have easily been made during this time was turbidity within the water column during the tidal period, as this would help in understanding the reason for this difference in light attenuation throughout the tidal cycle.

Working within such a small-time frame and trying to sample each site with similar conditions (e.g., tide and sun light) turned out to be harder than first anticipated. Sampling at the same point in the tidal period and spring or neap tide caused problems due to different time constrains for the divers because of turbidity differing at sites and there are only so many spring or neap tides during the summer months. Therefore, the sites (except ES) where sampled approaching high tide assuming less turbidity from the input of fresh sea water.

The microsensor technique used was based on Berg et al.'s (1998) method had limitations because of the increments of measurements during the profiling. The method

to analyze O_2 microprofiles requires the benthic boundary layer (BBL) to be accurately identified. The microsensor profiles were measured in 100 μm increments based on the electrode used which is a large increment for determining the BBL and would have been more accurate with an electrode with a finer tip. If the BBL is incorrectly identified this introduces error into the sediment flux calculation. Therefore, the microprofiles at lower light levels were subject to potential bias when setting the interface that could have affected the flux calculations.

Within microphytobenthic production work many different techniques of estimating are used and presented in different units. These techniques can also differ in what is defined as primary production indicating either net or gross based on the technique and whether the consumption was measured separately. If the methods used in a study are not clearly stated it becomes difficult to compare with other studies. Due to these circumstances in the field of microphytobenthic primary production a degree of "creativity" and clearly defined terminology is suggested by Glud et al. (2009) to evaluate the existing database of studies. Thus, when comparing this study to other it became difficult as most of the research done in temperate regions has been done on intertidal zones or sandy sediments. While the research in the Artic sites have sediment type conditions that are similar but differ in region. Therefore, not having any completely similar studies to compare to makes it difficult to understand whether the DRE is unusual in its high productivity of the benthic community or whether all temperate muddy subtidal sites have high productivity.

5.3 Future Work

Largely the two biggest variations of benthic community production estimates reported in other studies are seasonality and *in situ* versus *ex situ* estimations. Studies which investigated seasonality saw a change in production with the greatest amounts being reported in the spring and lowest in the Fall (Sospedra et al. 2015). In the case of the DRE during winter months, the upper part of the estuary can be ice covered significantly impacting the winter benthic production and possibility of sampling during these months. The most interesting changes in seasonal production to study in the DRE would be spring to determine if there is increased production during the spring phytoplankton bloom or if the estuary is nutrient rich year-round because of the large amount of aquaculture present. Other studies such as Gillespie et al. (2000) reported seasonal change with the month of April having the highest net production and the months of September and February having the least. This study had similar water depth in a subtidal bay in New Zealand. Further investigation into the production across the transect of the DRE during different seasons could lead to determining seasonal variation of production.

The importance of microphytobenthos in shallow water ecosystem is well established and the limiting factors of production all agree with light and biomass being key controlling variables while the fate of these communities are unknown (Middelburg et al. 2000). Research like this study aid in the growing database of benthic production estimations as the importance of the benthic community contribution is shown. To further the significance of this study the next step would be to compare these results to estimates of the pelagic primary production estimates performed in the DRE, the portion of the

benthic community contribution can be analyzed in comparison to that of the pelagic. Also looking into the sediment oxygen dynamics based on the microprofiles could lead to a diagenetic model of the sediment. This could be done with the pre-existing dataset to understand how the oxygen dynamics in the first few millimeters affect the rest of the redox cascade. To compare these results to other locations within the DRE or nearby estuaries would help to understand these results in a wider context and MPB PP in temperate subtidal estuaries more generally. Transects could be sampled at lower and middle locations of the DRE where there is significantly less aquaculture and with more sea water mixing which could lead to less nutrients present or different light attenuation to the sediment surface. The New Meadows estuary which is located south of the DRE is another river of interest for the region. It has similar conditions and an increasing amount of aquaculture each year. Conducting the same experiment within this estuary would be an opportunity to compare results with the same conditions for a study site.

Other concerns of the study that could have been measured during the process of the sampling season are identification of the benthic community rather than just the counts of diatoms present. This could lead to an understanding of whether there is a difference in diatom community composition to aid in the difference in biomass presented. Mainly this could help to understand site ES as it has a lower biomass but greater production than the two deep sites. Also, the heterotrophic community could have been examined to determine if the deep sites are net heterotrophic because of a larger biomass of heterotrophic organisms with diatoms present. Another measurement that could have been done was nutrient availability across the transect to see if that was a

factor for increasing respiration in the deeper sites compared to the shallow even though they had not statistically different parameters fitted from the PE curves.

This thesis describes the major differences in O_2 production and consumption across a transect with varying depths of diatom dominated MPB communities within an estuary. We conclude that the largest variation between the net production of each site was light limitation based on the water depth and the alignment of the tidal cycle with peak sunlight. However, site MC had the least amount of variation between low and high tide indicating that the shallow sites have greater variation in O_2 production dependant on light attenuation based on the tidal cycle. Variation in diatom species composition is hypothesized based on cell specific O_2 rates and may be the reason why similar production rates were observed at site East Shallow although less biomass was present. Moving forward with this study there are many factors that could be addressed when looking deeper into the variation within benthic net community production of the DRE.

BIBLIOGRAPHY

Ahmerkamp S, Winter C, Krämer K, Beer D de, Janssen F, Friedrich J, Kuypers M, Holtappels M (2017) Regulation of benthic oxygen fluxes in permeable sediments of the coastal ocean. Limnol Oceanogr 62:1935–1954.

An S, Joye SB (2001) Enhancement of coupled nitrification-denitrification by benthic photosynthesis in shallow estuarine sediments. Limnol Oceanogr.

Ask J, Rowe O, Brugel S, Strömgren M, Byström P, Andersson A (2016) Importance of coastal primary production in the northern Baltic Sea. Ambio 45:635–648.

Asmus R (1982) Field measurements on seasonal variation of the activity of primary producers on a sandy tidal flat in the northern Wadden sea. Netherlands J Sea Res.

Barranguet C, Kromkamp J (2000) Estimating primary production rates from photosynthetic electron transport in estuarine microphytobenthos. Mar Ecol Prog Ser 204:39–52.

Berg P, Risgaard-petersen N, Rysgaard S (1998) Interpretation of measured concentration profiles in sediment pore water. 1–10.

Blanchard GF, Montagna PA (1992) Photosynthetic response of natural assemblages of marine benthic microaglae to short- and long term variations of incident irradiance in Baffin bay, Texas. J Phycol.

Brotas V, Cabrita T, Portugal A, Serôdio J, Catarino F (1995) Spatio-temporal distribution of the microphytobenthic biomass in intertidal flats of Tagus Estuary (Portugal). Hydrobiologia.

Burkholder JM, Shumway SE (2011) Bivalve shellfish aquaculture and eutrophication. In: *Shellfish aquaculture and the environment*. John Wiley & Sons, Chichester, p 155–215

Cahoon LB (1999) The role of benthic microalgae in neritic ecosystems. Oceanogr Mar Biol an Annu Rev 37:47–86.

Cahoon LB, Cooke JE (1992) Benthic microalgal production in Onslow Bay, North Carolina, USA. Mar Ecol Prog Ser 84:185–196.

Cartaxana P, Ribeiro L, Goessling JW, Cruz S, Kühl M (2016) Light and O_2 microenvironments in two contrasting diatom-dominated coastal sediments. Mar Ecol Prog Ser 545:35–47.

Chandler EA, Belknap DF, Kelley JT (2016) Sedimentation Patterns in the Damariscotta River Estuary.

Christensen PB, Glud RN, Dalsgaard T, Gillespie P (2003) Impacts of longline mussel farming on oxygen and nitrogen dynamics and biological communities of coastal sediments. Aquaculture 218:567–588.

Christianen MJA, Middelburg JJ, Holthuijsen SJ, Jouta J, Compton TJ, van der Heide T, Piersma T, Sinninghe Damsté JS, van der Veer HW, Schouten S, Olff H (2017) Benthic primary producers are key to sustain the Wadden Sea food web: stable carbon isotope analysis at landscape scale. Ecology.

Cibic T, Blasutto O, Burba N, Fonda Umani S (2008) Microphytobenthic primary production as 14C uptake in sublittoral sediments of the Gulf of Trieste (northern Adriatic Sea): Methodological aspects and data analyses. Estuar Coast Shelf Sci 77:113–122.

Cole A (University of MARI, Langston A (University of MARI, Davis C (Maine AIC (2017) Maine Aquaculture Economic Impact Report.

Cook PLM, Røy H (2006) Advective relief of CO2 limitation in microphytobenthos in highly productive sandy sediments. Limnol Oceanogr.

Colijn F, de Jonge VN (1984) Primary production of micro- phytobenthos in the Ems-Dollard estuary. Mar Ecol Prog Ser 14:185–196

Davis M, Mclntire C (1983) Effects of physical gradients on the production dynamics of sediment-associated algae. Mar Ecol Prog Ser.

Denis L, Desreumaux PE (2009) Short-term variability of intertidal microphytobenthic production using an oxygen microprofiling system. Mar Freshw Res.

Denis L, Gevaert F, Spilmont N (2012) Microphytobenthic production estimated by in situ oxygen microprofiling: Short-term dynamics and carbon budget implications. J Soils Sediments 12:1517–1529.

Douglas EJ, Pilditch CA, Lohrer AM, Savage C, Schipper LA, Thrush SF (2018) Sedimentary Environment Influences Ecosystem Response to Nutrient Enrichment. Estuaries and Coasts.

Epping EHG, Jørgensen BB, Epping EHG, Barke B (1996) Light-enhanced oxygen phototrophic comm. 139:193–203.

Epping EHG, Khalili A, Thar R (1999) Photosynthesis and the dynamics of oxygen consumption in a microbial mat as calculated from transient oxygen microprofiles. Limnol Oceanogr.

Falkowski PG, Raven JA (2013) Aquatic Photosynthesis, 2nd ed. Princeton University Press, Princeton, NJ.

Fenchel T, Glud RN (2000) Benthic primary production and O2-CO2dynamics in a shallow-water sediment: Spatial and temporal heterogeneity. Ophelia 53:159–171.

Fodrie FJ, Rodriguez AB, Gittman RK, Grabowski JH, Lindquist NL, Peterson CH, Piehler MF, Ridge JT (2017) Oyster reefs as carbon sources and sinks. Proc R Soc B Biol Sci.

Gattuso JP, Gentili B, Duarte CM, Kleypas JA, Middelburg JJ, Antoine D (2006) Light availability in the coastal ocean: Impact on the distribution of benthic photosynthetic organisms and their contribution to primary production. Biogeosciences 3:489–513.

Gillespie PA, Maxwell PD, Rhodes LL (2000) Microphytobenthic communities of subtidal locations in New Zealand: Taxonomy, biomass, production, and food-web implications. New Zeal J Mar Freshw Res.

Glud (2008) Oxygen dynamics of marine sediments. Mar Biol Res 4:243–289.

Glud RN, Gundersen JK, Revsbech NP, Jørgensen BB (1994) Effects on the benthic diffusive boundary layer imposed by microelectrodes. Limnol Oceanogr.

Glud RN, Kühl M, Kohls O, Ramsing NB (1999) Heterogeneity of oxygen production and consumption in a photosynthetic microbial mat as studied by planar optodes. J Phycol 35:270–279.

Glud RN, Kühl M, Wenzhöfer F, Rysgaard S (2002a) Benthic diatoms of a high Arctic fjord (Young Sound, NE Greenland): Importance for ecosystem primary production. Mar Ecol Prog Ser 238:15–29.

Glud RN, Ramsing NB, Gundersen JK, Klimant I (1996) Planar optrodes: A new tool for fine scale measurements of two- dimensional O2 distribution in benthic communities. Mar Ecol Prog Ser.

Glud RN, Ramsing NB, Revsbech NP (1992) Photosynthesis and photosynthesis-coupled Respiration in Natural Biofilms Quantified with Oxygen Microsensors. J Phycol 28:51–60.

Glud RN, Rysgaard S, Kühl M (2002b) A laboratory study on O2 dynamics and photosynthesis in ice algal communities: Quantification by microsensors, O2 exchange rates, 14C incubations and a PAM fluorometer. Aquat Microb Ecol 27:301–311.

Glud RN, Woelfel J, Karsten U, Kühl M, Rysgaard S (2009) Benthic microalgal production in the Arctic: Applied methods and status of the current database. Bot Mar 52:559–571.

Grøntved J (1960) On the productivity of microbenthos and phytoplankton in some Danish fjords. Medd Dan Fisk- Havunders 3:1–17

Hammond DE, Cummins KM, Mcmanus J, Berelson WM, Smith G, Spagnoli F (2004) Methods for measuring benthic nutrient flux on the California Margin: Comparing shipboard core incubations to in situ lander results. Limnol Oceanogr Methods.

Heckman CW (1985) The Development of Vertical Migration Patterns in the Sediments of Estuaries as a Strategy for Algae to Resist Drift with Tidal Currents. Int Rev der gesamten Hydrobiol und Hydrogr.

Hope JA, Paterson DM, Thrush SF (2019) The role of microphytobenthos in soft-sediment ecological networks and their contribution to the delivery of multiple ecosystem services. J Ecol 108:815–830.

Hopes A, Mock T (2015) Evolution of Microalgae and Their Adaptations in Different Marine Ecosystems. eLS:1–9.

Jahnke RA, Nelson JR, Marinelli RL, Eckman JE (2000) Benthic flux of biogenic elements on the Southeastern US continental shelf: Influence of pore water advective transport and benthic microalgae. Cont Shelf Res 20:109–127.

Jesus B, Brotas V, Marani M, Paterson DM (2005) Spatial dynamics of microphytobenthos determined by PAM fluorescence. Estuar Coast Shelf Sci.

Kemp WM, Boynton WR, Adolf JE, Boesch DF, Boicourt WC, Brush G, Cornwell JC, Fisher TR, Glibert PM, Hagy JD, Harding LW, Houde ED, Kimmel DG, Miller WD, Newell RIE, Roman MR, Smith EM, Stevenson JC (2005) Eutrophication of Chesapeake Bay: Historical trends and ecological interactions. Mar Ecol Prog Ser.

Knap, A., A. Michaels, A. Close HD, (eds.) AD (1996) Protocols for the Joint Global Ocean Flux Study (JGOFS) Core Measurements. JGOFS Rep 19:1–170.

Kornman BA, De Deckere EMGT (1998) Temporal variation in sediment erodibility and suspended sediment dynamics in the Dollard estuary. Geol Soc Spec Publ.

Kowalski N, Dellwig O, Beck M, Grunwald M, Fischer S, Piepho M, Riedel T, Freund H, Brumsack HJ, Böttcher ME (2009) Trace metal dynamics in the water column and pore waters in a temperate tidal system: response to the fate of algae-derived organic matter. Ocean Dyn.

Krause-Jensen D, Markager S, Dalsgaard T (2012) Benthic and Pelagic Primary Production in Different Nutrient Regimes. Estuaries and Coasts 35:527–545.

Kritzer JP, DeLucia MB, Greene E, Shumway C, Topolski MF, Thomas-Blate J, Chiarella LA, Davy KB, Smith K (2016) The Importance of Benthic Habitats for Coastal Fisheries. Bioscience.

Kühl M (2005) Optical microsensors for analysis of microbial communities. Methods Enzymol 397:166–199.

Kühl M, Glud RN, Borum J, Roberts R, Rysgaard S (2001) Photosynthetic performance of surface-associated algae below sea ice as measured with a pulse-amplitude-modulated (PAM) fluorometer and O2 microsensors. 223:1–14.

Kühl M, Glud RN, Ploug H, Ramsing NB (1996) Photosynthesis-Coupled Respiration in an. J Phycol 32:799–812.

Kühl M, Lassen C, Revsbech NP (1997) A simple light meter for measurements of PAR (400 to 700 nm) with fiber-optic microprobes: Application for P vs E0(PAR) measurements in a microbial mat. Aquat Microb Ecol 13:197–207.

Light BR, Beardall J (2001) Photosynthetic characteristics of sub-tidal benthic microalgal populations from a temperate, shallow water marine ecosystem. Aquat Bot 70:9–27.

MacIntyre HL, Geider RJ, Miller DC, Shallow E, Science W, Jun MC, Miller DC (1996) Microphytobenthos : The Ecological Role of the " Secret Garden " of Unvegetated , Shallow- Water Marine Habitats . I . Distribution , Abundance and Primary Production Source : Estuaries , Vol . 19 , No . 2 , Part A : Selected Papers from the First Annual. Estuaries 19:186–201.

Mayer LM, Townsend DW, Pettigrew NR, Loder TC, Wong MW, Kristen-Morris D, Laursen AK, Schoudel AD, Conairis C, Brown J, Newell C (1996) The Kennebec, Sheepscot, and Damariscotta River Estuaries: Seasonal Oceanographic Data. 1–110.

McMinn A, Ashworth C, Bhagooli R, Martin A, Salleh S, Ralph P, Ryan K (2012) Antarctic coastal microalgal primary production and photosynthesis. Mar Biol 159:2827–2837.

Middelburg JJ, Barranguet C, Boschker HTS, Herman PMJ, Moens T, Heip CHR (2000) The fate of intertidal microphytobenthos carbon: An in situ 13C-labeling study. Limnol Oceanogr.

Mills KE, Pershing AJ, Brown CJ, Chen Y, Chiang FS, Holland DS, Lehuta S, Nye JA, Sun JC, Thomas AC, Wahle RA (2013) Fisheries management in a changing climate: Lessons from the 2012 ocean heat wave in the Northwest Atlantic. Oceanography 26.

Mitbavkar S, Anil AC (2002) Diatoms of the microphytobenthic community: Population structure in a tropical intertidal sand flat. Mar Biol 140:41–57.

Moreno S, Niell FX (2004) Scales of variability in the sediment chlorophyll content of the shallow Palmones River Estuary, Spain. Estuar Coast Shelf Sci.

Morioka H, Kasai A, Miyake Y, Kitagawa T, Kimura S (2017) Food composition for blue mussels (Mytilus edulis) in the Menai Strait, UK, based on physical and biochemical analyses. J Shellfish Res.

Murrell MC, Campbell JG, Hagy JD, Caffrey JM (2009) Effects of irradiance on benthic and water column processes in a Gulf of Mexico estuary: Pensacola Bay, Florida, USA. Estuar Coast Shelf Sci 81:501–512.

Ní Longphuirt S, Clavier J, Grall J, Chauvaud L, Le Loc'h F, Le Berre I, Flye-Sainte-Marie J, Richard J, Leynaert A (2007) Primary production and spatial distribution of subtidal microphytobenthos in a temperate coastal system, the Bay of Brest, France. Estuar Coast Shelf Sci 74:367–380.

Nielsen ES, Hansen VK (1958) Measurements with the carbon-14 technique of the respiration rates in natural populations of phytoplankton. Deep Sea Res.

Parsons TR, Maita Y, Lalli CM (1984) A Manual of Chemical & Biological Methods for Seawater Analysis.

Pinckney J, Zingmark RG (1991) Effects of tidal stage and sun angles on intertidal benthic microalgal productivity. Mar Ecol Prog Ser.

Pinckney JL, Tomas C, Greenfield DI, Reale-Munroe K, Castillo B, Hillis-Starr Z, Van Meerssche E, Zimberlin M (2018) Seasonal changes in phytoplankton community structure in a bioluminescent lagoon, st. Croix, US virgin islands. Aquat Microb Ecol 81:109–124.

Platt T, Gallegos CL (1980) Modelling Primary Production. In: *Primary Productivity in the Sea*.

Rabouille C, Denis L, Dedieu K, Stora G, Lansard B, Grenz C (2003) Oxygen demand in coastal marine sediments: Comparing in situ microelectrodes and laboratory core incubations. In: *Journal of Experimental Marine Biology and Ecology*.

Revsbech NP, Jørgensen BB (1983) Photosynthesis of benthic microflora measured with high spatial resolution by the oxygen microprofile method: Capabilities and limitations of the method. Limnol Oceanogr 28:749–756.

Revsbech NP, Jørgensen BB, Brix O (1981) Primary production of microalgae in sediments measured by oxygen microprofile, H14CO3 - fixation, and oxygen exchange methods. Limnol Oceanogr.

Rodil IF, Attard KM, Norkko J, Glud RN, Norkko A (2019) Towards a sampling design for characterizing habitat-specific benthic biodiversity related to oxygen flux dynamics using Aquatic Eddy Covariance. PLoS One 14:1–21.

Salleh S, McMinn A (2011) Photosynthetic response and recovery of Antarctic marine benthic microalgae exposed to elevated irradiances and temperatures. Polar Biol 34:855–869.

Santema M, Huettel M (2018) Dynamics of microphytobenthos photosynthetic activity along a depth transect in the sandy northeastern Gulf of Mexico shelf. Estuar Coast Shelf Sci 212:273–285.

Snelgrove PVR, Soetaert K, Solan M, Thrush S, Wei CL, Danovaro R, Fulweiler RW, Kitazato H, Ingole B, Norkko A, Parkes RJ, Volkenborn N (2018) Global Carbon Cycling on a Heterogeneous Seafloor. Trends Ecol Evol 33:96–105.

Sospedra J, Falco S, Morata T, Gadea I, Rodilla M (2015) Benthic fluxes of oxygen and nutrients in sublittoral fine sands in a north-western Mediterranean coastal area. Cont Shelf Res 97:32–42.

Sun MY, Aller RC, Lee C (1994) Spatial and temporal distributinos of sedimentary chloropigments as indicators of benthic processes in Long Island Sound. JMarRes 52:149–176.

Sundbäck K, Jönsson B (1988) Microphytobenthic productivity and biomass in sublittoral sediments of a stratified bay, southeastern Kattegat. J Exp Mar Bio Ecol.

Tang T, Tang T, Tan L, Gu Y, Jiang W, Cai Q (2017) Identifying community thresholds for lotic benthic diatoms in response to human disturbance. Sci Rep 7:1–10.

Testa JM, Brady DC, Cornwell JC, Owens MS, Sanford LP, Newell CR, Suttles SE, Newell RIE (2015) Modeling the impact of floating oyster (Crassostrea virginica) aquaculture on sediment-water nutrient and oxygen fluxes. Aquac Environ Interact 7:205–222.

Thompson B, Perry MJ, Davis C (2006) Phytoplankton in the Damariscotta River Estuary. Mar Res Focus 3:1–4.

Tolhursf TJ, Gust G, Paterson DM (2002) The influence of an extracellular polymeric substance (EPS) on cohesive sediment stability. In: *Proceedings in Marine Science*.

Underwood GJC, Kromkamp J (1999) Primary Production by Phytoplankton and Microphytobenthos in Estuaries. Adv Ecol Res 29:93–153.

Vadeboncoeur Y, Kalff J, Christoffersen K, Jeppesen E (2006) Substratum as a driver of variation in periphyton chlorophyll and productivity in lakes. J North Am Benthol Soc.

Vilbaste S, Sundbäck K, Nilsson C, Truu J (2000) Distribution of benthic diatoms in the littoral zone of the gulf of riga, the baltic sea. Eur J Phycol 35:373–385.

Wenzhöfer F, Glud RN (2004) Small-scale spatial and temporal variability in coastal benthic O 2 dynamics: Effects of fauna activity. Limnol Oceanogr.

Wenzhöfer F, Holby O, Glud RN, Nielsen HK, Gundersen JK (2000) In situ microsensor studies of a shallow water hydrothermal vent at Milos, Greece. Mar Chem 69:43–54.

Zhao C, Daewel U, Schrum C (2019) Tidal impacts on primary production in the North Sea. Earth Syst Dyn 10:287–317.

APPENDIX A

TOTAL OXYGEN EXCHANGE

A.1 Raw Oxygen with Experimental Light

Raw O_2 concentrations in mg L^{-1} measured every 5 minutes in the overlying water for the TOE whole core incubations for each experiment done in the summer of 2019. This was done for each site along the transect with 3 replication cores along with the corresponding experimental light levels recorded using a PME miniPAR sensor in the tank with core next to core 1.

A.1.1 West Deep Site

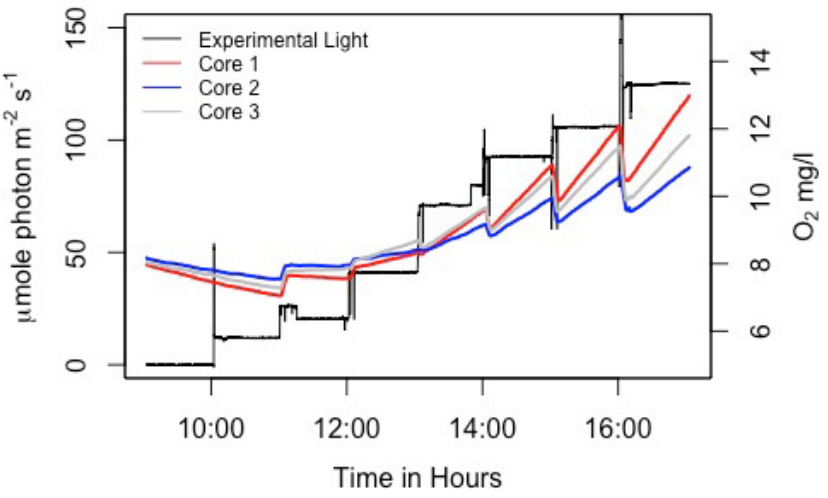

Figure A.1: *West Deep Site (June 25th, 2019) TOE raw oxygen concentration in mg L^{-1} for all 8 different intervals of light with three replication sediment cores. In black the corresponding light levels from the experiment in a core next to replication sediment core 1.*

A.1.2 East Shallow Site

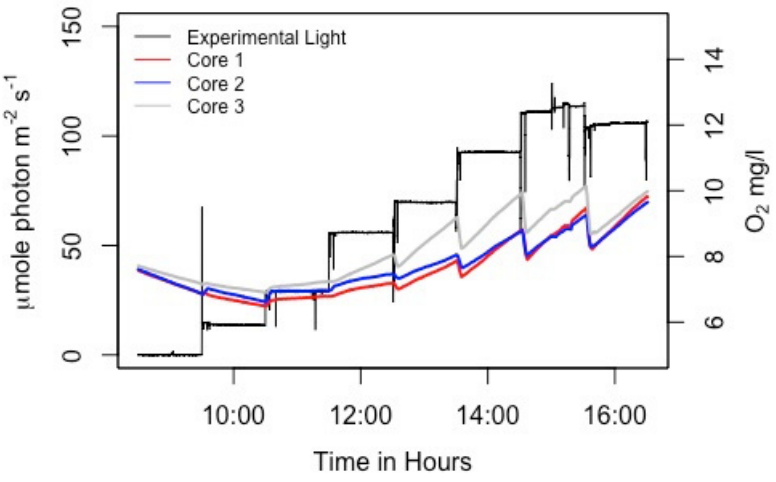

Figure A.2: *East Shallow Site (July 11th, 2019) TOE raw oxygen concentration in mg L^{-1} for all 8 different intervals of light with three replication sediment cores. In black the corresponding light levels from the experiment in a core next to replication sediment core 1.*

A.1.3 East Deep Site

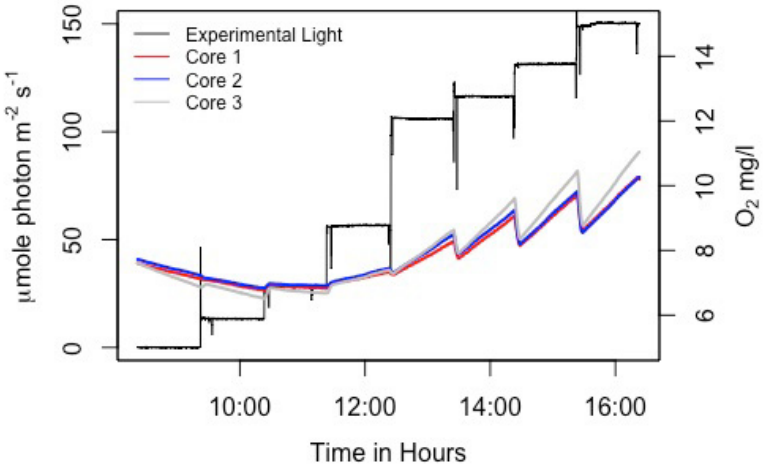

Figure A.3: *East Deep Site (July 23rd, 2019) TOE raw oxygen concentration in mg L^{-1} for all 8 different intervals of light with three replication sediment cores. In black the corresponding light levels from the experiment in a core next to replication sediment core 1.*

A.1.4 West Shallow Site

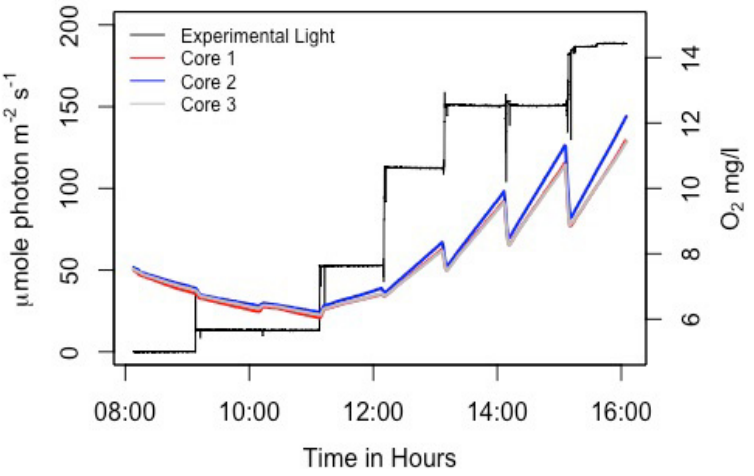

Figure A.4: *West Shallow Site (July 31st, 2019) TOE raw oxygen concentration in mg L^{-1} for all 8 different intervals of light with three replication sediment cores. In black the corresponding light levels from the experiment in a core next to replication sediment core 1.*

A.1.5 Middle of Channel Site

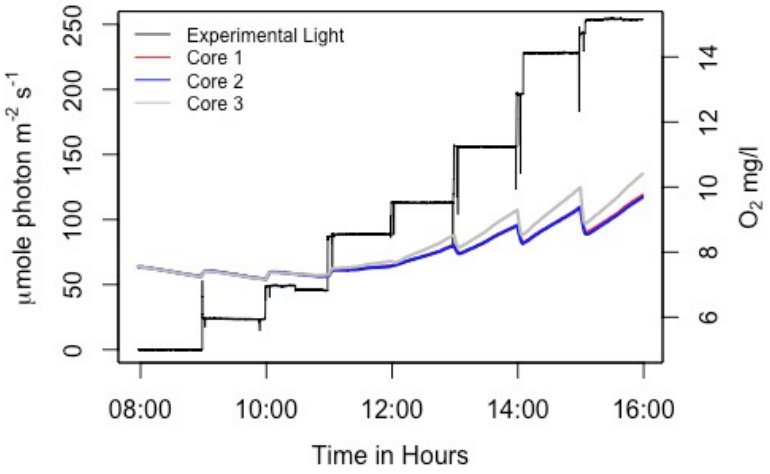

Figure A.5: Middle of Channel Site (August 13th, 2019) TOE raw oxygen concentration in mg L^{-1} for all 8 different intervals of light with three replication sediment cores. In black the corresponding light levels from the experiment in a core next to replication sediment core 1.

APPENDIX B

DIFFUSIVE OXYGEN EXCHANGE

B.1 Oxygen Microprofiles

Oxygen microsensor profiles for each DOE experiment done in summer 2019 for each site along the transect in the DRE is presented below. Three replication O_2 profiles were measured after each light interval in three different locations. The diffusive O_2 flux based on the curvature of the profiles was calculated for each profile based on the Berg et al. (1998) method to establish a diffusive PE relationship.

B.1.1 West Deep Site

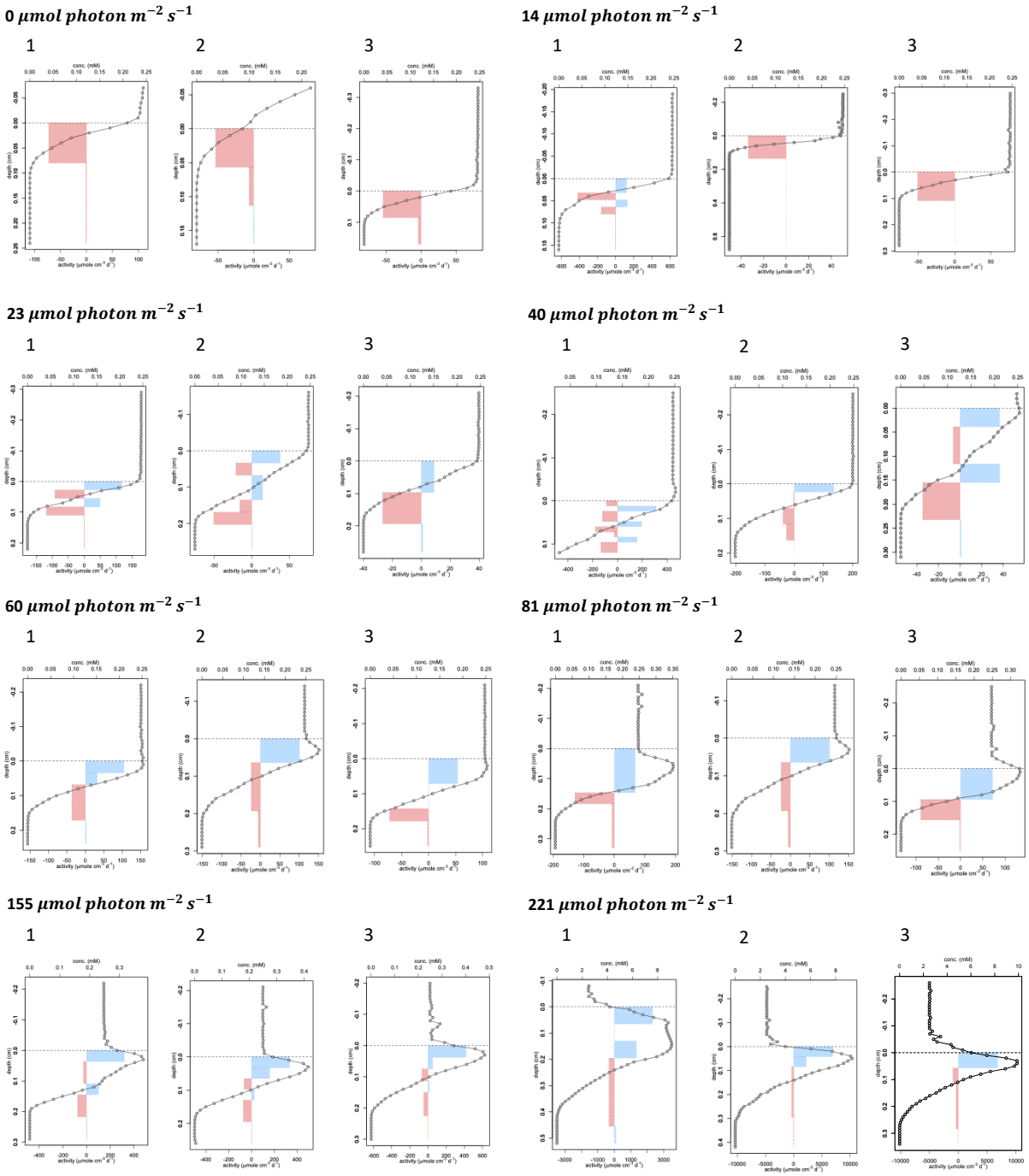

Figure B.1: West Deep Site (June 25th, 2019) DOE raw oxygen microprofiles in O_2 concentration with depth in cm with the activity of each section in μmol cm^{-3} d^{-1} for all 8 different intervals of light with three replication profiles. Profile activity separated into consumption in red and production in blue. Profile Dark replication 2 was not used.

B.1.2 East Shallow Site

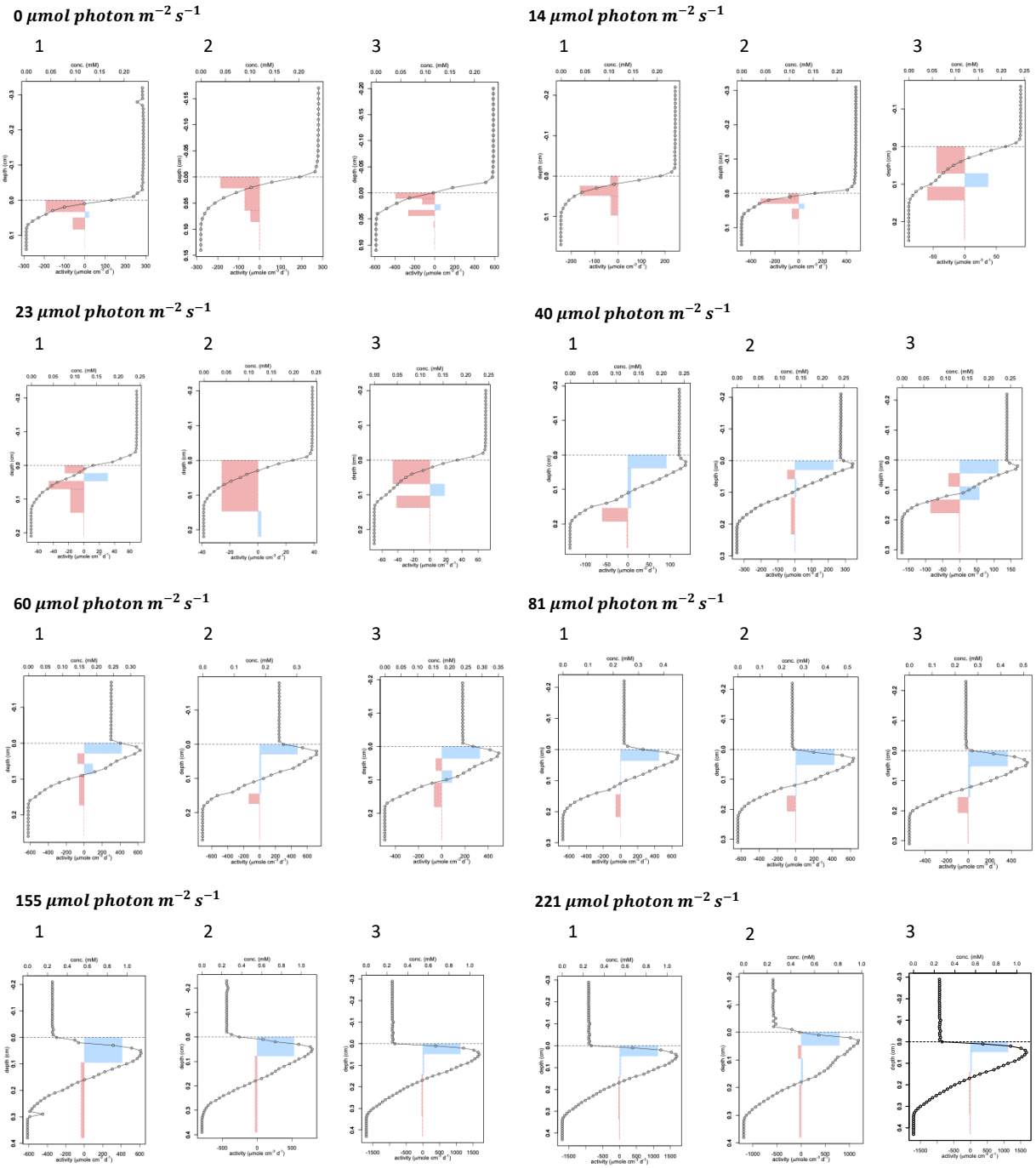

Figure B.2: East Shallow Site (July 11th, 2019) DOE raw oxygen microprofiles in O_2 concentration with depth in cm with the activity of each section in μmol cm^{-3} d^{-1} for all 8 different intervals of light with three replication profiles. Profile activity separated into consumption in red and production in blue.

B.1.3 East Deep Site

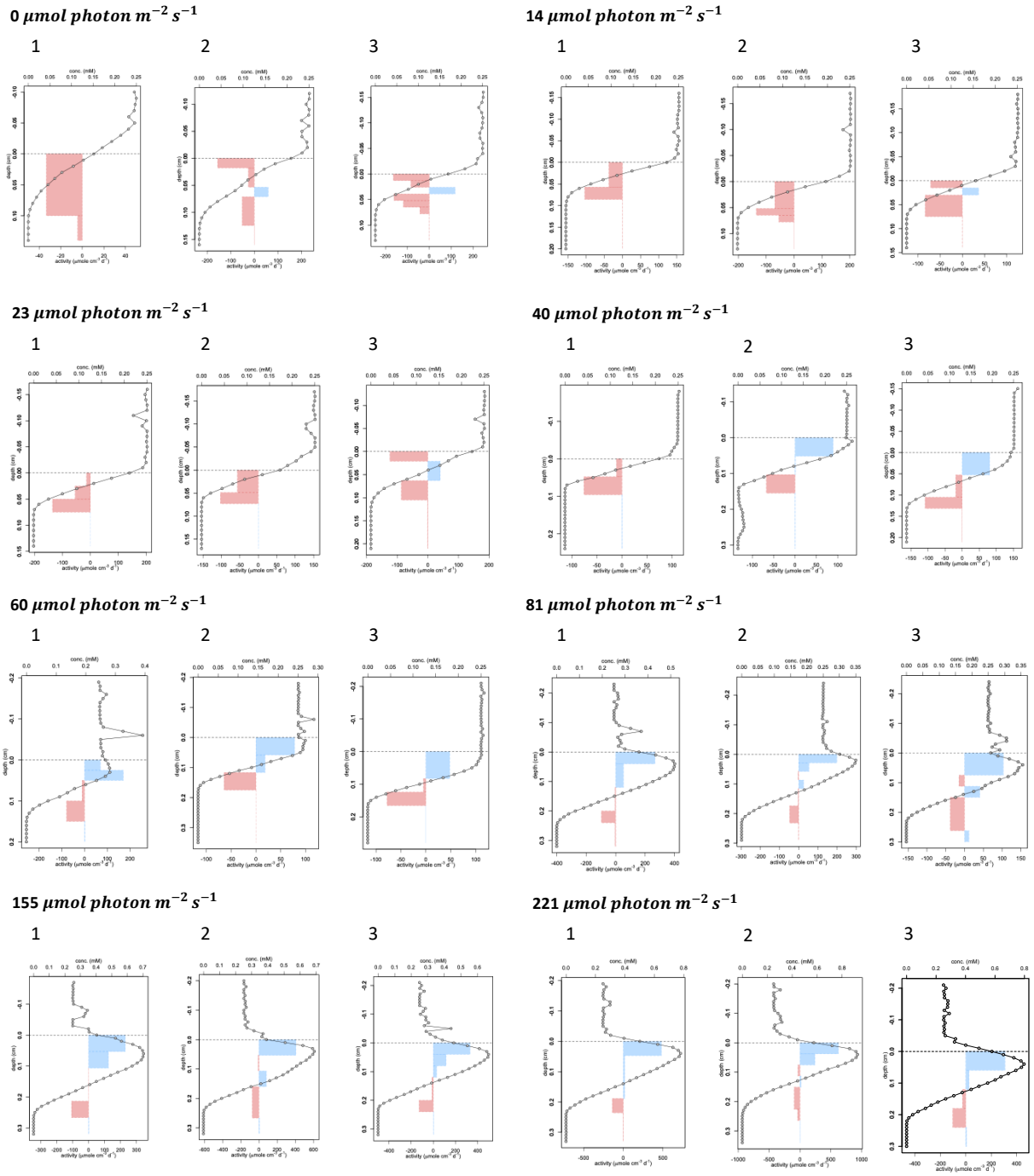

Figure B.3: East Deep Site (July 23rd, 2019) DOE raw oxygen microprofiles in O_2 concentration with depth in cm with the activity of each section in $\mu mol\ cm^{-3}\ d^{-1}$ for all 8 different intervals of light with three replication profiles. Profile activity separated into consumption in red and production in blue.

B.1.4 West Shallow Site

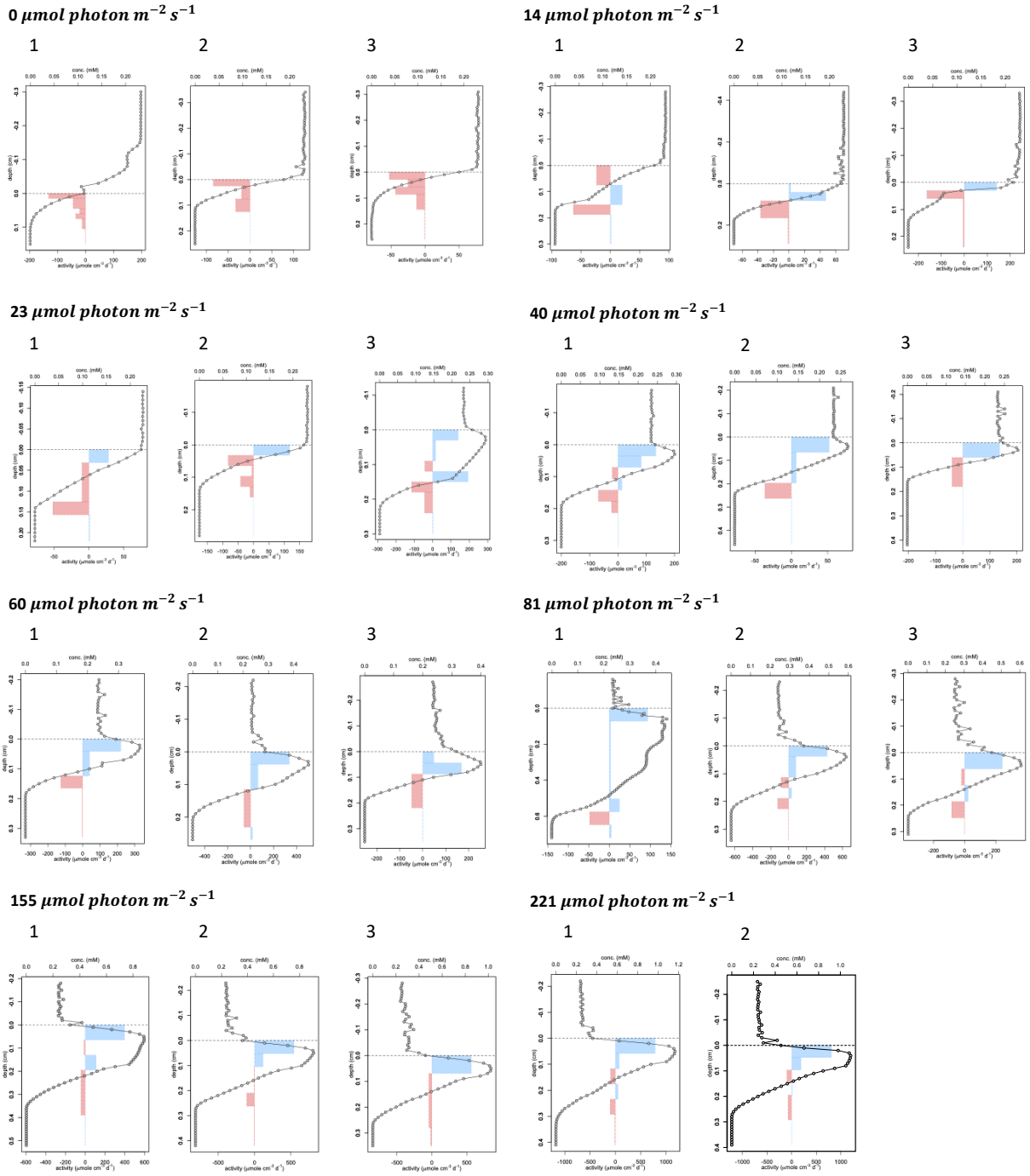

Figure B.4: West Shallow Site (July 31st, 2019) DOE raw oxygen microprofiles in O_2 concentration with depth in cm with the activity of each section in μmol cm^{-3} d^{-1} for all 8 different intervals of light with three replication profiles. Profile activity separated into consumption in red and production in blue. Profile 23 μmol photons m^{-2} s^{-1} replication 3 did not include.

B.1.5 Middle of Channel Site

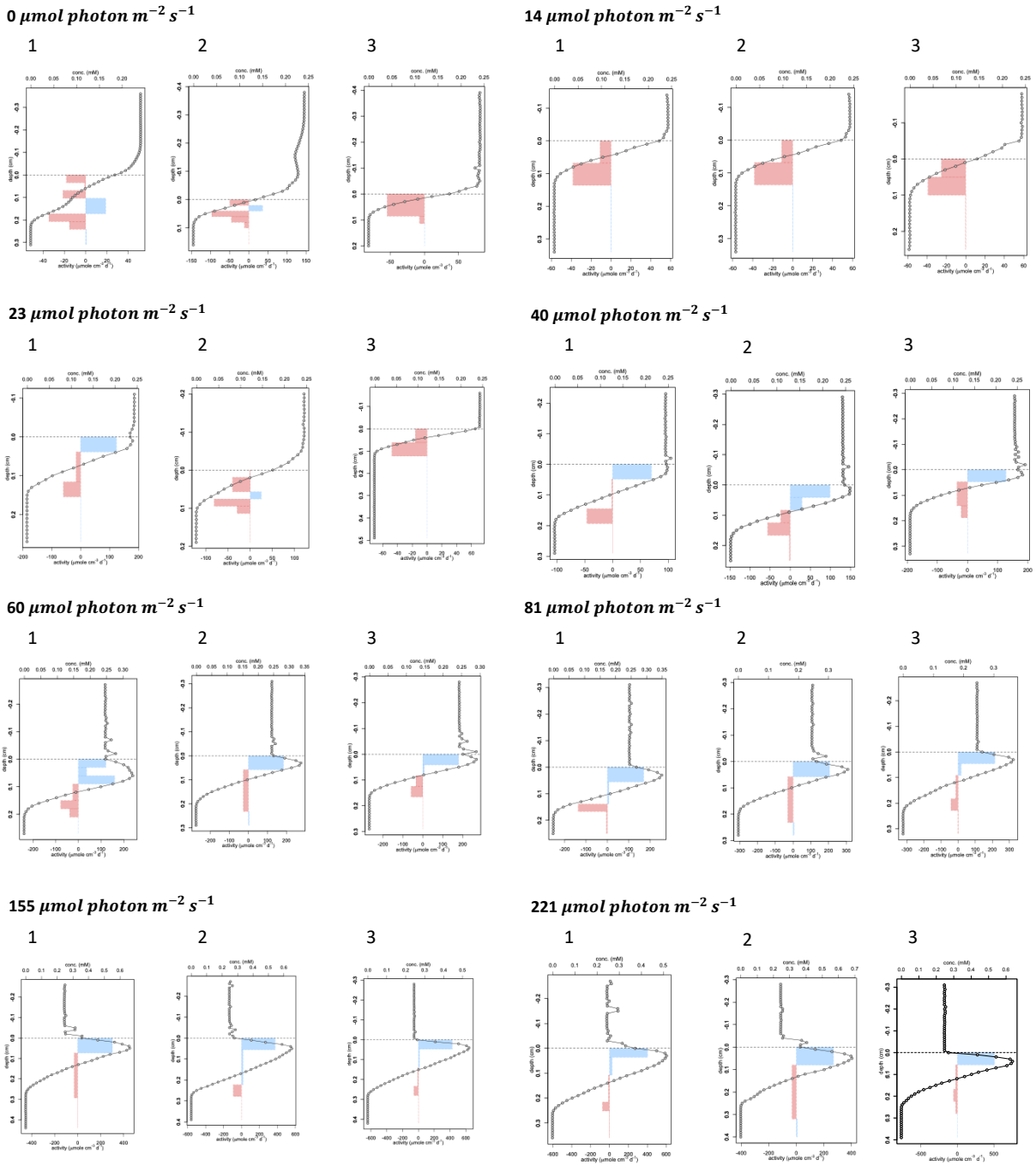

Figure B.5: Middle of Channel Site (August 13th, 2019) DOE raw oxygen microprofiles in O_2 concentration with depth in cm with the activity of each section in μmol cm^{-3} d^{-1} for all 8 different intervals of light with three replication profiles. Profile activity separated into consumption in red and production in blue.

APPENDIX C

EXPERIMENTAL LIGHT

C.1 TOE Tank Light Test

Light in the TOE whole core incubation tank was tested once all experiments during the summer of 2019 were completed. Testing of the light in the tank was done because the light levels during the experiments did not match the pre-experimental light levels tested for the experiments. The light level methods that were done before the experiments were completed the same during the experiments with the PME miniPAR sensor next to core 1 instead of in core 1. The light level methods were repeated after the completion of the experiments in fall 2019 to determine the error.

After the examination of the tested light levels to the original and experimental it was determined that the error between the light levels was only significant for the last light level where the largest difference between light was observed (Fig. C.1.1-5). Therefore, a correction factor was determined for the highest light level and the experimental light levels plus the corrected highest level was used for the PE relationship curves for each site.

C.1.1 West Deep Site

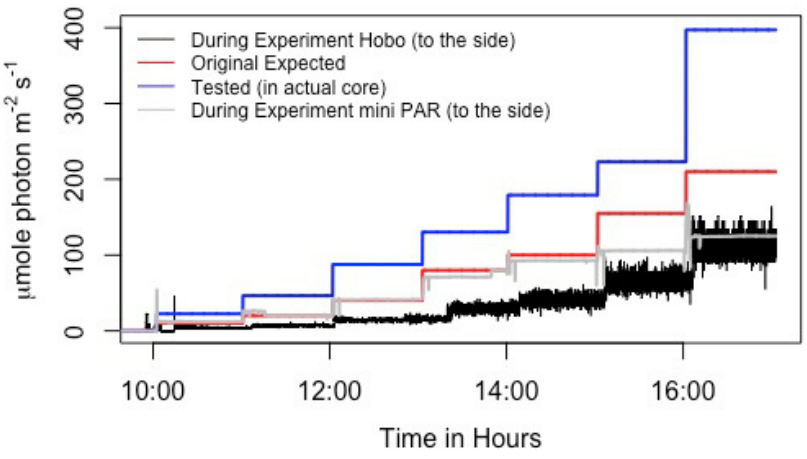

Figure C.1: West Deep (June 25th) experimental light with the original expected light, the light during the experiment from the miniPAR logger beside sediment core 1 and hobo logger that was between core 1 and 2 from summer 2019, and the tested light from fall of 2019.

C.1.2 East Shallow Site

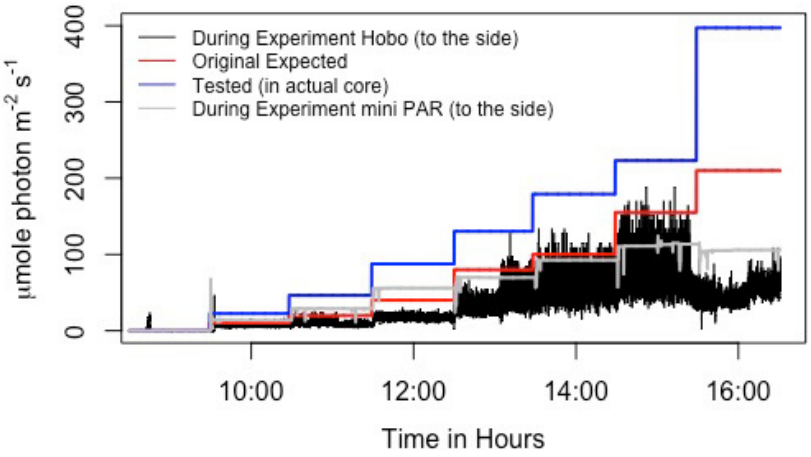

Figure C.2: East Shallow (July 12th) experimental light with the original expected light, the light during the experiment from the miniPAR logger beside sediment core 1 and hobo logger that was between core 1 and 2 from summer 2019, and the tested light from fall of 2019.

C.1.3 East Deep Site

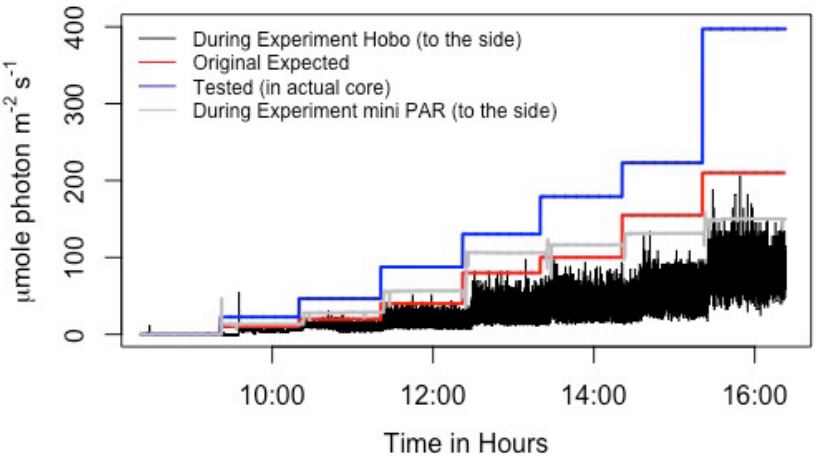

Figure C.3: East Deep (July 23rd) experimental light with the original expected light, the light during the experiment from the miniPAR logger beside sediment core 1 and hobo logger that was between core 1 and 2 from summer 2019, and the tested light from fall of 2019.

C.1.4 West Shallow Site

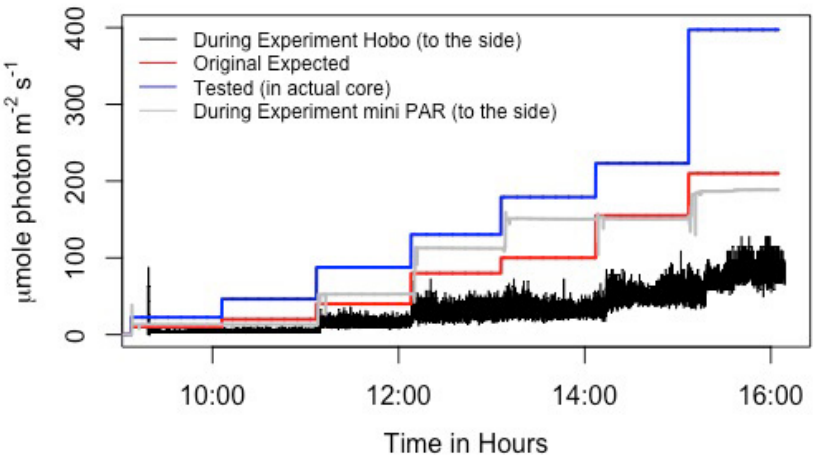

Figure C.4: West Shallow (July 31st) experimental light with the original expected light, the light during the experiment from the miniPAR logger beside sediment core 1 and hobo logger that was between core 1 and 2 from summer 2019, and the tested light from fall of 2019.

C.1.5 Middle of Channel Site

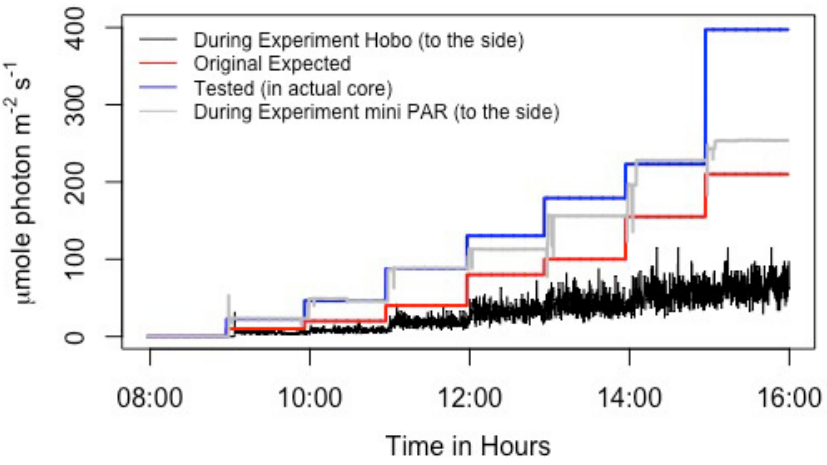

Figure C.5: Middle of channel (August 13th) experimental light with the original expected light, the light during the experiment from the miniPAR logger beside sediment core 1 and hobo logger that was between core 1 and 2 from summer 2019, and the tested light from fall of 2019.

C.2 DOE Tank Light Test

Light in the DOE microprofiling tank was tested once all experiments during the summer of 2019 were completed just like the TOE light levels. Testing of the light in the DOE tank was done because of the error in the TOE tank. The light level methods that were done before the experiments were completed the same during the experiments with only a Hobo logger in the DOE tank because the miniPAR logger would not fit in the tank while profiling was occurring. The light level methods were repeated after the completion of the experiments in fall 2019 to determine the error. After the examination of the tested light levels, it was observed that the tested and the original were similar and the during experimental Hobo was inaccurate due to the aeration in the tank scatter light over the Hobo and the position of the sensor created shadowing.

C.2.1 West Deep Site

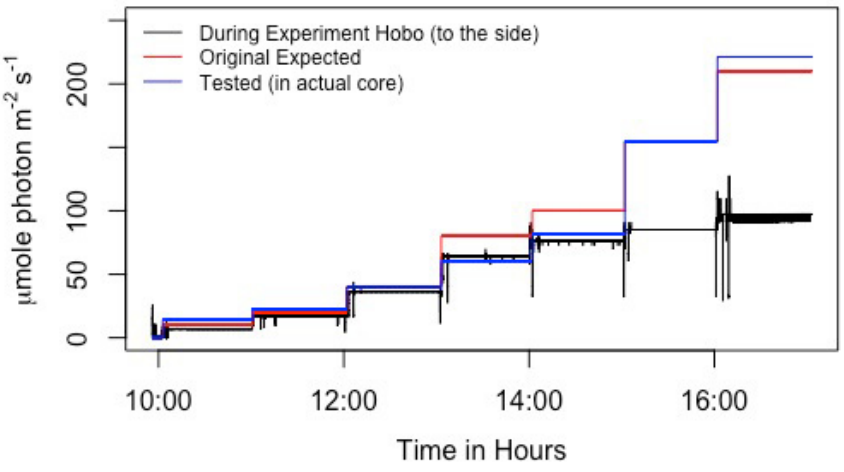

Figure C.6: West Deep (June 25th) experimental light with the original expected light, the light during the experiment from the hobo logger from summer 2019 and the tested light from fall 2019.

C.2.2 East Shallow Site

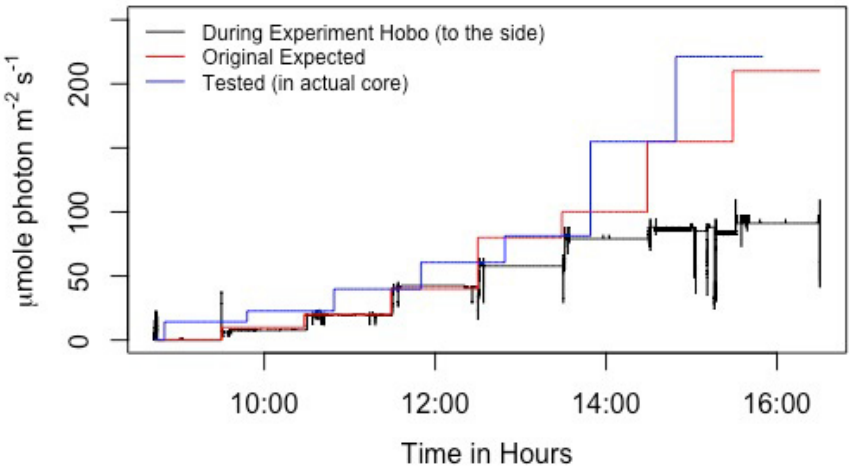

Figure C.7: East Shallow (July 12th) experimental light with the original expected light, the light during the experiment from the hobo logger from summer 2019 and the tested light from fall 2019.

C.2.3 East Deep Site

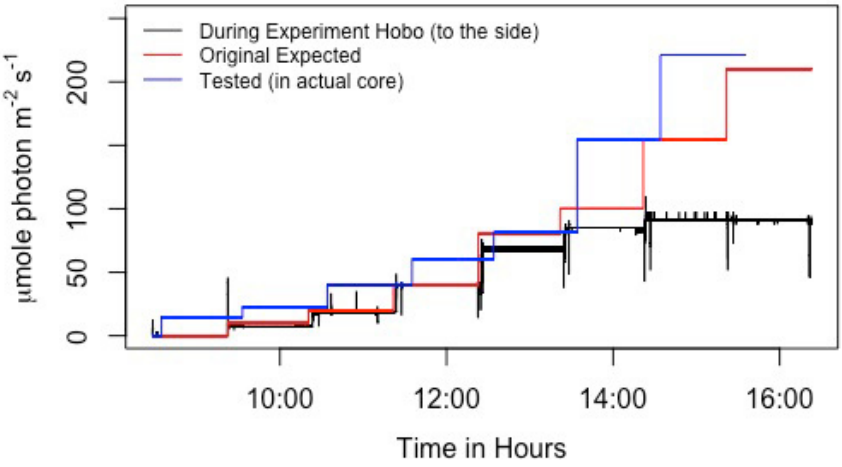

Figure C.8: East Deep (July 23rd) experimental light with the original expected light, the light during the experiment from the hobo logger from summer 2019 and the tested light from fall 2019.

C.2.4 West Shallow Site

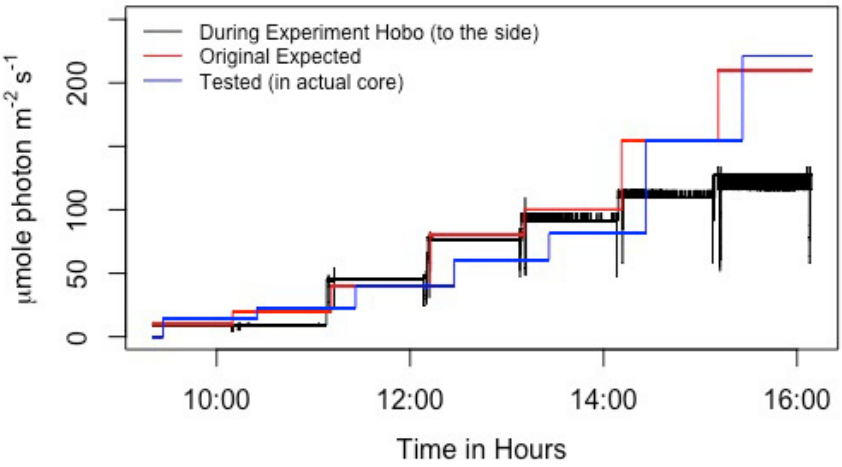

Figure C.9: West Shallow (July 31st) experimental light with the original expected light, the light during the experiment from the hobo logger from summer 2019 and the tested light from fall 2019.

C.2.5 Middle of Channel Site

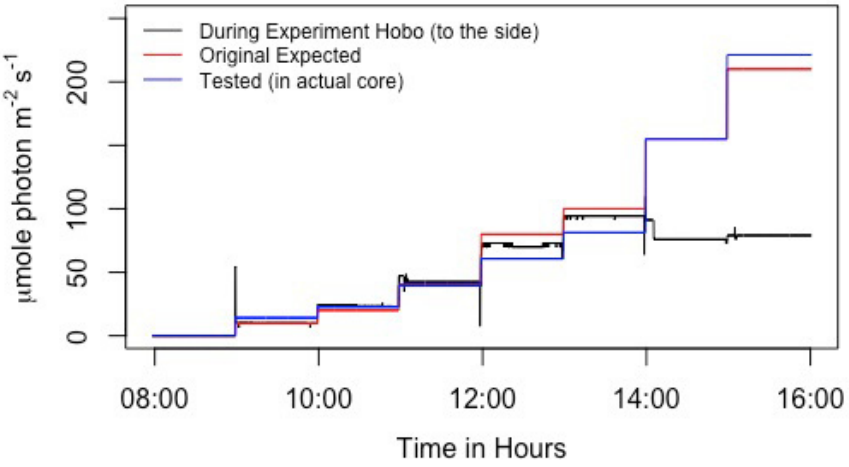

Figure C.10: Middle of channel (August 13th) experimental light with the original expected light, the light during the experiment from the hobo logger from summer 2019 and the tested light from fall 2019.

APPENDIX D

IN SITU LIGHT

D.1 Water Column Profiles

Water column light profiles taken at each site during the summer of 2019. The west side sites were done at low tide and east at high tide. The middle of the channel site was done at both low and high tide. This was done to determine the attenuation value for the water column at the sites to calculate the bottom irradiance level based on surface light readings. The profiles were exponentially fitted, and average low and high tide coefficients were determined.

D.1.1 East and West Side Sites

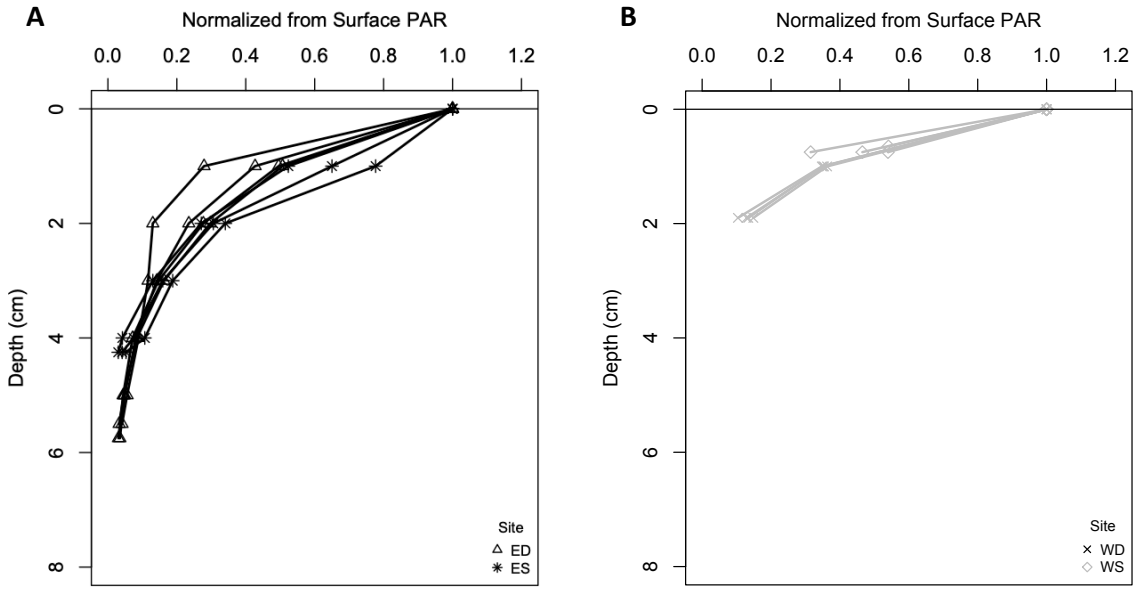

Figure D.1: (A) East side of the channel sites light with depth water column profiles done during high tide on July 18th, 2019 for both the shallow and deep. (B) West side of the channel sites light with depth water column profiles done during low tide on August 9th, 2019 for both the shallow and deep.

D.1.2 Middle of Channel Site

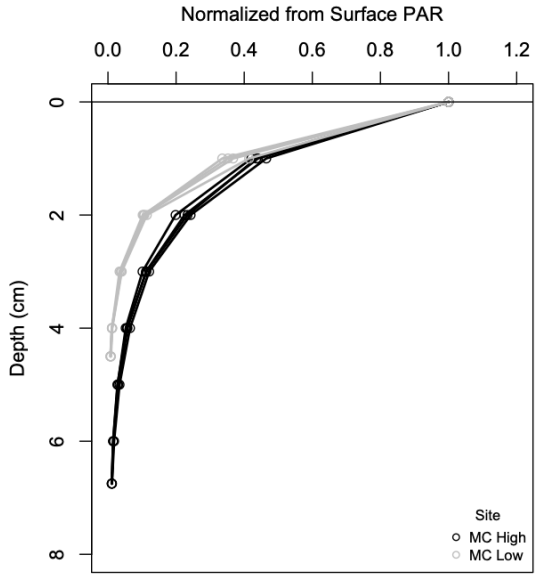

Figure D.2: Middle of the channel site light with depth water column profiles done on two separate days. Low tide was measured on August 9th, 2019 and high tide was measured on August 12th, 2019 the core sampling day of the site.

D.1.3 All Sites

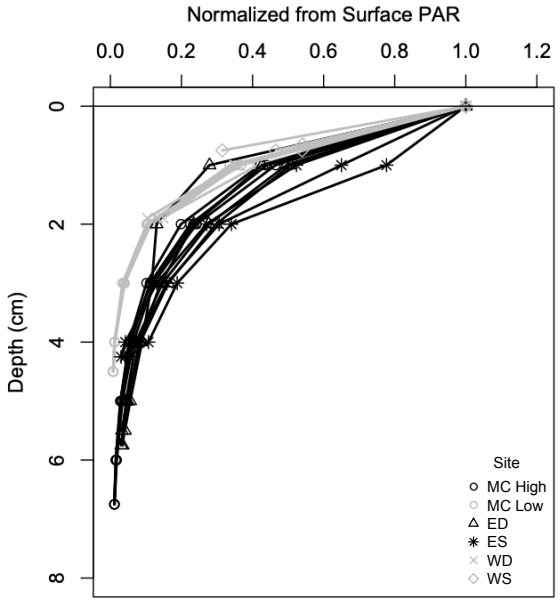

Figure D.3: All of the Light with depth water column profiles done across the transect to determine the attenuation coefficient. Profiles in black are ones taken at high tide and ones in grey are from low tide. Average low and high tide coefficients where determined based off these profiles of the water column to calculate the bottom irradiance.

APPENDIX E

BENTHIC ESTIMATES

E.1 Parameters and NCP Calculation

In situ water depth, attenuation coefficient and surface irradiance values used to calculate the benthic NCP. The hourly surface irradiance recorded by the LOBO buoy used to calculate the downwelling irradiance at the sediment level combined with the k_{par} and water depth. The k_{par} hourly values calculated from the *in situ* water column profiles in Appendix D. Water depth was determined from the NOAA tide and currents buoy (Walpole, Damariscotta River, ME, 43°56.0 N, 69°34.8 W).

E.1.1 West Deep Site

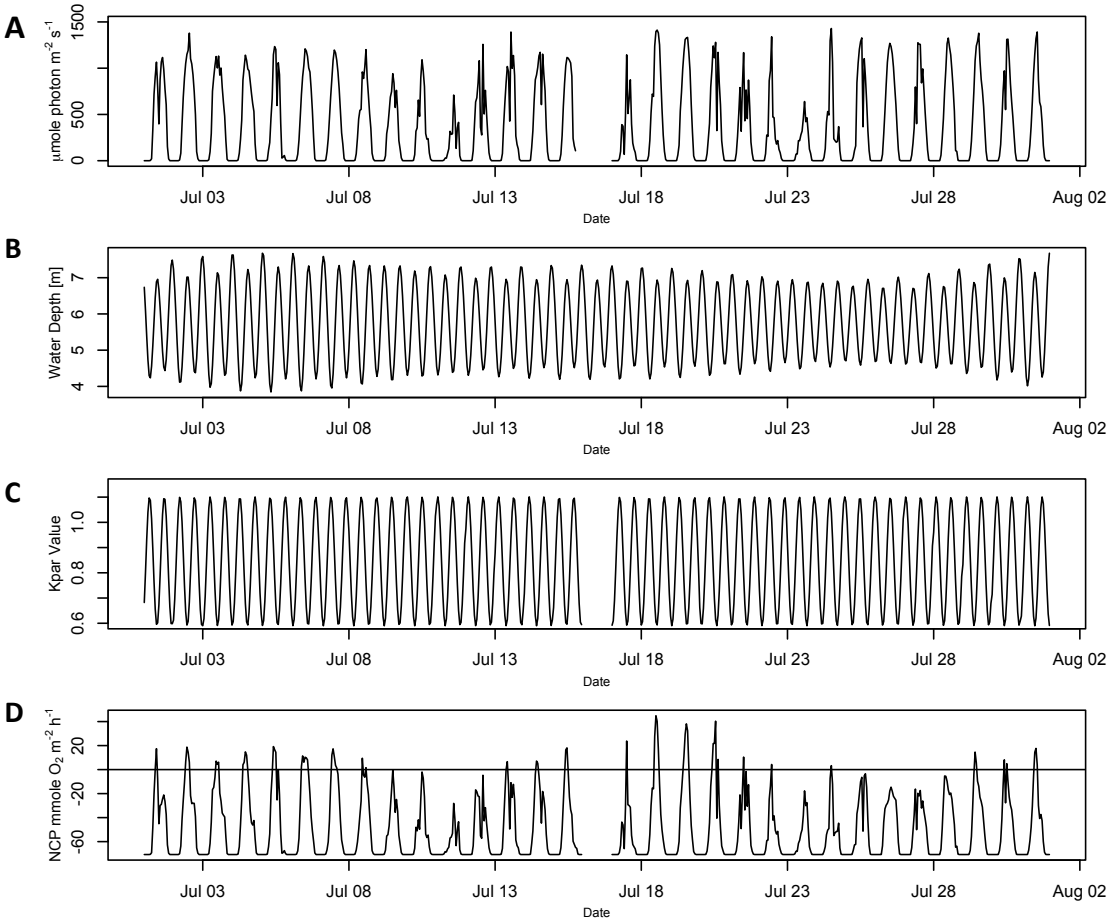

Figure E.1: In situ hourly values from the month of July used to calculate the NCP for site West Deep (WD). (A) is the irradiance at the surface of the water, (B) is the water depth at the specific site and (C) is the attenuation value calculated. (D) is the calculated NCP for site west shallow for the month of July. July 16th missing for plot (A), (C) and (D) due to Lobo buoy cleaning.

E.1.2 East Shallow Site

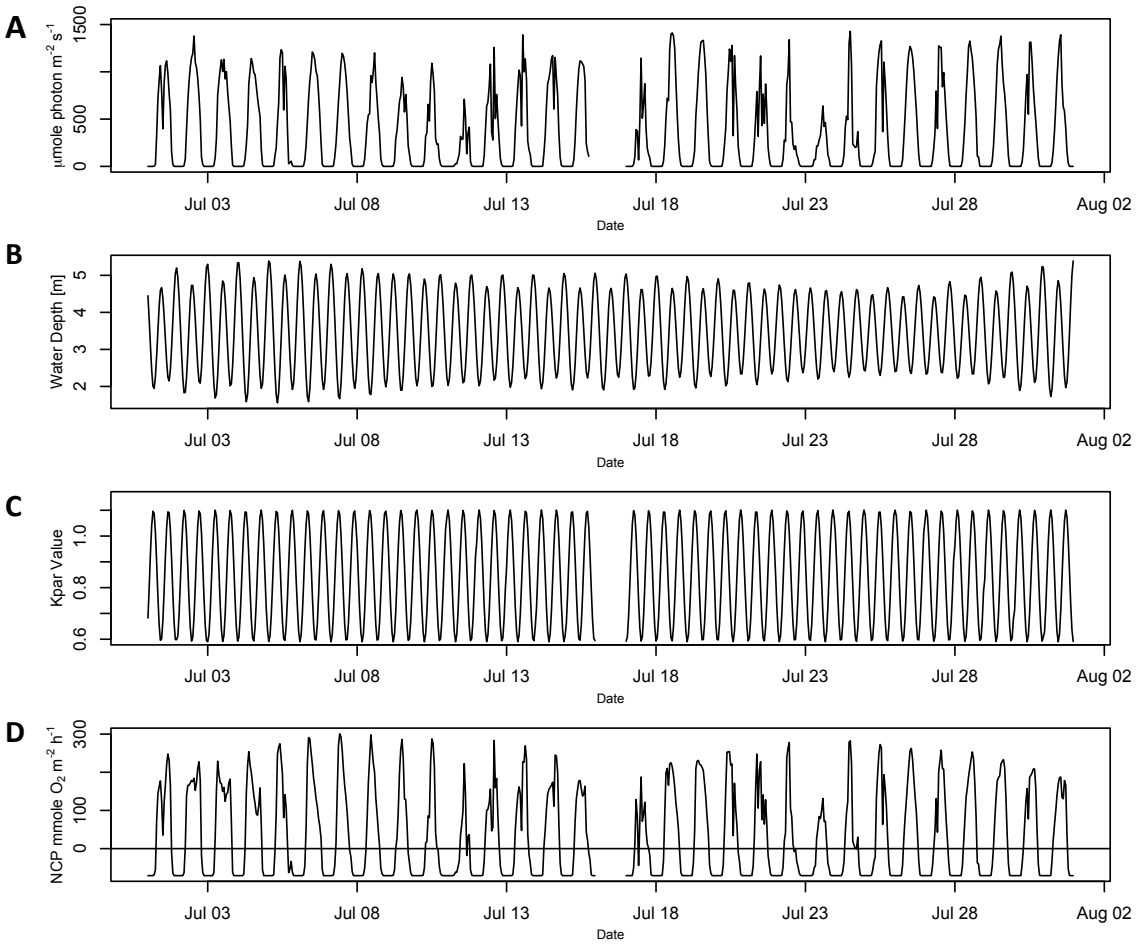

Figure E.2: In situ hourly values from the month of July used to calculate the NCP for site East Shallow (ES). (A) is the irradiance at the surface of the water, (B) is the water depth at the specific site and (C) is the attenuation value calculated. (D) is the calculated NCP for site west shallow for the month of July. July 16th missing for plot (A), (C) and (D) due to Lobo buoy cleaning.

E.1.3 East Deep Site

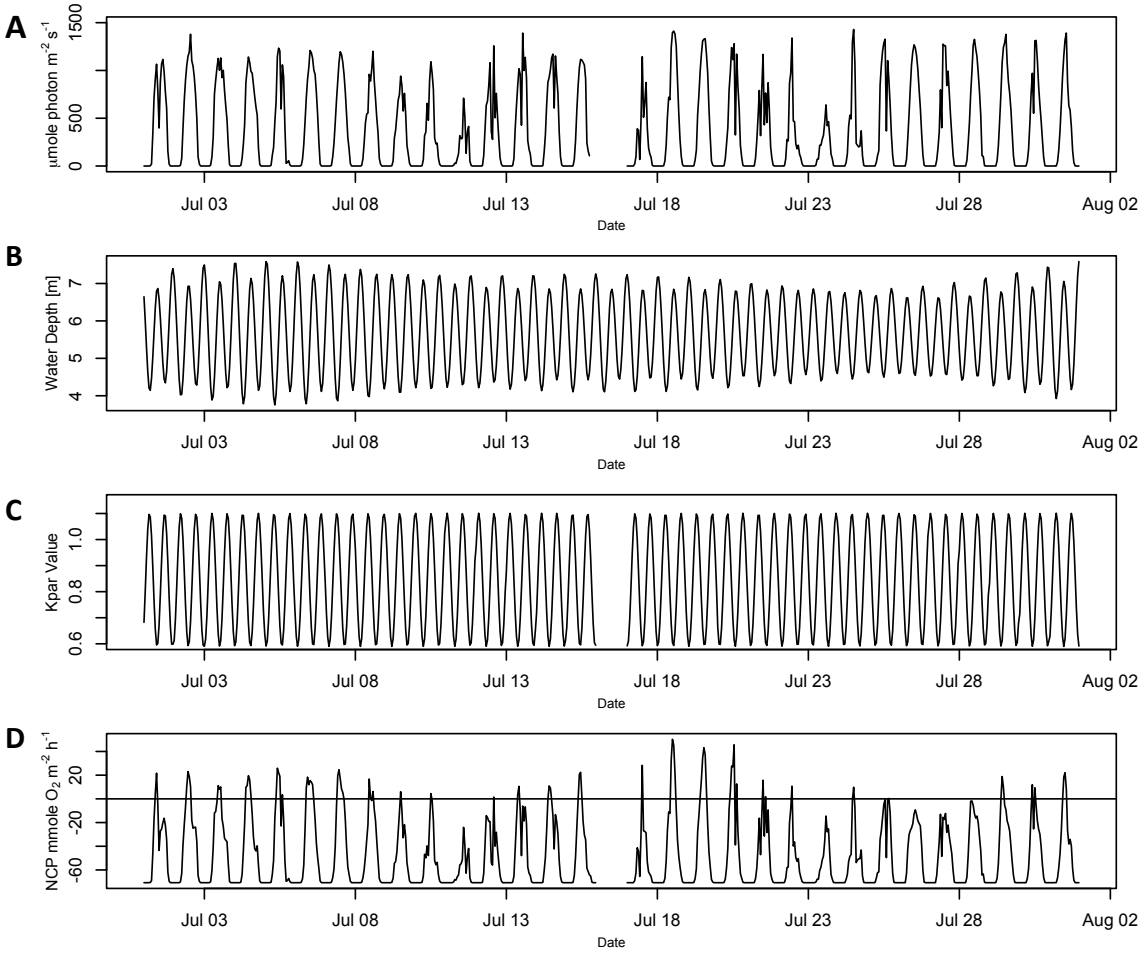

Figure E.3: In situ hourly values from the month of July used to calculate the NCP for site East Deep (ED). (A) is the irradiance at the surface of the water, (B) is the water depth at the specific site and (C) is the attenuation value calculated. (D) is the calculated NCP for site west shallow for the month of July. July 16th missing for plot (A), (C) and (D) due to Lobo buoy cleaning.

E.1.4 West Shallow Site

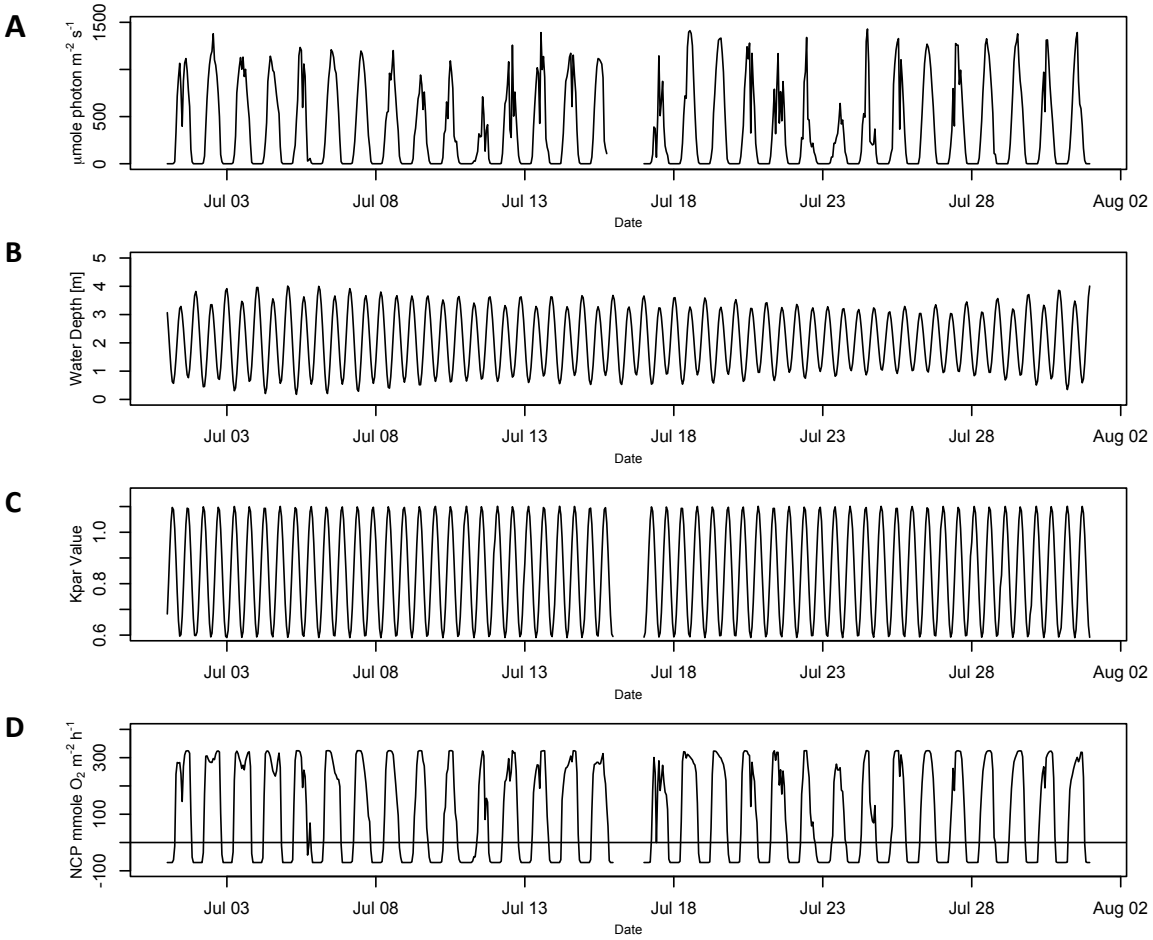

Figure E.4: In situ hourly values from the month of July used to calculate the NCP for site West Shallow (WS). (A) is the irradiance at the surface of the water, (B) is the water depth at the specific site and (C) is the attenuation value calculated. (D) is the calculated NCP for site west shallow for the month of July. July 16th missing for plot (A), (C) and (D) due to Lobo buoy cleaning.

E.1.5 Middle of Channel Site

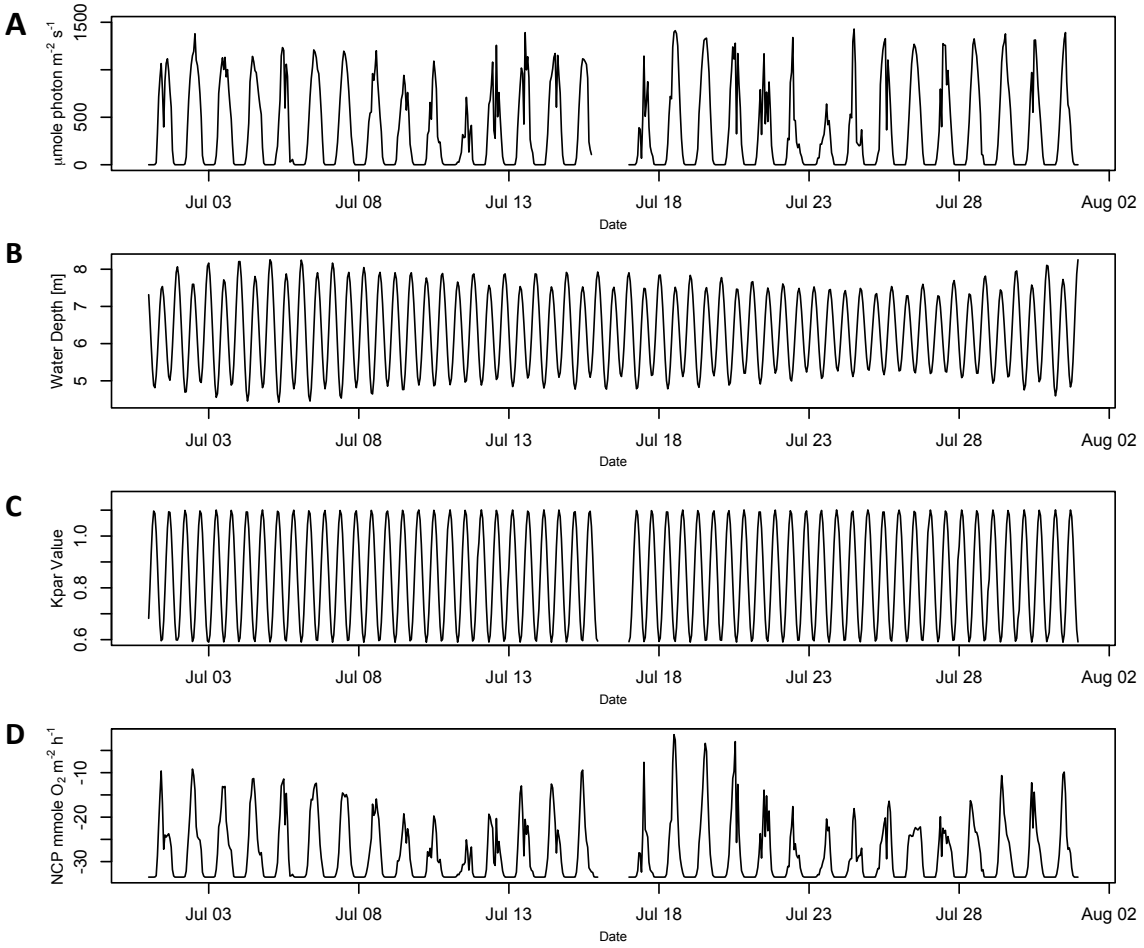

Figure E.5: In situ hourly values from the month of July used to calculate the NCP for site Middle of Channel (MC). (A) is the irradiance at the surface of the water, (B) is the water depth at the specific site and (C) is the attenuation value calculated. (D) is the calculated NCP for site west shallow for the month of July. July 16th missing for plot (A), (C) and (D) due to Lobo buoy cleaning.

E.2 NCP Box Plots

Box plots were used to determine which site were net autotrophic during periods of photosynthesising time (day light) for the benthic NCP estimates for the month of July. Based on Fig. 4.4 only the shallow sites are net autotrophic which was not expected. Therefore, the parameter α was examined to see if the standard deviation would affect

these results. The parameter *R* was also changed from Fig. 4.4 from the average *R* (except site MC) to the individual *R* parameters. After changing both of these parameters the results did not significantly change and the deep sites still remained net heterotrophic. α was calculated based on the *in situ* irradiance to determined what the parameter α had to be for each site to be net autotrophic on three days in July. From this calculation in Table E.2, it was determined that both deep sites were not close to being net autotrophic based on the estimates from the TOE parameters.

E.2.1 Alpha (α) Upper and Lower Range

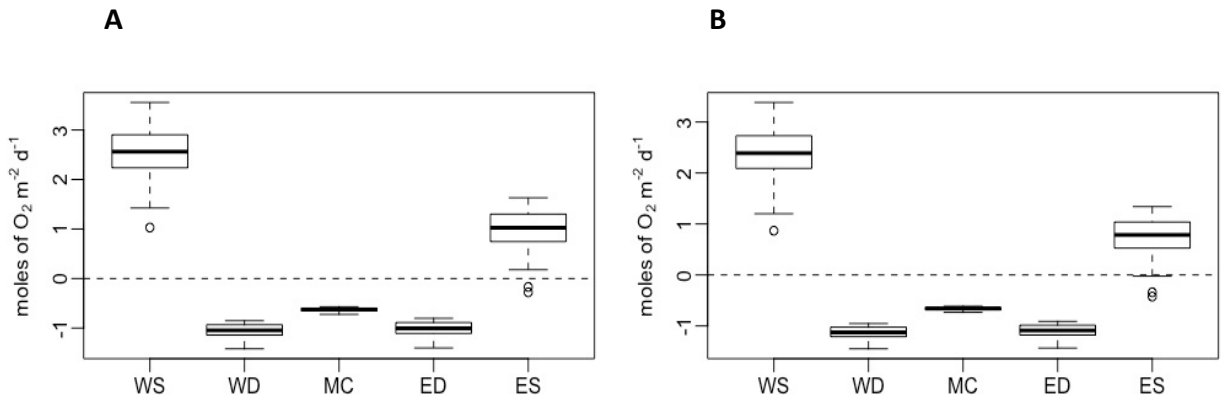

Figure E.6: (A) *NCP box plot using the upper standard error of α parameter. (B) NCP box plot using the lower standard error of α parameter. Both (A) and (B) estimate the month of July for periods of potential photosynthesising (day light) for each site on the transect. Below zero on the plot is net heterotrophic and above is net autotrophic.*

Table E.1: Parameters used for the upper and lower Alpha (α) ($mmol\ O_2\ m^{-2}\ d^{-1}\ (\mu mol\ photons\ m^{-2}\ s^{-1})^{-1}$) standard error ranges for the boxplots above with individual dark respiration (R) ($mmol\ O_2\ m^{-2}d^{-1}$) parameters for Table E.2 calculation.

Site Name	Alpha (α)	Standard Deviation	Upper α (+)	Lower α (-)	Respiration (R)
West Shallow (WS)	4.5	0.3961	4.9	4.1	81.9
West Deep (WD)	4.3	0.5897	4.9	3.7	51.3
Middle of Channel (MC)	1.4	0.1774	1.6	1.2	33.5
East Deep (ED)	3.5	0.3601	3.8	3.1	67.1
East Shallow (ES)	4.8	0.5275	5.3	4.2	82.8
Average (w/o MC)	3.9	0.3085	4.2	3.6	70.8

Table E.2: Calculated Alpha (α) ($mmol\ O_2\ m^{-2}\ d^{-1}\ (\mu mol\ photons\ m^{-2}\ s^{-1})^{-1}$) determined from average 24 hr light levels from the sampling days in July and dark respiration (R) ($mmol\ O_2\ m^{-2}d^{-1}$) from Table E.1 to determine $\alpha = R/E$. These calculated Alpha's are the values alpha would have to be for each site to be net autotrophic with the average in situ irradiance levels.

Site Name	July 11th		July 22nd		July 30th	
	Irradiance (E)	Alpha (R/E)	Irradiance (E)	Alpha (R/E)	Irradiance (E)	Alpha (R/E)
West Shallow (WS)	72.7	0.97	133.3	0.53	139.9	0.51
West Deep (WD)	2.1	33.5	3.8	18.8	6.1	11.7
Middle of Channel (MC)	1.3	26.8	2.2	15.1	3.8	8.7
East Deep (ED)	2.3	30.8	4.1	17.3	6.5	10.9
East Shallow (ES)	18.5	3.8	33.7	2.1	40.7	1.7

E.2.2 *R* Upper and Lower Range

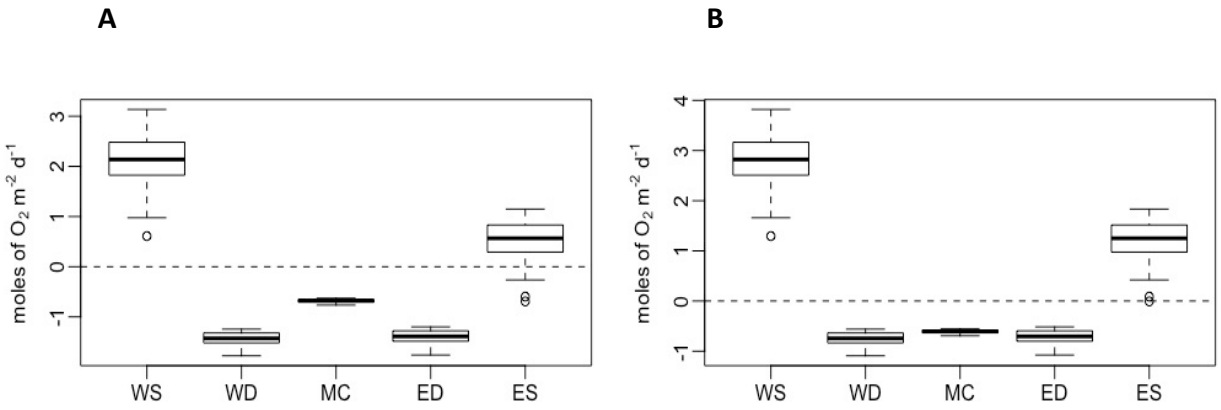

Figure E.7: (A) *NCP box plot using the upper standard error of R parameter. (B) NCP box plot using the lower standard error of R parameter. Both (A) and (B) estimate the month of July for periods of potential photosynthesising (day light) for each site on the transect. Below zero on the plot is net heterotrophic and above is net autotrophic.*

E.2.3 Individual *R* Parameters

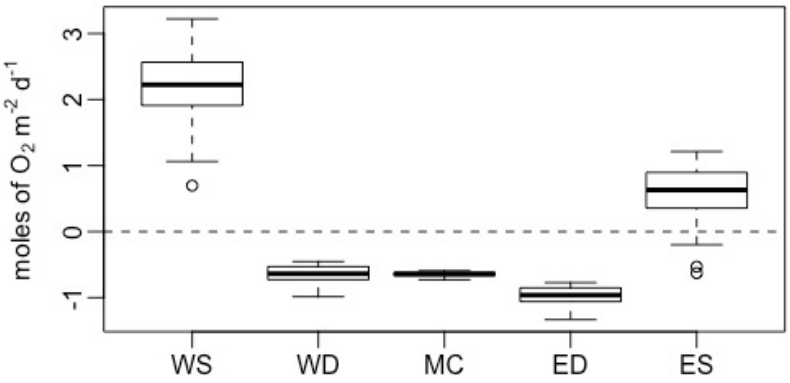

Figure E.8: *NCP box plot using the individual site R parameters for the month of July for periods of potential photosynthesising (day light) for each site on the transect. Below zero on the plot is net heterotrophic and above is net autotrophic.*

APPENDIX F

BIOMASS

F.1 Cell Counts

The cell concentration at each site when compared to the parameters showed linear dependence for the parameter P_{max} but not for α or R. In Fig. 4.3 the linear trend infers that the difference in rates at the higher light levels when P_{max} was reached was due to a cell specific increase in biomass present at each site. For α and R the slope of the curve is flat indicating no dependence on biomass for the rate of production or consumption at the lower light levels for the parameter α or the dark period for R.

F.1.1 *R* Parameter with Cell Concentration

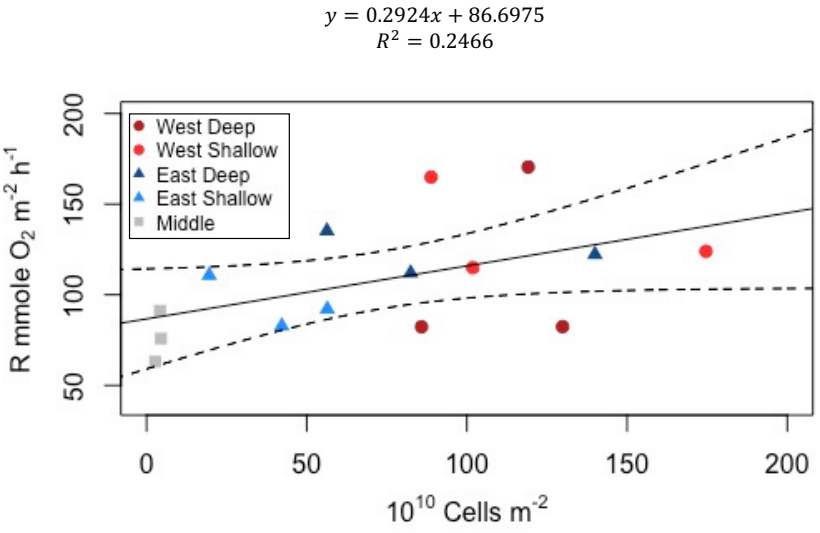

Figure F.1: TOE R parameters for each individual site-specific core with the microphytobenthic cell concentration from the diatom counts. Dashed lines are the 95% confidence intervals.

F.2 Chlorophyll a Concentrations

When comparing the sediment chlorophyll a concentration to the parameters fitted from the PE relationship the chl a concentrations showed no correlation. Therefore, the sediment chl a concentration has no specific effect on the difference in rates from site to site. This is determined based on the flat trend of the slope of the line fitted to the parameters versus the chl a concentration for Fig. 2.1-3.

F.2.1 *Pmax* Parameters with Chl a Concentration

$$y = -0.2273x + 430.2127$$
$$R^2 = -0.0767$$

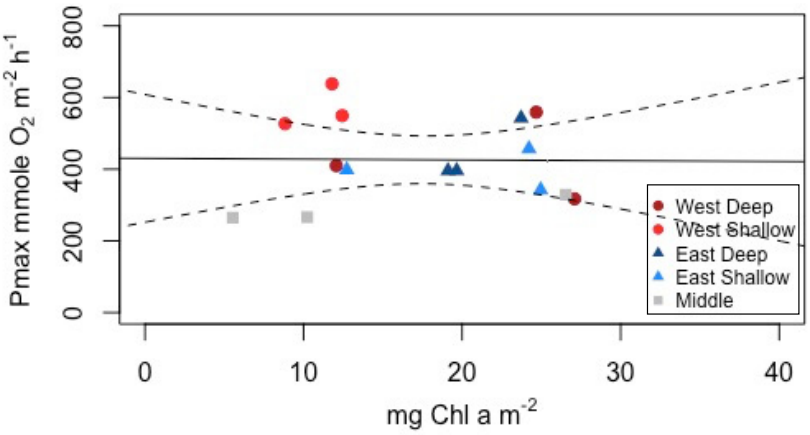

Figure F.2: TOE P_{max} parameters for each individual site-specific core with the chlorophyll a sediment concentration for each site. Dashed lines are the 95% confidence intervals.

F.2.2 Alpha (α) Parameters with Chl a Concentrations

$$y = 0.04803x + 2.88002$$
$$R^2 = -0.0153$$

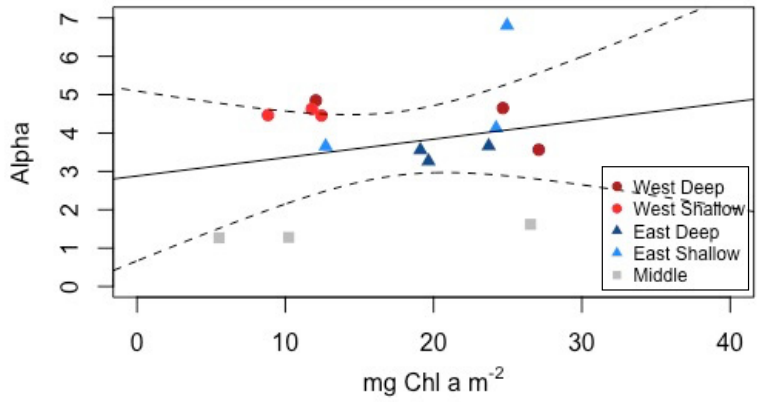

Figure F.3: TOE α parameters for each individual site-specific core with the chlorophyll a sediment concentration for each site. Dashed lines are the 95% confidence intervals.

F.2.3 *R* Parameters with Chl a Concentrations

$$y = 0.1383x + 105.8696$$
$$R^2 = -0.07581$$

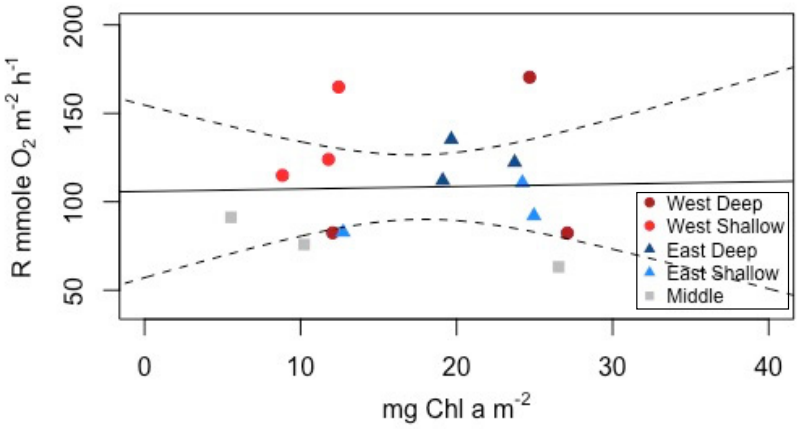

Figure F.4: TOE R parameters for each individual site-specific core with the chlorophyll a sediment concentration for each site. Dashed lines are the 95% confidence intervals.